KATHOLIEKE
UNIVERSITEIT
LEUVEN

Faculteit Wetenschappen

Departement Chemie

Moleculair Design en Synthese

Laboratorium voor Coördinatiechemie

Metallomesogens based on
1,10-phenanthroline

Proefschrift ingediend voor het behalen van de graad van

Doctor in de Wetenschappen

Jan Ramaekers

Leuven, 2008

Promotor: Prof. Dr. C. Görller-Walrand

Promotor: Prof. Dr. K. Binnemans

Co-Promotor: Dr. T. Cardinaels

Leden van de examencommissie:

Prof. Dr. Christiane Görller-Walrand (promotor)
Prof. Dr. Koen Binnemans (promotor)
Dr. Thomas Cardinaels (co-promotor)
Prof. Dr. Wim Dehaen
Prof. Dr. Steven De Feyter
Prof. Dr. Thierry Verbiest
Prof. Dr. Mario Smet
Prof. Dr. Andreas Taubert

Dankwoord

Hier sta ik dan, op het einde van een vier jaar durende wandeling doorheen het land der vloeibare kristallen. Vele wegen zijn bewandeld, sommige met groot succes, anderen met matig, weer anderen helemaal zonder succes. Maar aan het einde van deze lange wandeling kan ik niet anders dan zeggen dat ik enorm veel heb bijgeleerd. En dit dankzij de vele mensen die ik ontmoet heb op deze weg. Daarom wil ik ze heel graag bedanken.

In de eerste plaats wil ik mijn twee promotoren, Prof. Dr. Christiane Görller-Walrand en Prof. Dr. Koen Binnemans, bedanken voor de mogelijkheid die ze mij hebben gegeven om in hun labo onderzoek te doen. Prof. Dr. Koen Binnemans wil ik ook bedanken voor de wetenschappelijke ondersteuning tijdens deze periode.

Ten tweede wil ik mijn co-promotor, Thomas Cardinaels bedanken. Een paragraaf gaat te kort zijn om dit correct te doen maar we gaan het proberen. Wetenschappelijk is thomas mijn steunpilaar geweest gedurende mijn doctoraat, altijd heeft hij mij bijgestaan met raad. Aan hem heb ik grotendeels dit werk te danken. Maar ook buiten de wetenschappen heeft hij het leven in de F en buiten de F kleur gegeven. Gezapige fietstochtjes, tennis"les", snowboarden, ne curry nu en dan, noem maar op... Master nog veel succes verder en heel hard bedankt.

Dan wil ik mijn jaargenootjes bedanken bij COC (Ben, Els en Karen), dit voor samen deze vier jaar door te brengen en met regelmaat elkaar bij te staan met de nodige hulp. Ben wil ik ook nog even speciaal bedanken en dit niet enkel voor de jaren van mijn doctoraat, maar voor de volle acht jaar die we samen "wetenschappelijk" hebben doorgebracht. Merci Benson.

Niet te vergeten onze post-docs: Dr. Kris Driesen voor de steun bij de spectroscopie en voor de leuke babbels over XIII dingen, Dr. Peter Nockemann voor het antwoord op al mijn vragen en alle tips, Dr. Tanja Parac-Vogt voor de hulp bij de interpretatie van NMR-spectra en Dr. Rik Van Deun voor de wetenschappelijke discussies.

Vervolgens wil ik nog enkele professoren bedanken: Prof. Dr. Bart Goderis voor zijn hulp bij de X-stralen metingen in Grenoble en de interpretatie van deze data. Prof. Dr. Steven De Feyter voor de STM-metingen. Prof. Dr. Wim Dehaen en Prof. Dr. Mario Smet voor de discussies betreffende de vele organische synthesereacties die ik heb gedaan. Last but not least, I want to thank Dr. Bertrand Donnio and Dr. Daniel Guillon for two interesting weeks in Strasbourg and also for the help with the X-ray diffraction and the modelling of these structures.

Graag zou ik Dirk Henot, Leen Van Nerum en Petra Bloemen willen bedanken voor de CHN-analyses en de massaspecta, maar ook voor alle andere dingen waarmee ze ons dagelijks helpen. Paul Wijnants voor de hulp met bestellingen en nog zoveel meer. Karel Duerinckx wil ik graag bedanken voor zijn hulp bij het opnemen van de NMR-spectra. Rita u wil ik zeker niet vergeten, dank je wel voor al de dingen die je voor mij geregeld hebt tijdens mijn doctoraat.

Dan zou ik graag nog mijn collega's en ex-collega's bedanken. Allemaal heel fel bedankt voor de geweldige sfeer in ons labo, de feestjes, de koffiepauzes, de vrijdag-alma-dag, six flags en La Roche en ga zo maar door. Tonio, Bompa, T en Benson voor het koloniseren, den Grande en 999 anderen. Karel, Katleen en Thomas, we were the LC-people. Zij die pas begonnen zijn wil ik heel veel succes wensen met hun onderzoek.

Als laatste en niet in het minste wil ik mijn familie en vrienden bedanken. Mijn vrienden om het constant informeren naar mijn onderzoek en zeker

Table of contents

Abbreviations

A	cross-sectional area
bipy	bipyridine
ca.	circa
cmc	critical micelle concentration
Col_h	hexagonal columnar phase
Col_o	oblique columnar phase
Col_r	rectangular columnar phase
Cr	crystalline or semicrystalline phase
Cub	cubic phase
d	layer spacing
dec	decomposition
DMF	*N,N*-dimethylformamide
DMSO	dimethyl sulfoxide
DSC	differential scanning calorimetry
ESI-MS	electron spray ionization mass spectrometry
HOPG	highly oriented pyrolytic graphite
I	isotropic phase
λ	wavelength
L_α	lamellar phase
LMCT	ligand to metal charge transfer
Ln	lanthanide ion
MLCT	metal to ligand charge transfer
N	nematic phase
ñ	director of the liquid crystal
N_{col}	columnar nematic
N_D	discotic nematic
NMR	nuclear magnetic resonance
NTf_2	bistriflimide
Phen	1,10-phenanthroline
POM	polarizing optical microscopy

ppm	parts per million
rt	room temperature
SAXS	small angle X-ray scattering
Sm	smectic phase
STM	scanning tunneling microscopy
TCB	1,2,4-trichlorobenzene
TGB	twisted grain boundary
THF	tetrahydrofuran
XRD	X-ray diffraction

Introduction: objective and outline

For a long time general belief was that matter existed in three states of matter. However this is not entirely correct. Certain materials possess an intermediate state of matter between disordered liquids and ordered solids. These materials are called liquid crystals and they combine the anisotropic properties of crystals and the fluidity of liquids.

The objective of this PhD thesis was to design *metallomesogens* with d-block and f-block metals. These are metal-containing liquid crystals which combine the properties of both metals and liquid crystals. The reason to choose for the d-block and f-block transition metals was based on two different reasons. The first is related to the research history of the lab, which has great experience in the synthesis of luminescent lanthanide complexes. We wanted to combine the luminescent properties of the lanthanides and some d-block metals with the properties of a liquid crystal. Secondly, the use of transition metals would give us the ability to design complexes with a geometry that is impossible to obtain with pure organic compounds.

1,10-Phenanthroline is an interesting building block to synthesize ligands because of its versatile coordination chemistry. In addition, the extended conjugated π-system and the permanent dipole moment are favorable for the emergence of mesophases via π-π stacking and dipole-dipole interactions of the rigid cores. 1,10-Phenanthroline can form complexes with a wide variety of metals. The reason that few liquid crystals based on 1,10-phenanthroline are known is because of the difficulty to synthesize the substituted starting materials. Taking advantage of the binding ability of 1,10-phenanthroline with metals, metallomesogens can be formed. Specific properties can be obtained by a suitable choice of the metal or by changing the structure of the 1,10-phenanthroline-based ligand.

Two different approaches of ligand-design were investigated. The first series of ligands is based on 1,10-phenanthrolines with a 5,6-substitution pattern, the second series on 1,10-phenanthrolines with a 3,8-substitution

pattern. In the first case, the ligand is an amphiphilic compound which has an aromatic core combined with apolar, terminal alkyl chains. In case of a 3,8-substitution, a polycatenar ligand is formed. The major part of this research was the synthesis of the ligands and the study of the thermal behavior of the ligands and the corresponding metal complexes. Also STM-studies were performed and luminescent properties were investigated for some of the compounds.

Outline

To introduce the reader to this work, a general introduction about the basics of liquid crystals is given in chapter 1. The different types of mesophases are described and the techniques for characterization are shortly explained.

The literature overview gives an insight in earlier work done on metallomesogens based on 1,10-phenanthroline. Related work on thermotropic cubic phases and lyomesogens is covered in chapter 2.

Lanthanide(III) complexes of substituted imidazo*[4,5-f]*-1,10-phenanthroline ligands were synthesized. The influence of the size of the lanthanide(III) ion and the substitution pattern of the alkyl chains on the thermal properties of these complexes is described in chapter 3.

Imidazo*[4,5-f]*-1,10-phenanthroline and pyrazino*[2,3-f]*-1,10-phenanthroline substituted with long alkyl chains were used as ligands for the design of metallomesogens. Rhenium(I) and ruthenium(II) complexes were synthesized and their thermal behavior was investigated. Chapter 4 gives also the introduction to the lyotropic liquid-crystalline behavior of these compounds.

Furthermore, as demonstrated in chapter 5, a rigid, extended, tetracatenar system derived from 1,10-phenanthroline was examined. The 1,10-phenanthroline unit was extended in the 3- and 8-positions using acetylene linking groups. The mesophase behavior of these ligands and their corresponding rhenium(I) complexes was investigated as a function of the alkoxy chain length. Self-assembled monolayers of the ligands and corresponding rhenium(I) complexes were studied by scanning tunnelling microscopy (STM). Also the photophysical properties of the ligands and corresponding rhenium(I) complexes were investigated.

Chapter 1: Liquid crystals

1.1 History of liquid crystals

It was the Austrian botanist Friedrich Reinitzer (1857-1927) who first noted liquid-crystallinity in 1888. Working at the University of Prague, he carried out research on the function of cholesterol. He synthesized several cholesterol-related substances and he noticed that one of the esters, cholesteryl benzoate (Figure 1.1), seemed to have two melting points.[1] At 145.5 °C, the solid melted into a cloudy liquid. Upon further heating, he observed that the cloudiness suddenly disappeared at 178.5 °C, and a clear transparent liquid was formed.
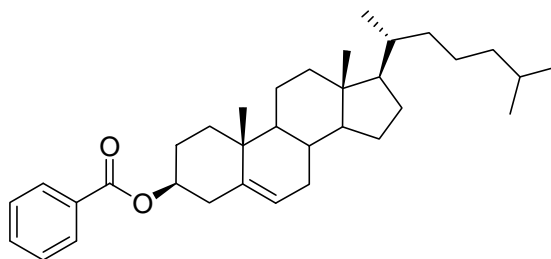
Figure 1.1: Structure of cholesteryl benzoate.

The German physicist Otto Lehmann (1855-1922), a professor at the University of Karlsruhe, studied Reinitzer's compound by hot-stage polarizing optical microscopy and became convinced that the cloudy liquid was a thermodynamically distinct phase with a unique molecular order. Lehmann was also the first to use the term "Flüssige Kristalle" in 1889.[2] Within the same year Ludwig Gattermann (1860-1920), an assistant

professor at the University of Heidelberg, reported the same behavior for para-azoxyanisole (Figure 1.2).
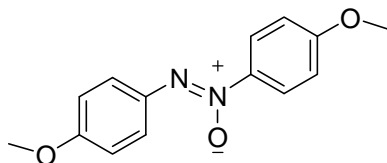
Figure 1.2: Structure of para-azoxyanisole.

The article of Gattermann reports a cloudy liquid phase, which is formed at 116 °C and disappears at 134 °C. The temperature at which the cloudiness disappeared, became later known as the *clearing point*.[3] Whereas Gattermann lost interest in these compounds, Daniel Vorländer (1867-1941) gained interest. As a professor at the University of Halle (Germany), Vorländer tried to find a structural explanation for the *crystalline liquids*, the term he used for liquid crystals.[4] In the meanwhile a lively discussion was going on about the real nature of liquid crystals. Emulsions as well as polymorphism were brought forward as possible explanations. None of them survived the criticism.

In 1909, Lehmann gave at Geneva and Paris seminars with an experimental demonstration, which inspired Charles Mauguin (1878-1958), Georges Friedel (1865-1933) and François Grandjean (1882-1975). Mauguin, an assistant of Fréderic Wallerant (1858-1936) at the École Normale Supérieure at Paris, started to study the behavior of liquid crystals between thin layers. He was confronted with the pitch that appeared between layers and also found that the orientation could be changed by applying a magnetic field. Simultaneously Friedel's assistant Grandjean studied liquid-crystallinity (Friedel was at that time director of the School of Mines at St. Étienne). In 1922, Friedel gave the first acceptable and valuable explanation. His interpretation of the phenomena was published in the

Annales de Physique.[5] He used the term "*mésomorphe*" which underlines the intermediate character of the phase between solid (crystalline) and fluid. George William Gray (born in 1926) is an emeritus professor of Organic Chemistry at the University of Hull (U.K.). He synthesized the cyano-biphenyl liquid crystals, which were the first compounds which exhibited stable nematic phases at room temperature.[6] The best known is the 4-*n*-pentyl-4'-cyanobiphenyl (5CB) shown in Figure 1.3.

*Figure 1.3: Structure of 4-*n-*pentyl-4'-cyanobiphenyl.*

In the following years numerous new mesogenic compounds were synthesized. It's difficult to imagine a world without liquid crystals, since they are nowadays used in the most diverse applications: wristwatches, laptops, TV screens, spatial light modulators, temperature sensors and many more.

1.2 Introduction to liquid crystals

Compounds are classified into three different physical aggregation states: solid, liquid and gas. In the crystalline solid state, atoms or molecules are ordered in a crystal lattice. The atoms or molecules possess positional and orientational order. In the amorphous solid state, the molecules have no longe-range orientational order, similar to a frozen liquid. In the liquid phase, the molecules have neither positional nor orientational order. They are free to flow and are randomly oriented.

The liquid-crystalline phase represents an intermediate situation between the crystalline phase and liquid phase. It is also called the *mesomorphic phase* or *mesophase* (*mesos* = between). In this phase, the molecules still have orientational and sometimes some positional order, but can move through the solution. Liquid-crystalline molecules are usually highly anisometric, which gives rise to the preferred orientations of neighboring molecules. Compounds that are able to form liquid-crystalline phases are also termed *mesogens*.

There are two different kinds of liquid crystals: *thermotropic* liquid crystals and *lyotropic* liquid crystals. For thermotropic liquid crystals, the mesophase is obtained by heating a crystalline phase or by cooling an isotropic liquid phase. At the melting point, the solid compound will melt into the liquid-cristalline phase. At a higher temperature the sample will become an isotropic liquid. This temperature is called the *clearing point*.
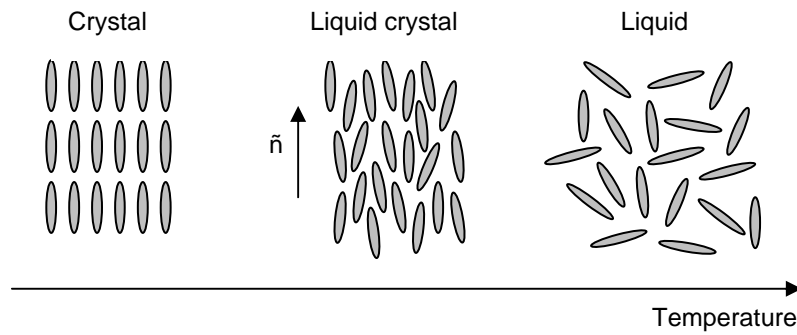
Figure 1.4: Schematic thermal behavior of a thermotropic liquid crystal.

When a mesophase appears both on heating as on cooling, it is called an *enantiotropic* mesophase. When a mesophase only appears on cooling from the isotropic liquid, it is termed *monotropic*. Many thermotropic liquid crystals exhibit a variety of phases when the temperature is changed. This is called *polymorphism*.

For lyotropic liquid crystals, the mesophase is formed upon addition of a solvent, which is usually water.

1.3 Thermotropic liquid crystals

1.3.1 Classification of mesophases

Mesophases can be easily classified based on the shape of the mesogens. This shape can be: rodlike (*calamitic* mesogens), disklike (*discotic* mesogens) or V-shaped (*bent-core* or *banana shaped* mesogens). *Polycatenar* liquid crystals have an intermediate structure between rodlike and disklike and are considered as a different class of liquid crystals. The cubic mesophases will be discussed separately.

1.3.1.1 Mesophases formed by calamitic molecules

Nematic phase
The *nematic* (N) phase has no positional order, but only orientational order. The mesogens all point with their long molecular axis on average to the same direction, defined by the *director ñ* (Figure 1.5). The nematic phase is the least ordered mesophase. Because of the low molecular order in the nematic phase, this phase has a low viscosity and is very fluid.
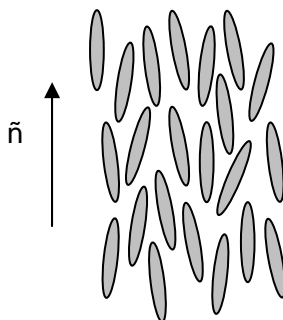
*Figure 1.5: Schematic representation of the molecular order
in the nematic phase.*

Chiral nematic phase

The *chiral nematic* (N*) phase possesses chirality. This phase is also called the *cholesteric phase* because it was first observed for cholesterol derivatives. In this phase, the director describes a helix through the material (Figure 1.6). The distance (along the director) over which the director undergoes a full 360° twist is called the *pitch*.
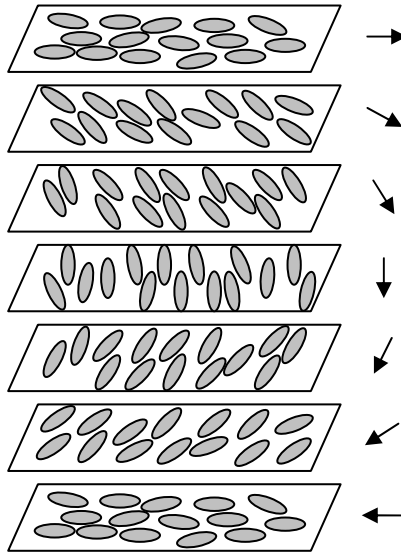
Figure 1.6: Schematic representation of the molecular order in the chiral nematic phase.

Smectic phases

The *smectic* (Sm) phases are more ordered than the nematic phase. Smectic phases have orientational order, and some degree of positional order. Typical for a smectic phase is the arrangement of molecules into layers.

In the *smectic A* (SmA) phase, the director is perpendicular to the smectic layer plane, and there is no particular positional order within the layers

(Figure 1.7). The smectic A phase is the most disordered smectic phase and therefore the most fluid one.

In the *smectic C* (SmC) phase, molecules are arranged in layers as they do in the smectic A phase, but the director is not perpendicular to the smectic layer plane (Figure 1.7). Thus the molecules are tilted within the layers.
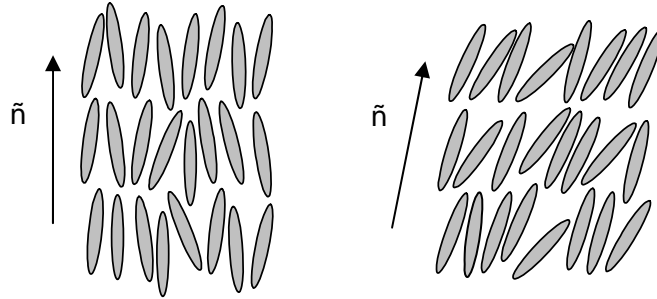
Figure 1.7: Schematic representation of the SmA (left) and the SmC (right) phase.

When hexagonal symmetry is introduced in the smectic A phase, the *smectic B* (SmB) phase is obtained (Figure 1.8). It is a more ordered, and hence less fluid phase than the SmA and the SmC phase.
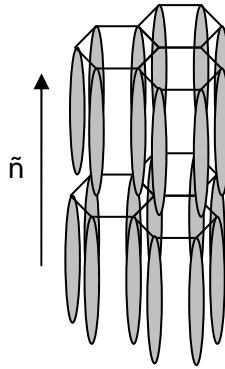
Figure 1.8: Schematic representation of the SmB phase.

12

The *smectic F* (SmF) phase and the *smectic I* (SmI) phase are tilted hexagonal structures. SmC, SmF and SmI phases can also exist as chiral modifications (SmC*, SmF* and SmI*). Soft crystal phases (B, E, G, H, J and K) are characterized by the appearance of inter-layer correlations. They exhibit long-range positional order in three dimensions.

1.3.1.2 Mesophases formed by discotic molecules

Discotic nematic phase
The *discotic nematic* (N_D) phase is the least ordered discotic liquid-crystalline phase. This phase only possesses orientational order of the molecules (Figure 1.9). Whereas in the calamitic nematic phase, the long molecular axis is parallel to a preferential direction (the director), the preferential direction of the molecules in the discotic nematic phase is established by the short molecular axis.

Figure 1.9: Schematic representation of the discotic nematic phase (N_D).

Columnar nematic phase
In the *columnar nematic* (N_{col}) phase, the molecules are stacked into short colums and these columns are ordered as the molecules in the calamitic nematic phase.

Columnar phases

In the *columnar* phases, the molecules are also stacked into columns and these columns are arranged according to the symmetry of a 2D lattice (Figure 1.10). It were Chandrasekhar et al. who discovered the columnar phases in 1977.[7]

Figure 1.10: Schematic representation of a columnar phase.

There exist several types of discotic columnar phases, which differ by the positioning of the columns. Moreover, the stacking of the molecules within the columns can be ordered or disordered. In the *hexagonal columnar* (Col_h) phase, the columns are positioned in a 2D hexagonal pattern (Figure 1.11).
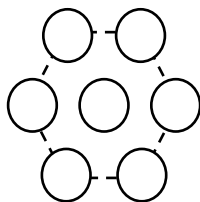
Figure 1.11: Schematic representation of the 2D lattice of the hexagonal columnar phase (plane group p6mm).

The *oblique columnar* (Col_o) or the *rectangular columnar* (Col_r) *phase* are two other types of columnar phases. Here, the columns are positioned in a rectangular pattern. A schematic representation of the 2D lattices of the Col_o and the Col_r phase is shown in Figure 1.12.

14
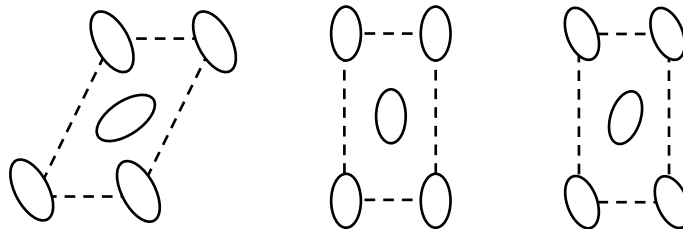
Figure 1.12: Schematic representation of the 2D lattices of the oblique columnar phase (left, plane group p1) and the rectangular columnar phase (middle, plane group c2mm; right, plane group p2gg).

1.3.1.3 Cubic phases

Cubic phases are mesophases with a cubic symmetry. They are optically isotropic, which makes it difficult to distinguish them from the isotropic solution by polarizing optical microscopy. The cubic phases are very viscous and their formation kinetics are slow. The molecules possess long-range positional order, accompanied by rotational disorder and conformational mobility. Although cubic mesophases are very common for lyotropic liquid crystals, where a cubic phase is possible between any pair of phases, there are relatively few examples of cubic mesophases for thermotropic liquid crystals.[8] The cubic mesophases will be further discussed in the part of the lyotropic liquid crystals.

1.3.1.4 Polycatenar mesogens

Polycatenar mesogens or *polycatenars* are molecules with a long rod-like rigid core to which several aliphatic chains are attached.[9,10] They bridge the gap between rodlike and disklike mesogenic compounds (Figure 1.13).
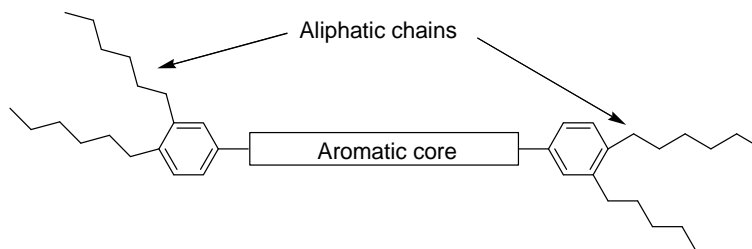
Figure 1.13: General structure of polycatenar liquid crystals. In this figure a tetracatenar liquid crystal is shown.

"Polycatenar" literally means "many-tailed" and the nomenclature reflects to the number of terminal chains. Tetra-, penta- or hexacatenars contain four, five or six terminal chains, respectively. Different isomers are possible by placing the chains in various positions. In order to obtain mesomorphic properties a balance must be kept between the number of chains grafted to the core and the length of the core. Generally, the core must have as many rings as terminal chains. Polycatenars have aroused interest due to their rich mesomorphism and tetracatenar mesogens are the most interesting when the terminal chains are in the 3- and 4-positions. They can show nematic, smectic C, cubic and columnar mesophases in the same series at differing chain lengths, making them quite unique liquid-crystalline materials.[11-14] At short chain lengths, nematic and/or SmC phases are observed, while at longer chain lengths, columnar phases are formed (Figure 1.14).
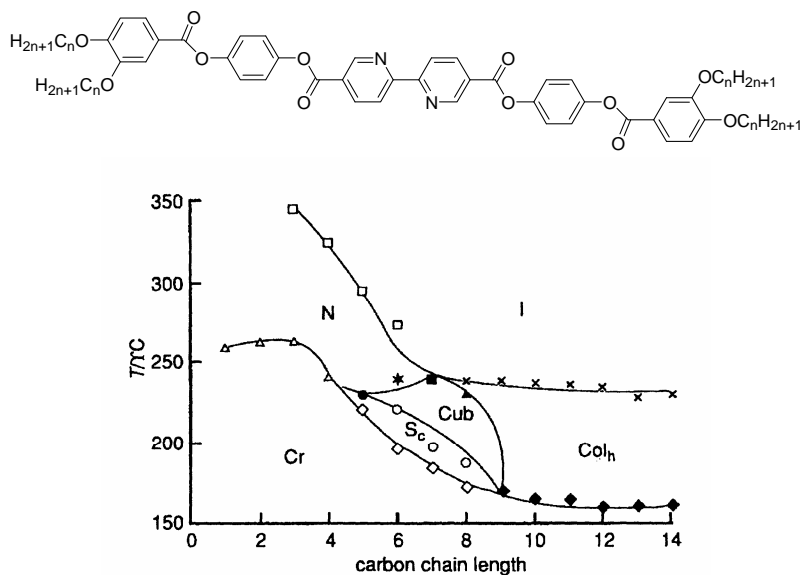
Figure 1.14: Structure and phase diagram for the tetracatenar bipyridines (Cr = crystalline phase; N = nematic phase, Sm$_C$ = smectic C phase; Cub = cubic phase and Col$_h$ = hexagonal columnar phase).[13]

When the chain length is short, the materials have a rodlike shape and so nematic or smectic phases are expected. For these systems, it is always the SmC phase which is observed: at the interface between the rigid core and the chains, the cross-sectional area of the chains is greater than that of the core and so to fill space efficiently, the cores must tilt. However, at longer chain lengths and/or at higher temperatures, the chains occupy a greater volume and, in order to compensate this additional volume, the cores have to tilt even more. Eventually, the smectic layers can no longer hold together and they break up, leading to the formation of a columnar phase (Figure 1.15). The transition from the SmC phase to the columnar phase normally takes place gradually (one or two compounds showing both phases) and is classically achieved via a cubic phase.
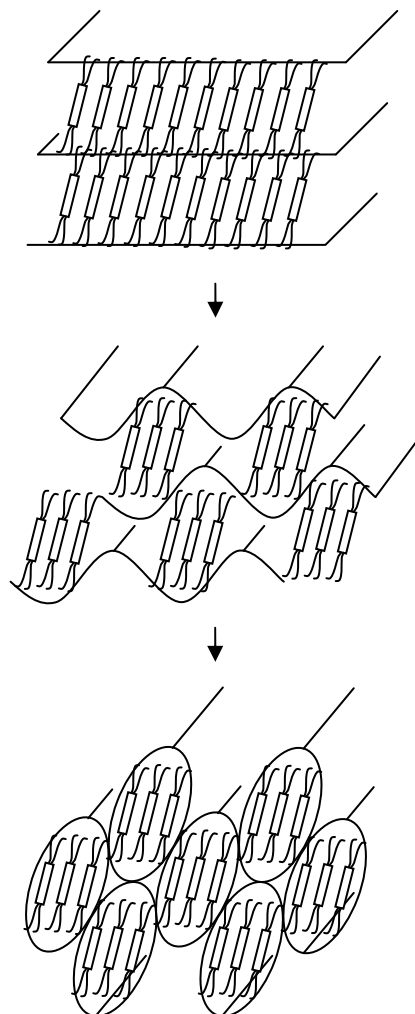
Figure 1.15: Model for the formation of the columnar mesophases.[15]

1.3.1.5 Banana-shaped mesogens

It was Vorländer who discovered the liquid-crystalline behavior of banana-shaped molecules in 1923.[4] Recently, the banana-shaped liquid crystals have attracted much scientific attention due to their unique mesomorphic properties.[16-18] Their shape and polarity lead to a stacking of the molecules in layers, with the polar bend of the molecules in the same direction (Figure 1.16).
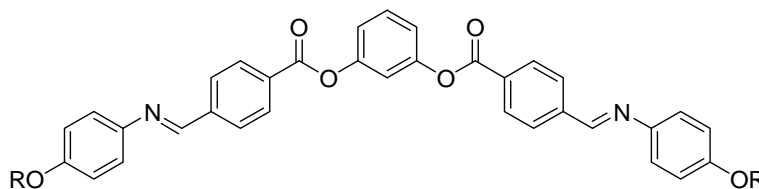
Figure 1.16: General structure of the most intensively investigated type of bent-core (banana-shaped) liquid crystals.

The important consequence of the directed packing of such molecules is the occurrence of a polar order parallel to the layers. The layer structures are modified in order to destroy the macroscopic polarization. This leads to new types of mesophases (Figure 1.17). The formation of a rectangular columnar mesophase (Col$_r$ or *B1 phase*), built up by antiparallel aligned ribbons of collapsed layers seems to be the simplest way to escape from a macroscopic polar order. This organization is usually formed if the core-core interactions are dominant. It becomes unstable for molecules with elongated alkyl chains. For these molecules, a lamellar arrangement is more favorable, leading to antiferroelectric, switchable smectic phases (*SmP$_A$ phases*). By

application of an electric field, the antiparallel stacking of the layers can be transformed into a parallel stacking, resulting in a ferroelectric polar smectic phase (*SmP$_F$*). In most of these phases, the molecules are additionally tilted (*SmCP phases*), and this leads to a further reduction of the phase symmetry. For these SmCP phases, a handedness (and thus chirality) is observed, depending on the tilt sense of the molecules. This inherent chirality can lead to mesophases with chiral supramolecular structures, even though the molecules themselves are achiral. Examples are the *plastic crystal B4 phase*, which has a *twisted grain boundary structure* (*TGB phase*) and the *B7 phase*, which has a very complex structure. The non-polar intercalated phases are called Sm_{int} or B_6 phases.
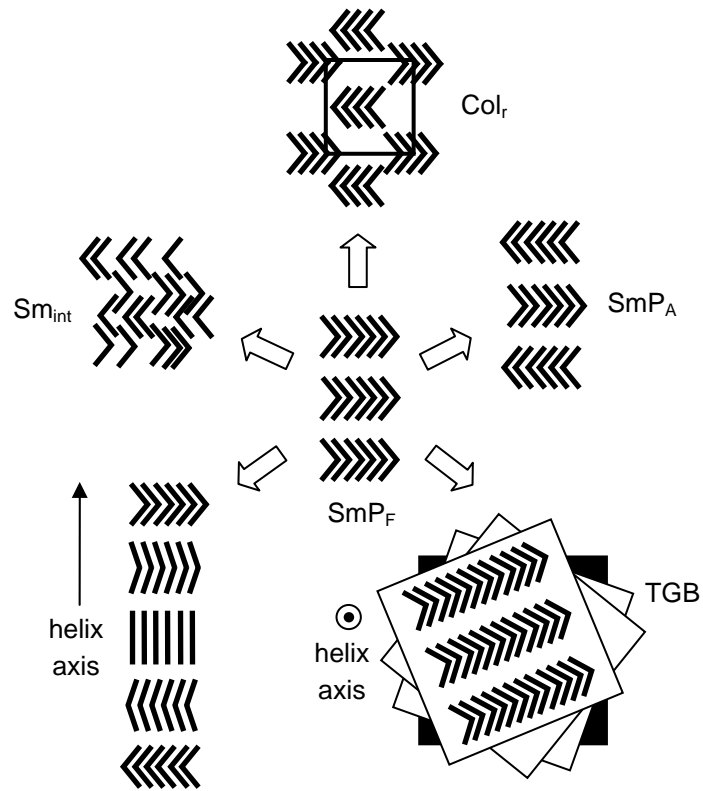
Figure 1.17: Possible ways to escape from a macroscopic polarization in mesophases built up from bent-core molecules. Abbreviations: Sm$_{int}$ = intercalated smectic phase; SmP$_A$ = smectic phase with antiferroelectric correlation between adjacent layers; SmP$_F$ = smectic phase with ferroelectric correlation between adjacent layers (macroscopically polar ordered); TGB = twisted grain boundary structure.[17]

1.3.1.6 Metallomesogens

The rationale for incorporation of transition metals into liquid crystals is to combine the properties of liquid crystals (anisotropic fluids) with the unique properties of d-block and f-block transition metals (magnetic and photophysical properties, redox behavior).[19-22] The design of metal-containing liquid crystals (metallomesogens) is a challenge, because the presence of a metal center often modifies the mesomorphic behavior of the free ligand (stabilization, modification or suppression of the mesophases of the ligand, or induction of mesophases).[23,24] On the other hand, transition metals aid in the construction of mesogenic materials with original molecular architectures which are not reachable by the use of pure organic systems. Examples are lanthanide(III) complexes,[25-29] gold metallacrowns,[30] macrocyclic azacrown complexes,[31-33] and long-chain carboxylate metal salts.[21,34] Additionally, the radius of the metal ion can influence the transition temperatures and even the type of mesophase. This effect has been studied in mesogens of trivalent lanthanide ions[35-37] and of divalent transition metal ions.[15,19-21,38-43] Taking advantage of the variation of the coordination number by a proper choice of the metal ion, it is possible to obtain complexes with different metal-to-ligand ratios and molecular geometry, and thus modifications in the mesophase behavior are expected. However, in order to study the influence of the metal ion on the thermal behavior of metallomesogens, it is necessary to have ligand systems that are able to form complexes with many different types of metal ions. Good examples are provided by the metal alkanoates for which depending on the choice of the metal, covalent or ionic bonding between the metal and the carboxylate groups is observed.[21,34]

1.4 Lyotropic liquid crystals

Lyotropic mesophases (*lyomesophases*) are built up by *amphiphilic* compounds, which consist of two chemically incompatible parts: one or more hydrophobic hydrocarbon tails and a hydrophilic head. Typical examples are salts of fatty acids and phospholipids. Many amphiphiles are used as detergents. When the molecules are dissolved in an appropriate polar solvent in sufficiently high concentrations (above the so-called *critical micelle concentration* (*cmc*)), they self-assemble so that the polar (hydrophilic) heads protect the non-polar (hydrophobic) tails. An opposite situation is found for a non-polar solvent. Lyotropic mesophases formed in polar solvents are termed *normal* phases (I_1, H_1, R_1 and V_1 in Figure 1.19), while lyomesophases formed in apolar solvents are termed *inverse* phases (I_2, H_2, R_2 and V_2 in Figure 1.19). The parameter *V/Al* can predict the type of aggregate that will be formed, and so the mesophase that will be formed. *V* is the volume of the hydrocarbon chains, *l* the length of these chains and *A* is the cross-sectional area of the hydrophilic head (Figure 1.18).[44]
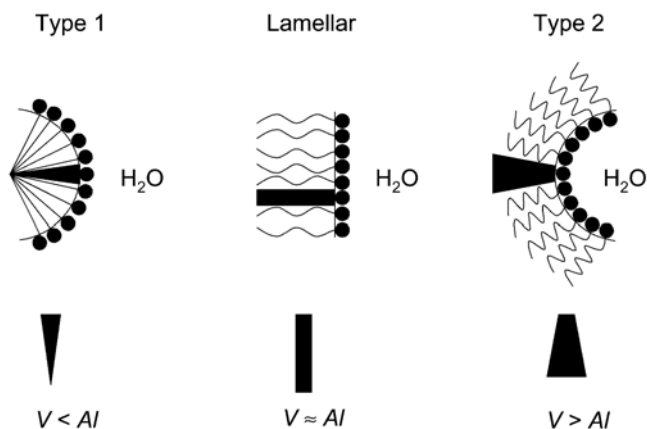
Figure 1.18: Molecular shape and aggregate morphology.[44]

23

Thus, the chemical incompatibility contained in the molecular structure leads to the association of molecules into micellar aggregates. At low surfactant concentrations, the micelles are roughly spherical and there is no aggregation of the micelles. Above the critical micelle concentration and above a boundary temperature, referred to as the *Krafft point* (temperature below which micelles are not soluble), the micelles interact and self-assemble into ordered arrays of supramolecular aggregates or lyotropic mesophases. The nature of the mesophase is strongly connected to the type of aggregation, and the curvature between the polar/apolar interface (Figure 1.19).
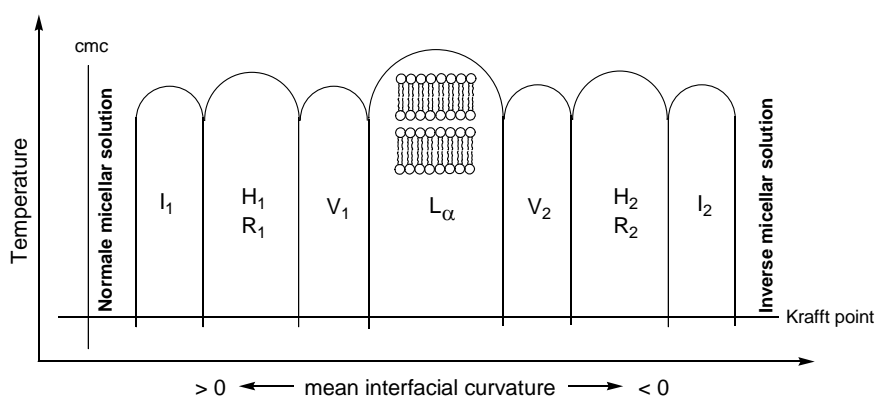
Figure 1.19: Representation of the lyotropic phase diagram of an amphiphilic compound. L_α represents the lamellar phase, H_1 and H_2 hexagonal columnar phases, R_1 and R_2 rectangular columnar phases, I_1 and I_2 micellar (discontinuous) cubic phases, and V_1 and V_2 bicontinuous cubic phases.

Disklike micelles will form discotic nematic (N_D) and lamellar (L_α) phases. Cylindrical micelles will organize into columnar phases (N_{Col}, H, R). The structure of the hexagonal columnar phase is shown in Figure 1.20.
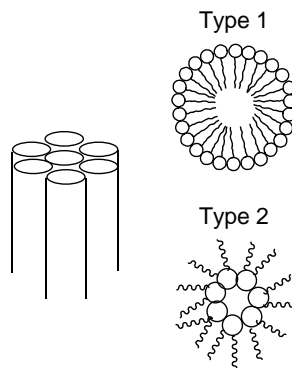
Type 1

Type 2

Figure 1.20: Schematic representation of the hexagonal columnar phase (left), top view of the columns type 1 and type 2 (right).

Spherical micelles will give rise to micellar cubic phases (I). Micellar cubic phases have symmetries associated with the cubic space groups like *Im*-3*m* and *Pm*-3*n* (Figure 1.21).

Im-3*m*   *Pm*-3*n*
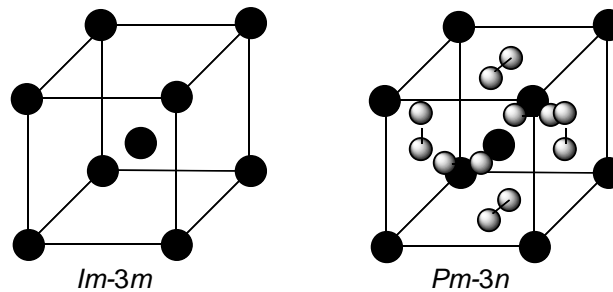
Figure 1.21: 3D cubic lattices of the Im-*3*m *and* Pm-*3*n *phases.*

The non-micellar bicontinuous cubic phases (V), located between the lamellar and hexagonal phases, are not directly formed from such basic molecular assemblies but are the result of a multiple step process and a passage through rather complicated intermediate structures. The *bicontinuous cubic* phases consist of a single continuous bilayer which

divides the space into two interwoven labyrinths (Figure 1.22). It is important to note that these cubic phases occupy narrow regions of stability, in comparison with the lamellar and hexagonal phases.
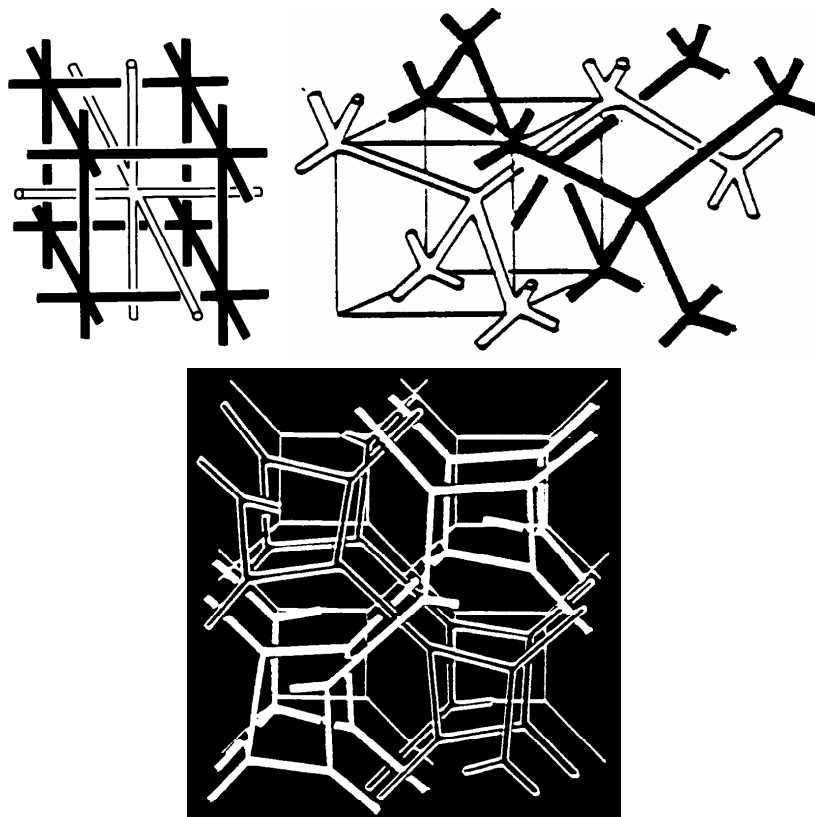
Figure 1.22: The two labyrinths of rods in the structures associated to the three most frequent cubic space groups in surfactant liquid crystals (left top: Im-*3*m*, right top:* Pn-*3*m*, bottom:* Ia-*3*d).[45]

Chromonic liquid crystals present an unusual example of lyotropic mesomorphism. These materials can be classified between the conventional lyotropic liquid crystals and the thermotropic liquid crystals. The molecules

have aromatic structures and are disk-like or plank-like, a general structure is shown in Figure 1.23.[46] In solution the molecules don't arrange into micelles but into columns, caused by face-to-face arrangement of the aromatic cores. Aggregation is observed at very low concentrations of solvent, there seems to be no threshold concentration like the critical micelle concentration in amphiphilic systems.[47-51]
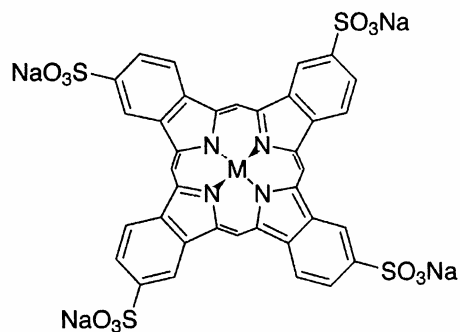
Figure 1.23: General structure of a chromonic liquid crystal.[52]

1.5 Mesophase characterization

Full characterization of the mesophase behavior is achieved using three techniques: hot-stage polarizing optical microscopy (POM), differential scanning calorimetry (DSC) and X-ray diffraction (XRD).

1.5.1 Polarizing optical microscopy

Polarizing optical microscopy is based on the fact that a mesophase is birefringent, which means that the ray of light is split into two rays when it passes through the mesophase depending on the polarization of the light. Two different refractive indices can be assigned to the mesophase. Figure 1.24 illustrates the experimental setup which is used to perform microscopy studies.

Figure 1.24: Picture of the experimental setup for hot-stage microscopy.

The microscope contains two polarizers. The first is localized between the light source and the hot-stage, the second is placed between the hot-stage and the observer. The polarizers can be rotated, but are typically placed in a crossed configuration, meaning that the polarization directions are perpendicular to another. In this way, only birefrigent materials, like liquid crystals, can form an image, due to their ability to change the polarization direction of the incident light. Isotropic materials, like isotropic molten samples, possess only one refractive index and cannot show an image.

In a typical microscopy experiment, a small amount of product is placed between two glass cover slips and these are positioned on the hot-stage. The sample is heated into the mesophase and when the light passes through, two refracted rays are formed, which interact with each other to give a characteristic interference pattern. This pattern is called a *texture* (or *defect texture*), and is different for each mesophase. The best-formed textures are obtained on cooling the sample from the isotropic liquid (*natural texture*). Some typical textures are shown below (Figure 1.25, Figure 1.26 and Figure 1.27).
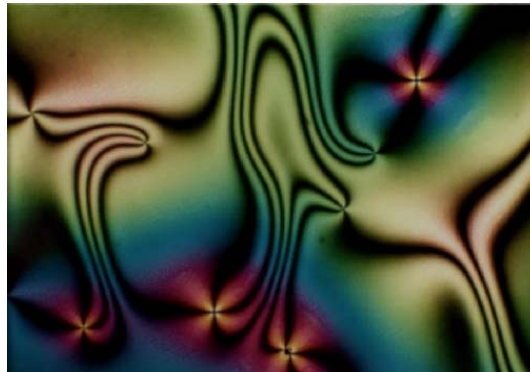
Figure 1.25: Schlieren texture of a nematic mesophase.[53]

29
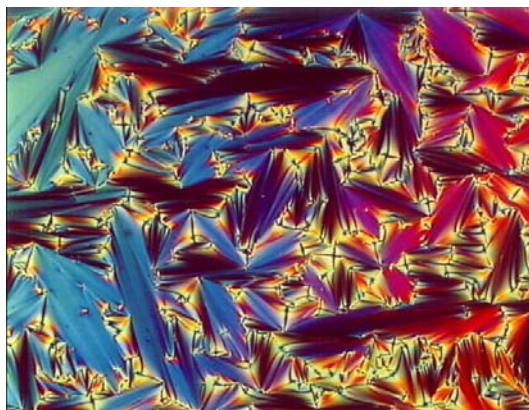
Figure 1.26: Fan-shaped texture of a smectic A mesophase.[54]
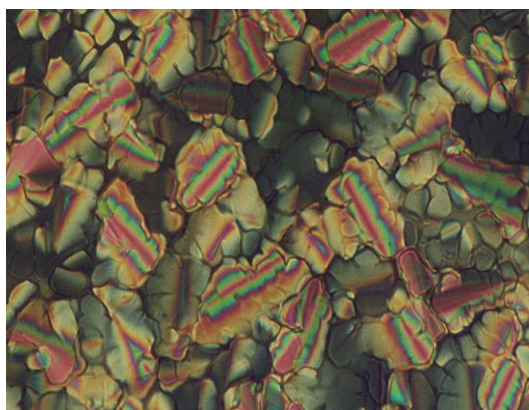
Figure 1.27:Texture of a hexagonal columnar mesophase.

1.5.2 Differential scanning calorimetry

All the phase transitions (solid-mesophase, mesophase-mesophase and mesophase-isotropic phase) are accompanied by an enthalpy change (and consequently by an entropy change $\Delta S = \Delta H/T$). The mesophase-mesophase transition can also be a second order transition, which results in a change of heat capacity (ΔC_p). The magnitude of the enthalpy change is related to the amount of order that is lost or gained during the transition. In a DSC experiment, the enthalpy change related to a phase transition is measured. Two types of DSC techniques exist: *power compensating* DSC and *heat flux* DSC. Heat flux DSC will be described, because only this technique was used for all the DSC experiments performed for this PhD study.
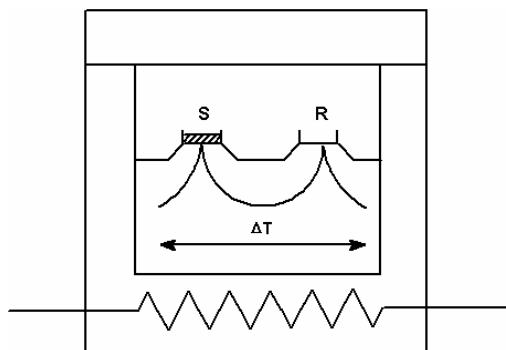
Figure 1.28: Heat flux DSC cell; S = sample, R = reference, ΔT = temperature difference .

As shown in Figure 1.28 a heat flux DSC uses one furnace to heat both the sample and reference. At the moment the sample undergoes a phase transition, it will have a temperature lag compared to the reference. Because the mass of the sample is known and the temperature lag is measured very accurately, it is possible to calculate the energy of the transition (the

enthalpy change). A typical DSC experiment of the liquid-crystalline para-nonyloxybenzoic acid (Cr · 93 · SmC · 111 · N · 141 · I) is shown in Figure 1.29. Not all the information gattered by DSC can be obtained by microscopy. Therefore, the DSC technique is complementary to optical microscopy and they should be used in combination. It's possible that a phase transition is accompanied with only a very small textural change, easily overlooked by the observer. On the other hand not all textural changes are an indication for a phase transition.
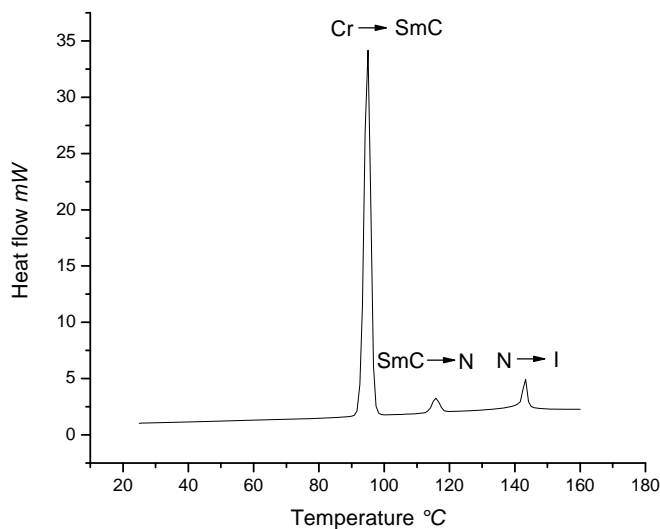
Figure 1.29: DSC curve of para-nonyloxybenzoic acid.

1.5.3 X-ray diffraction

The best method for the characterization of mesophases is X-ray diffraction. X-rays interact with the clouds of electrons, present in the mesophase and are scattered accordingly. The various scattered wavelets combine, undergoing constructive or destructive interference. The X-ray technique is based on Bragg's law, which relates the angle of incidence of the X-ray beam θ with the X-ray wavelength λ and the distance d between two planes:

$$\mathrm{n}\lambda = 2d\sin\theta \qquad\qquad\qquad (1.2)$$

A powder sample is placed in a glass capillary which can be heated. When the X-ray beam strikes the sample, diffraction will take place. The diffracted beams that interfere coherently result in a pattern, which is collected by a detector. The intensity I of the diffracted X-rays is measured as a function of the diffraction angle (2θ), leading to a diffraction pattern containing several diffraction peaks. The position of the diffraction peaks is related to the separation between layers of scattering atoms. The sharpness of the peaks is related to the extent to which these separations extend periodically over large distances. The intensity of diffraction peaks is related to the number of scattering atoms. Using this information (position, intensity and sharpness of diffraction peaks), the structure of the mesophase can be revealed.[42,55-58]

1.6 References

1. Reinitzer, F. *Monatsh. Chem.* **1888,** *9,* 421-441.

2. Lehmann, O. *Z. Phys. Chem.* **1889,** *4,* 462-472.

3. Gattermann, L. *Ber. Dtsch. Chem. Ges.* **1890,** *23,* 1218-1228.

4. Vorländer, D. *Z. Phys. Chem.* **1923,** *105,* 211-254.

5. Friedel, G. *Ann. Phys.* **1922,** *18,* 273-474.

6. Gray, G. W.; Harrison, K. J.; Nash, J. A. *Electron. Lett.* **1973,** *9,* 130-131.

7. Chandrasekhar, S.; Sadashiva, B. K.; Suresh, K. A. *Pramana* **1977,** *9,* 471-480.

8. Diele, S.; Goring, P. Thermotropic Cubic Phases. In *Handbook of Liquid Crystals;* Demus, D.; Goodby, J. W.; Gray, G. W.; Spiess, H.-W.; Vill, V., Eds.; Wiley-VCH: Weinheim, 1998; pp 887-900.

9. Malthête, J.; Nguyen, H. T.; Destrade, C. *Liq. Cryst.* **1993,** *13,* 171-187.

10. Nguyen, H. T.; Destrade, C.; Malthête, J. *Adv. Mater.* **1997,** *9,* 375-388.

11. Fazio, D.; Mongin, C.; Donnio, B.; Galerne, Y.; Guillon, D.; Bruce, D. W. *J. Mater. Chem.* **2001,** *11,* 2852-2863.

12. Guillon, D.; Heinrich, B.; Ribeiro, A. C.; Cruz, C.; Nguyen, H. T. *Mol. Cryst. Liq. Cryst.* **1998,** *317,* 51-64.

13. Rowe, K. E.; Bruce, D. W. *J. Mater. Chem.* **1998,** *8,* 331-341.

14. Smirnova, A. I.; Fazio, D.; Iglesias, E. F.; Hall, C. G.; Guillon, D.; Donnio, B.; Bruce, D. W. *Mol. Cryst. Liq. Cryst.* **2003,** *396,* 227-240.

15. Donnio, B.; Bruce, D. W. *J. Chem. Soc. , Dalton Trans.* **1997,** 2745-2755.

16. Dantlgraber, G.; Eremin, A.; Diele, S.; Hauser, A.; Kresse, H.; Pelzl, G.; Tschierske, C. *Angew. Chem. Int. Ed.* **2002,** *41,* 2408-2412.

17. Tschierske, C. *J. Mater. Chem.* **2001,** *11,* 2647-2671.

18. Tschierske, C. *Curr. Opin. Colloid Interface Sci.* **2002,** *7,* 69-80.

19. *Metallomesogens, Synthesis, Properties and Applications;* Serrano, J. L., Ed.; VCH: Weinheim, Germany, 1996.

20. Binnemans, K.; Görller-Walrand, C. *Chem. Rev.* **2002,** *102,* 2303-2345.

21. Donnio, B.; Guillon, D.; Deschenaux, R.; Bruce, D. W. Metallomesogens. In *Comprehensive Coordination Chemistry II;* McCleverty, J. A.; Meyer, T. J., Eds.; Elsevier: Oxford, United Kingdom, 2003; pp 357-627.

22. Piguet, C.; Bünzli, J. C. G.; Donnio, B.; Guillon, D. *Chem. Commun.* **2006,** 3755-3768.

23. Bruce, D. W. *Adv. Mater.* **1994,** *6,* 699-701.

24. Terazzi, E.; Suarez, S.; Torelli, S.; Nozary, H.; Imbert, D.; Mamula, O.; Rivera, J. P.; Guillet, E.; Benech, J. M.; Bernardinelli, G.; Scopelliti, R.; Donnio, B.; Guillon, D.; Bünzli, J. C. G.; Piguet, C. *Adv. Funct. Mater.* **2006,** *16,* 157-168.

25. Binnemans, K.; Galyametdinov, Y. G.; Collinson, S. R.; Bruce, D. W. *J. Mater. Chem.* **1998,** *8,* 1551-1553.

26. Binnemans, K.; Galyametdinov, Y. G.; Van Deun, R.; Bruce, D. W.; Collinson, S. R.; Polishchuk, A. P.; Bikchantaev, I.; Haase, W.; Prosvirin, A. V.; Tinchurina, L.; Litvinov, I.; Gubajdullin, A.; Rakhmatullin, A.; Uytterhoeven, K.; Van Meervelt, L. *J. Am. Chem. Soc.* **2000,** *122,* 4335-4344.

27. Galyametdinov, Y. G.; Athanassopoulou, M. A.; Griesar, K.; Kharitonova, O.; Bustamante, E. A. S.; Tinchurina, L.; Ovchinnikov, I. V.; Haase, W. *Chem. Mater.* **1996,** *8,* 922-926.

28. Galyametdinov, Y. G.; Haase, W.; Malykhina, L. V.; Prosvirin, A. V.; Bikchantaev, I.; Rakhmatullin, A.; Binnemans, K. *Chem. Eur. J.* **2001,** *7,* 99-105.

29. Nozary, H.; Torelli, S.; Guenee, L.; Terazzi, E.; Bernardinelli, G.; Donnio, B.; Guillon, D.; Piguet, C. *Inorg. Chem.* **2006,** *45,* 2989-3003.

30. Barbera, J.; Elduque, A.; Gimenez, R.; Lahoz, F. J.; Lopez, J. A.; Oro, L. A.; Serrano, J. L. *Inorg. Chem.* **1998,** *37,* 2960-2967.

31. Lattermann, G.; Schmidt, S.; Kleppinger, R.; Wendorff, J. H. *Adv. Mater.* **1992,** *4,* 30-33.

32. Neve, F.; Ghedini, M.; Demunno, G.; Levelut, A. M. *Chem. Mater.* **1995,** *7,* 688-693.

33. Schmidt, S.; Lattermann, G.; Kleppinger, R.; Wendorff, J. H. *Liq. Cryst.* **1994,** *16,* 693-702.

34. Binnemans, K. *Chem. Rev.* **2005,** *105,* 4148-4204.

35. Binnemans, K.; Van Deun, R.; Bruce, D. W.; Galyametdinov, Y. G. *Chem. Phys. Lett.* **1999,** *300,* 509-514.

36. Binnemans, K.; Sleven, J.; De Feyter, S.; De Schryver, F. C.; Donnio, B.; Guillon, D. *Chem. Mater.* **2003,** *15,* 3930-3938.

37. Terazzi, E.; Torelli, S.; Bernardinelli, G.; Rivera, J. P.; Benech, J. M.; Bourgogne, C.; Donnio, B.; Guillon, D.; Imbert, D.; Bünzli, J. C. G.; Pinto, A.; Jeannerat, D.; Piguet, C. *J. Am. Chem. Soc.* **2005,** *127,* 888-903.

38. Bruce, D. W. Metal-Containing Liquid Crystals. In *Inorganic Materials;* 2nd ed.; Bruce, D. W.; O' Hare, D., Eds.; Wiley: Chichester, United Kingdom, 1996; pp 429-522.

39. Donnio, B.; Bruce, D. W. *Struct. Bond.* **1999,** *95,* 193-247.

40. Giroud-Godquin, A. M.; Maitlis, P. M. *Angew. Chem. Int. Ed.* **1991,** *30,* 375-402.

41. Hudson, S. A.; Maitlis, P. M. *Chem. Rev.* **1993,** *93,* 861-885.

42. Morale, F.; Date, R. W.; Guillon, D.; Bruce, D. W.; Finn, R. L.; Wilson, C.; Blake, A. L.; Schroder, M. W.; Donnio, B. *Chem. Eur. J.* **2003,** *9,* 2484-2501.

43. Sleven, J.; Cardinaels, T.; Görller-Walrand, C.; Binnemans, K. *Arkivoc* **2003,** 68-82.

44. Donnio, B. *Curr. Opin. Colloid Interface Sci.* **2002,** *7,* 371-394.

45. Donnio, B. Mesomorphic metal complexes of polycatenar stilbazoles : a structure/property study. University of Sheffield (UK), 1996.

46. Kimura, M.; Muto, T.; Takimoto, H.; Wada, K.; Ohta, K.; Hanabusa, K.; Shirai, H.; Kobayashi, N. *Langmuir* **2000,** *16,* 2078-2082.

47. Lydon, J. *Curr. Opin. Colloid Interface Sci.* **1998,** *3,* 458-466.

48. Lydon, J. *Curr. Opin. Colloid Interface Sci.* **2004,** *8,* 480-490.

49. Horowitz, V. R.; Janowitz, L. A.; Modic, A. L.; Heiney, P. A.; Collings, P. J. *Phys. Rev. E* **2005,** *72*.

50. Nastishin, Y. A.; Liu, H.; Shiyanovskii, S. V.; Lavrentovich, O. D.; Kostko, A. F.; Anisimov, M. A. *Phys. Rev. E* **2004,** *70*.

51. Attwood, T. K.; Lydon, J. E.; Hall, C.; Tiddy, G. J. T. *Liq. Cryst.* **1990,** *7,* 657-668.

52. Bykova, V.; Usoltseva, N.; Ananjeva, G.; Semeikin, A.; Karmanova, T. *Mol. Cryst. Liq. Cryst.* **1995,** *265,* 651-657.

53. http://www.lci.kent.edu/polmicpic.html. 2007.

54. Van Deun, R. Liquid Crystals with Lanthanides. K.U.Leuven, 2001.

55. Bruce, D. W.; Donnio, B.; Hudson, S. A.; Levelut, A. M.; Megtert, S.; Petermann, D.; Veber, M. *J. Phys. II* **1995,** *5,* 289-302.

56. Donnio, B.; Heinrich, B.; Allouchi, H.; Kain, J.; Diele, S.; Guillon, D.; Bruce, D. W. *J. Am. Chem. Soc.* **2004,** *126,* 15258-15268.

57. Guillon, D. *Struct. Bond.* **1999,** *95,* 41-82.

58. Cardinaels, T. Liquid-crystalline complexes of transition metals and rare earths with substituted 1,10-phenanthroline ligands. K.U.Leuven, 2006.

Chapter 2: Literature overview

2.1 Liquid crystals based on 1,10-phenanthroline

It is known that 1,10-phenanthrolines (Figure 2.1) are able to form complexes with a variety of metal ions in different oxidation states. These complexes exhibit interesting luminescent properties when they are properly designed.[1-6] Because of the fixed conformation of 1,10-phenanthroline, it is set up for N,N´-coordination. 1,10-Phenanthroline has a permanent lateral dipole moment of 4.1 D.[7]
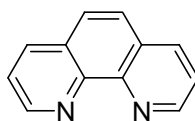
Figure 2.1: Structure of 1,10-phenanthroline.

Bousquet and Bruce reported on the first 1,10-phenanthroline-containing liquid crystals.[8] These were linear 3,8-disubstituted 1,10-phenanthrolines (Figure 2.2) with an alkylated phenyl group coupled to the 1,10-phenanthroline via a single bond or a triple C-C bond.
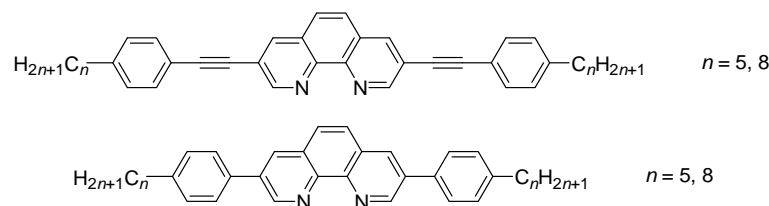
Figure 2.2: 3,8-Disubstituted 1,10-phenanthrolines reported by Bousquet and Bruce.[8]

The 3,8-disubstituted 1,10-phenanthrolines melted above 100 °C and cleared at *ca*. 300 °C or decomposed before clearing. They showed nematic and smectic phases. By introducing methyl groups in the 2- and 9-positions (Figure 2.3), the clearing and decomposition temperatures decreased and these compounds exhibited a nematic phase.
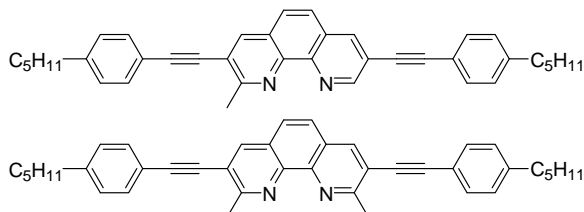
Figure 2.3: 3,8-Disubstituted 1,10-phenanthrolines with additional methyl groups in the 2- and 9-positions.[8]

Also 3-monosubstituted 1,10-phenanthrolines were reported by Bousquet and Bruce, but these did not show liquid-crystalline behavior (Figure 2.4).[8]
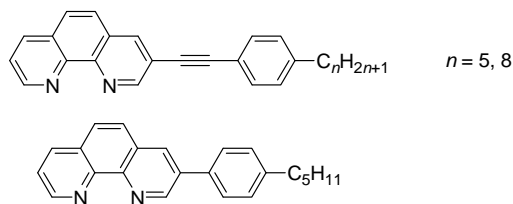
Figure 2.4: 3-Monosubstituted 1,10-phenanthroline reported by Bousquet and Bruce.[8]

Related tetracatenar ligands of 1,10-phenanthroline and corresponding rhenium(I) complexes were made by Bruce and co-workers (Figure 2.5).[9,10] In the case of the short chain lengths, the ligands showed nematic and smectic C phases. For longer chain lengths, the ligands showed a hexagonal columnar phase. The rhenium(I) complexes with shorter chain lengths were not liquid-crystalline. The longer-chain homologues showed hexagonal

columnar phases, but with higher clearing points and a wider mesophase range than the corresponding ligands.
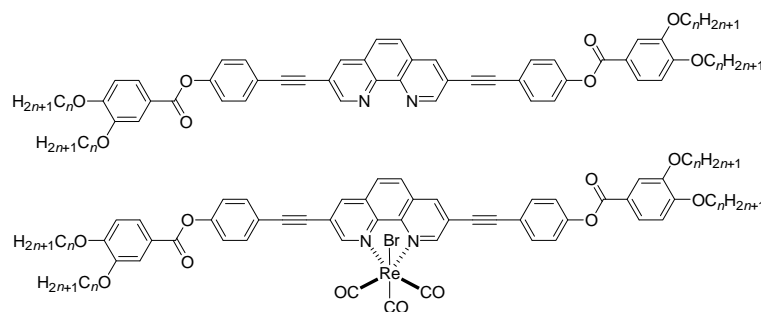
Figure 2.5: Tetracatenar 1,10-phenanthrolines and corresponding rhenium(I) complexes reported by Bruce and co-workers.[9,10]

Mesomorphic copper(I) complexes derived from non-symmetrical 1,10-phenanthroline were reported by Ziessel and co-workers.[11] The structure of the ligands is shown in Figure 2.6. The ligands were mesomorphic only at longer chain lengths ($n = 12, 16$) and exhibited an unstable ($n = 12$) and a stable cubic phase ($n = 16$).
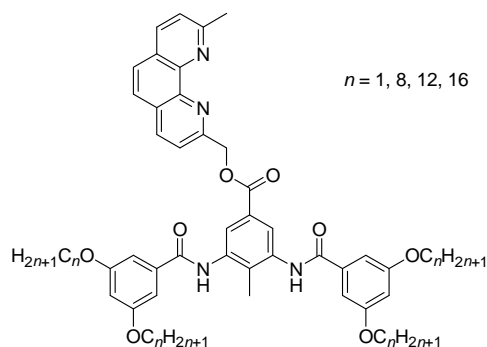
Figure 2.6: Structure of the non-symmetrical 1,10-phenanthroline reported by Ziessel and co-workers.[11]

The corresponding copper(I) complexes (Figure 2.7) were only liquid-crystalline at longer chain lengths (n = 12, 16) and have a non-planar geometry. These copper(I) complexes exhibited an oblique columnar phase (Col$_o$). The driving force for the organization into liquid-crystalline phases is hydrogen bonding.
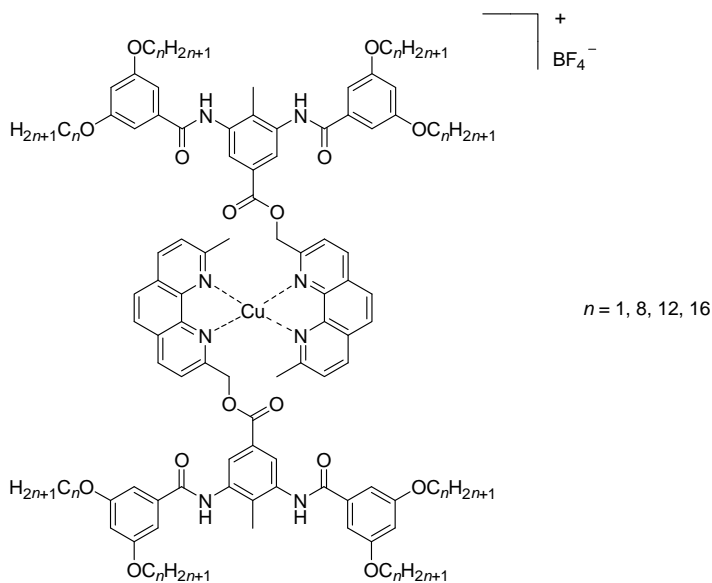
Figure 2.7: Structure of the copper(I) complexes of non-symmetrical 1,10-phenanthrolines reported by Ziessel and co-workers.[11]

Cardinaels and co-workers reported on imidazo*[4,5-f]*-1,10-phenanthrolines containing mesogenic groups (4-cyanobiphenyl).[12] The ligands are shown in Figure 2.8. Ligands L_I and L_{II} formed a nematic phase, while ligand L_{III} formed a lamello-columnar phase.
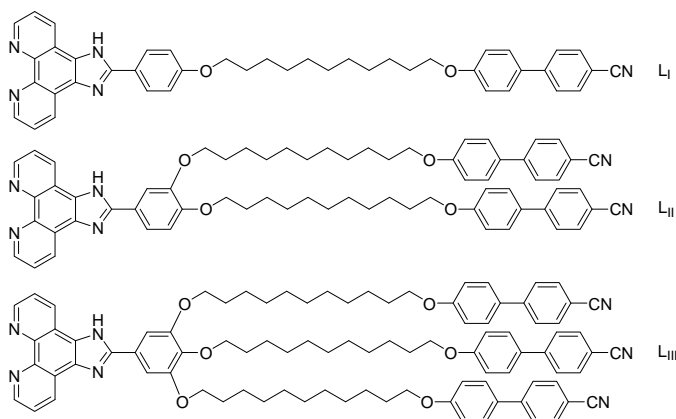
Figure 2.8: Structure of the imidazo[4,5-f]-1,10-phenanthroline ligands reported by Cardinaels and co-workers.[12]

The rhenium(I) complex of ligand L_I exhibited only a monotropic nematic phase, while the rhenium(I) complex of ligand L_{II} showed a nematic phase and a monotropic smectic A phase. The rhenium(I) complex of ligand L_{III} showed a rectangular columnar phase.

The corresponding lanthanide(III) complexes (Ln = Y, La, Nd, Sm, Eu, Er and Yb) formed a nematic phase.

The structure of the rhenium(I) and lanthanide(III) complexes of ligand L_{II} are shown in Figure 2.9.
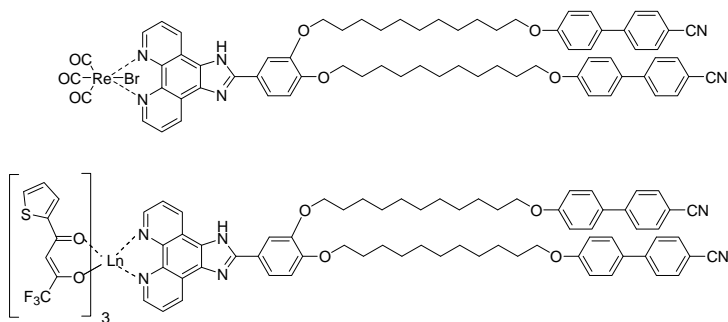
Figure 2.9: Structure of rhenium(I) and lanthanide(III) (Ln = Y, La, Nd, Sm, Eu, Er and Yb) complexes of ligand L$_{II}$ reported by Cardinaels et al.[12]

Cardinaels et al. reported on a propeller-like uranyl metallomesogen (Figure 2.10).[13] The uranyl complex of the imidazo*[4,5-f]*-1,10-phenanthroline ligand bearing three long alkyl chains showed a hexagonal columnar phase.
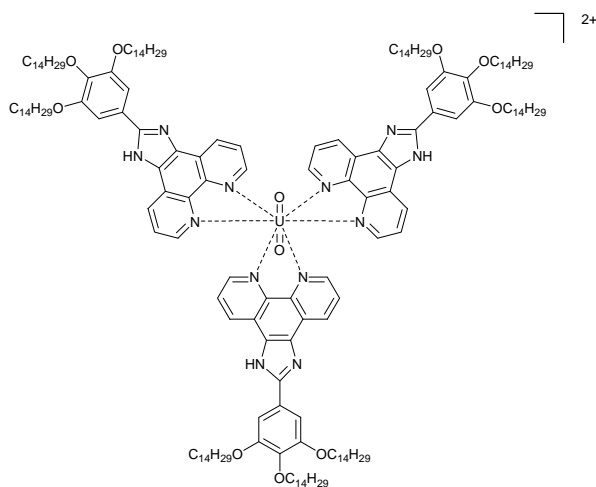
Figure 2.10: Structure of the uranyl complex reported by Cardinaels et al.[13]

2.2 Thermotropic cubic phases of metallomesogens

The discussion of the thermotropic cubic phases begins in 1957 with Gray et al.. They reported on the mesophase behavior of 4'-*n*-alkoxy-3'-nitro-biphenyl-4-carboxylic acids for which $n = 16$ and 18 (Figure 2.11).[14]
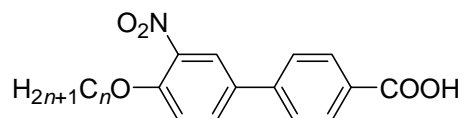
*Figure 2.11: Structure of the 4'*n-*alkoxy-3'-nitro--biphenyl-4-carboxylic acids.*[14]

They wrote: "For the hexadecyl and octadecyl ether the changes occurring on heating are solid - smectic I – smectic II – smectic III – isotropic, … . Smectic III has a marked tendency to homeotropy." A new analysis of these compounds by Demus et al. in 1968 confirmed the observed results.[15] By miscibility studies, they proved the existence of a new type of liquid-crystalline phase. In 1971, Pelzl and Sackmann measured the refractive index of these samples and in 1972 Diele et al. performed X-ray studies which proved the existence of a cubic phase.[16,17] A structural model based on micelles was assumed for reasons of simplicity. During the same period, different groups were investigating lyotropic liquid-crystalline phases, including cubic mesophases. Some of these compounds also exhibited a thermotropic cubic mesophase, as reported by Spegt and Skoulios.[18] Luzzati and Spegt reported on their research of strontium(II) alkanoates (Figure 2.12) which exhibited a thermotropic cubic mesophase.[19]
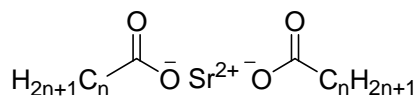
Figure 2.12: Structure of the strontium(II) alkanoates.[18,19]

45

Based on the detailed small-angle X-ray measurements, they suggested the cubic space group *Ia*-3*d* and developed a complicated structural model. The model consisted of a network of rods linked three-by-three and interwoven, but the two networks are not connected (representation of the *Ia*-3*d* structure is given in Chapter 1, Figure 1.22).

The repeated small-angle X-ray measurements of the 4'*n*-octadecyloxy-3'-nitro-biphenyl-4-carboxylic acid by Tardieu and Billard gave six reflections instead of four.[20] This allowed a more precise interpretation and resulted in a body-centered cubic phase, which is compatible with the space group *Ia*-3*d*. Miscibility studies pointed out that the phase was not miscible with smectic A, smectic B or smectic C and the new phase was designated smectic D.[15] Later obtained results proved that the phase could not belong to the group of smectic phases. Therefore Demus et al. and later Etherington et al. and others stated that it was wrong to use the term smectic.[21-23] The cubic phase was thought to be a new group of thermotropic liquid-crystalline phases different than the smectic and discotic ones.[21] Therefore the abbreviation Cub was used instead of smectic D.

There is no typical class of compounds that exhibit cubic phases. Nevertheless, polycatenar systems can show a cubic phase between the smectic and the columnar phase (see chapter 1) and also dendritic molecules can form a cubic phase. Figure 2.13 shows the retrostructural analysis of a cubic phase formed by *dendrimers*. The top line shows the essential structural building block for dendrimers of different generations.
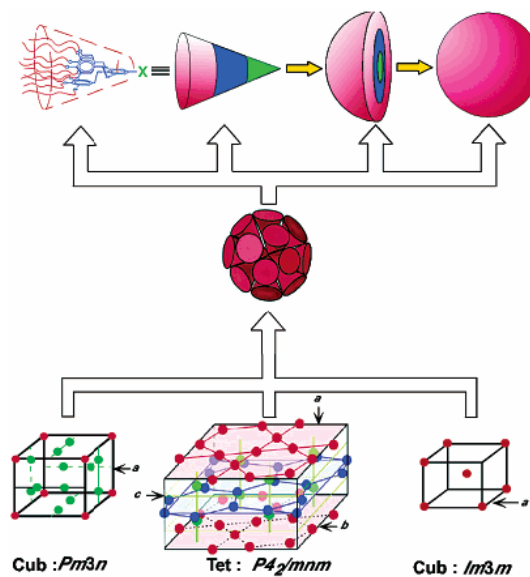
Figure 2.13: Retrostructural analysis of cubic phases by dendritic molecules.[24]

Several reviews on thermotropic cubic phases have been published.[25-28] However, metallomesogens displaying a thermotropic cubic phase are rare while for lyotropic systems, a cubic phase can exist between any two types of phases. The review on metallomesogens by Donnio et al. includes thermotropic cubic metallomesogens reported until 2003.[29] Thermotropic cubic metallomesogens reported after 2003 are described next.

In 2003, Dukeson et al. reported on a rubidium(I) complex of the dendritic ligand shown in Figure 2.14.[30] This complex exhibited a micellar cubic *Pm-3n* mesophase.

47
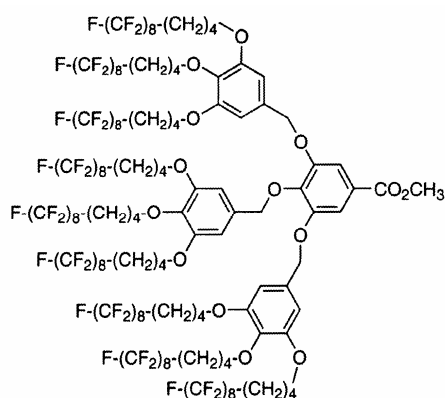
Figure 2.14: Structure of the dendritic ligand.[30]

In 2003, Terazzi et al. reported on hexacatenar tridentate ligands.[31] The corresponding europium(III) and the dysprosium(III) nitrate complexes of ligand L_{T1} (Figure 2.15) exhibited a cubic phase.

In 2005, Terazzi et al. reported on the lanthanide(III) nitrate complexes of ligand L_{T1} and ligand L_{T2} (Figure 2.15).[32] The lanthanide(III) complexes (Ln = Pr, Nd, Sm, Eu, Gd, Tb, Dy and Ho) of ligand L_{T1} and ligand L_{T2} showed a cubic phase, only the erbium(III) complex of ligand L_{T2} exhibited a cubic phase.

Ligand L_{T1} : R = C_2H_5, Y = H, X =

Ligand L_{T2} : R = C_2H_5, X = H, Y =
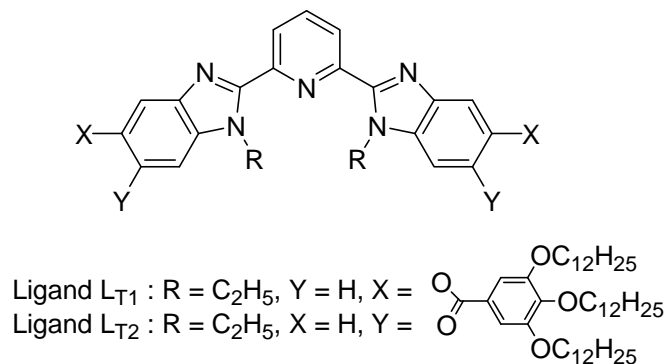
Figure 2.15: Structure of the hexacatenar tridentate ligand.[31,32]

48

In 2004, Neve and Impéror-Clerc reported on a thermotropic cubic phase formed by *N*-pentadecylpyridinium tetrahalocuprates.[33] The chloride complex exhibited a cubic phase between 77 °C and 105 °C, while the bromide complex showed a cubic phase between 64 °C and 81 °C.
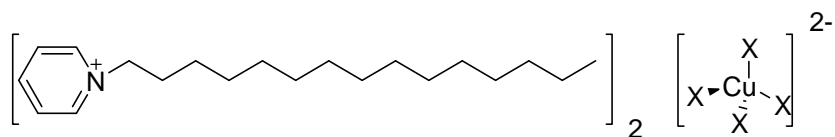
Figure 2.16: Structure of the N-*pentadecylpyridinium tetrahalocuprates (X = Br or Cl).[33]*

In 2005, Massiot et al. reported on metallomesogens which display bicontinuous cubic phases.[34] The ferrocene-containing liquid crystals (**1b**, **1c**, **2a**, **2b** and **2c** in Figure 2.17) exhibited a *Ia-3d* cubic phase.

1a (*m* = 6, *n* = 8) **2a** (*m* = 10, *n* = 8)
1b (*m* = 6, *n* = 10) **2b** (*m* = 10, *n* = 10)
1c (*m* = 6, *n* = 12) **2c** (*m* = 10, *n* = 12)
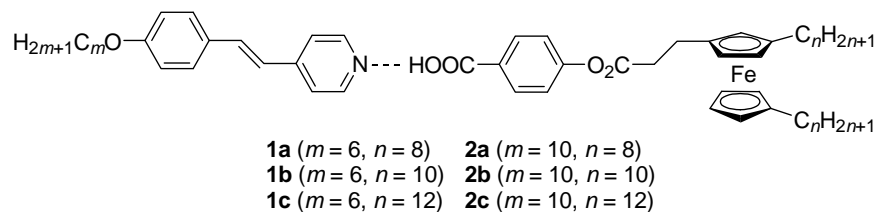
Figure 2.17: Structures of the ferrocene-containing liquid crystals.[34]

2.3 Lyotropic metallomesogens

In 2002, Donnio published a review on lyotropic mettallomesogens.[35] This review covers the most important research in this field up to 2002. The compounds and their mesophase behavior related to our research are described below.

In 1993, Bruce et al. reported on cationic tris-2,2'-(bipyridine)ruthenium(II) surfactants (Figure 2.18).[36] These compounds exhibited a lyotropic mesophase in water between room temperature and 100 °C. Trihydrated chloride salts and anhydrous hexafluorophosphate salts were studied. All the dichloride salts of the monoalkylated bipyridine ligands ($m = 1$, $n = 12$, 19, 21, and 31) exhibited a cubic phase. An additional hexagonal H_1 phase was observed for the complex with the longest chain. No mesomorphism was observed for the hexafluorophosphate salts. The two-chain derivative of the chloride salt with $m = 19$, $n = 19$ showed a H_1 hexagonal phase only.
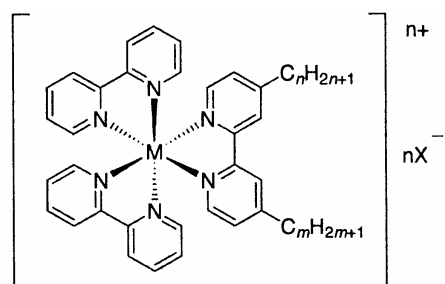
Figure 2.18: Structure of the cationic tris-2,2'-(bipyridine)metal surfactant.[36]

In 1995, Holbrey et al. reported on salts of several bis(terpyridine) complexes.[37] The complexes of ruthenium(II) and rhodium(II) with the general formula ($[M(terpy)(L^n)]^{x+}[X^-]_x$) (M = Ru ($x = 2$), Rh ($x = 3$); $n = 19$, 31; X = Cl, PF_6) were prepared (Figure 2.19). The $[M(terpy)(L^{19})][Cl]_x$

complex showed a cubic phase. The longer chain homologue ($n = 31$) did not dissolve in water at room temperature and only showed a mesophase above 70 °C. In ethylene glycol, the short-chain complex did not show a mesophase, while the long-chain complex showed a cubic mesophase between 96 °C and 150 °C.
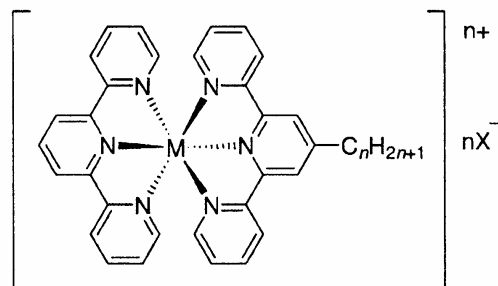
Figure 2.19: Structure of the bis(terpyridine) complexes.[37]

In 2000, Draeger et al. reported on an amphiphilic bis(bipyridine)-dipyrilmethylene distearyl ester ruthenium(II) complex (Figure 2.20).[38] The hexafluorophosphate and perchlorate salts were prepared. The hexafluorophosphate salt showed a lamellar mesophase in water.
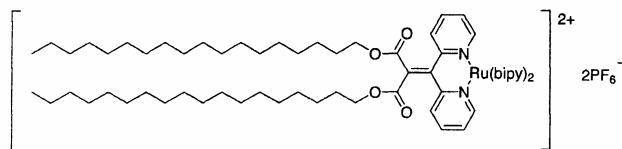
Figure 2.20: Structure of the bis(bipyridine)-dipyrilmethylene distearyl ester ruthenium(II) complex.[38]

In 2002, Yam et al. reported on mixed phenanthroline-bipyridine ruthenium(II) complexes (Figure 2.21).[39] The chloride salts exhibited a hexagonal H_1 phase in water.
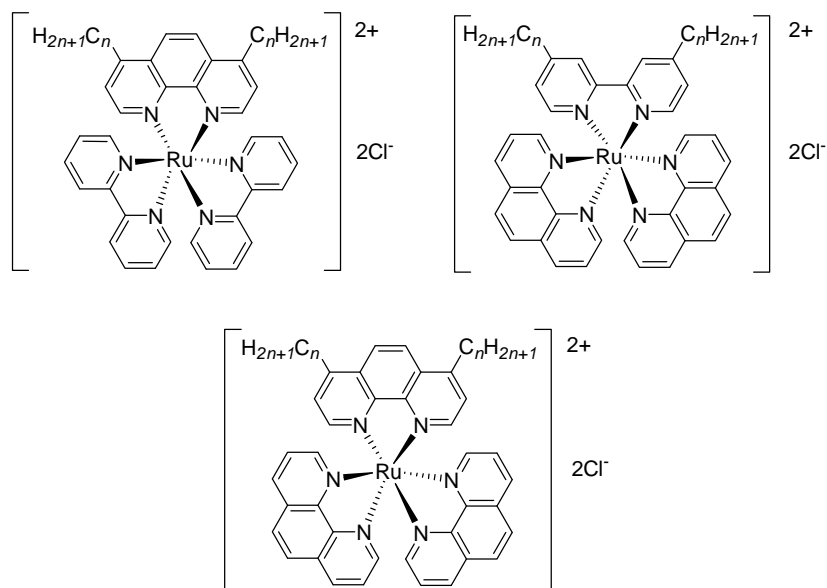
Figure 2.21: Structure of the mixed phenanthroline-bipyridine ruthenium(II) complexes.[39]

In 2002, Smirnova and Bruce reported on the lyotropic behavior of tetracatenar silver(I) complexes (Figure 2.22).[40] Four classes of solvents were used: linear alcohols, linear alkanes, cyclic hydrocarbons and small, polar, aprotic solvents. The complexes exhibited several lyomesophases depending on the temperature and surfactant concentration lamellar, cubic, hexagonal and tetragonal phases.

a: $m = 10$, $n = 4$; b: $m = 14$, $n = 4$; c: $m = 14$; $n = 6$

Figure 2.22: Structure of the tetracatenar silver(I) complexes.[40]

In 2006, Smirnova and Bruce reported on the mesomorphism of analogous polycatenar silver(I) complexes.[41] 3,5-, 2,4-, 3,4,5- and 2,3,4- alkoxystilbazole complexes of silver(I) were dissolved in several organic solvents and showed a rich lyomesomorphism.

2.4 References

1. Sammes, P. G.; Yahioglu, G. *Chem. Soc. Rev.* **1994,** *23,* 327-334.

2. Hiort, C.; Lincoln, P.; Norden, B. *J. Am. Chem. Soc.* **1993,** *115,* 3448-3454.

3. Hartshorn, R. M.; Barton, J. K. *J. Am. Chem. Soc.* **1992,** *114,* 5919-5925.

4. Binnemans, K.; Lenaerts, P.; Driesen, K.; Görller-Walrand, C. *J. Mater. Chem.* **2004,** *14,* 191-195.

5. Bellusci, A.; Barberio, G.; Crispini, A.; Ghedini, M.; La Deda, M.; Pucci, D. *Inorg. Chem.* **2005,** *44,* 1818-1825.

6. Bunzli, J. C. G.; Moret, E.; Foiret, V.; Schenk, K. J.; Wang, M. Z.; Jin, L. P. *J. Alloy. Compd.* **1994,** *207,* 107-111.

7. Fielding, P. E.; Le Fevre, R. J. W. *J. Chem. Soc.* **1951,** 1811.

8. Bousquet, S. J. P.; Bruce, D. W. *J. Mater. Chem.* **2001,** *11,* 1769-1771.

9. Date, R. W.; Iglesias, E. F.; Rowe, K. E.; Elliott, J. M.; Bruce, D. W. *Dalton Trans.* **2003,** 1914-1931.

10. Smirnova, A. I.; Fazio, D.; Iglesias, E. F.; Hall, C. G.; Guillon, D.; Donnio, B.; Bruce, D. W. *Mol. Cryst. Liq. Cryst.* **2003,** *396,* 227-240.

11. Ziessel, R.; Pickaert, G.; Camerel, F.; Donnio, B.; Guillon, D.; Cesario, M.; Prange, T. *J. Am. Chem. Soc.* **2004,** *126,* 12403-12413.

12. Cardinaels, T.; Driesen, K.; Parac-Vogt, T. N.; Heinrich, B.; Bourgogne, C.; Guillon, D.; Donnio, B.; Binnemans, K. *Chem. Mater.* **2005,** *17,* 6589-6598.

13. Cardinaels, T.; Ramaekers, J.; Guillon, D.; Donnio, B.; Binnemans, K. *J. Am. Chem. Soc.* **2005,** *127,* 17602-17603.

14. Gray, G. W.; Jones, B.; Marson, F. *J. Chem. Soc.* **1957,** 393-&.

15. Demus, D.; Kunicke, G.; Neelsen, J.; Sackmann, H. *Z. Naturforsch.* **1968,** *A 23,* 84-90.

16. Pelzl, G.; Sackmann, H. *Symp. Chem. Soc. Faraday* **1971,** *5,* 68-88.

17. Diele, S.; Sackmann, H.; Brand, P. *Mol. Cryst. Liq. Cryst.* **1972,** *17,* 163-169.

18. Spegt, P. A.; Skoulios, A. E. *Acta Cryst.* **1966,** *21,* 892-&.

19. Luzzati, V.; Spegt, P. A. *Nature* **1967,** *215,* 701-&.

20. Tardieu A.; Billard J. *J. Phys. Colloq. France* **1976,** *37,* C3-79-C3-81.

21. Demus, D.; Gloza, A.; Hartung, H.; Hauser, A.; Rapthel, I.; Wiegeleben, A. *Cryst. Res. Technol.* **1981,** *16,* 1445-1451.

22. Demus, D.; Diele, S.; Grande, S.; Sackmann, H. *Adv. Liq. Cryst.* **1983,** *6,* 1-107.

23. Etherington, G.; Leadbetter, A. J.; Wang, X. J.; Gray, G. W.; Tajbakhsh, A. *Liq. Cryst.* **1986,** *1,* 209-214.

24. Percec, V.; Peterca, M.; Sienkowska, M. J.; Ilies, M. A.; Aqad, E.; Smidrkal, J.; Heiney, P. A. *J. Am. Chem. Soc.* **2006,** *128,* 3324-3334.

25. Diele, S.; Goring, P. Thermotropic Cubic Phases. In *Handbook of Liquid Crystals;* Demus, D.; Goodby, J. W.; Gray, G. W.; Spiess, H.-W.; Vill, V., Eds.; Wiley-VCH: Weinheim, 1998; pp 887-900.

26. Diele, S. *Curr. Opin. Colloid Interface Sci.* **2002,** *7,* 333-342.

27. Imperor-Clerc, M. *Curr. Opin. Colloid Interface Sci.* **2005,** *9,* 370-376.

28. Kutsumizu, S. *Curr. Opin. Solid State Mater. Sci.* **2002,** *6,* 537-543.

29. Donnio, B.; Guillon, D.; Deschenaux, R.; Bruce, D. W. Metallomesogens. In *Comprehensive Coordination Chemistry II;* McCleverty, J. A.; Meyer, T. J., Eds.; Elsevier: Oxford, United Kingdom, 2003; pp 357-627.

30. Dukeson, D. R.; Ungar, G.; Balagurusamy, V. S. K.; Percec, V.; Johansson, G. A.; Glodde, M. *J. Am. Chem. Soc.* **2003,** *125,* 15974-15980.

31. Terazzi, E.; Benech, J. M.; Rivera, J. P.; Bernardinelli, G.; Donnio, B.; Guillon, D.; Piguet, C. *Dalton Trans.* **2003,** 769-772.

32. Terazzi, E.; Torelli, S.; Bernardinelli, G.; Rivera, J. P.; Benech, J. M.; Bourgogne, C.; Donnio, B.; Guillon, D.; Imbert, D.; Bünzli, J. C. G.; Pinto, A.; Jeannerat, D.; Piguet, C. *J. Am. Chem. Soc.* **2005,** *127,* 888-903.

33. Neve, F.; Imperor-Clerc, M. *Liq. Cryst.* **2004,** *31,* 907-912.

34. Massiot, P.; Imperor-Clerc, M.; Veber, M.; Deschenaux, R. *Chem. Mater.* **2005,** *17,* 1946-1951.

35. Donnio, B. *Curr. Opin. Colloid Interface Sci.* **2002,** *7,* 371-394.

36. Bruce, D. W.; Holbrey, J. D.; Tajbakhsh, A. R.; Tiddy, G. J. T. *J. Mater. Chem.* **1993,** *3,* 905-906.

37. Holbrey, J. D.; Tiddy, G. J. T.; Bruce, D. W. *J. Chem. Soc. , Dalton Trans.* **1995,** 1769-1774.

38. Draeger, C.; Bottcher, C.; Messerschmidt, C.; Schulz, A.; Ruhlmann, L.; Siggel, U.; Hammarstrom, L.; Berglund-Baudin, H.; Fuhrhop, J. H. *Langmuir* **2000,** *16,* 2068-2077.

39. Yam, V. W. W.; Li, B.; Zhu, N. Y. *Adv. Mater.* **2002,** *14,* 719-722.

40. Smirnova, A. I.; Bruce, D. W. *Chem. Commun.* **2002,** 176-177.

41. Smirnova, A. I.; Bruce, D. W. *J. Mater. Chem.* **2006,** *16,* 4299-4306.

Chapter 3: Thermotropic cubic lanthanide(III) complexes of imidazo-phenanthrolines

3.1 Introduction

It is known that 1,10-phenanthrolines are able to form complexes with a variety of metal ions.[1] However, there are only very few examples of metallomesogens with 1,10-derivatives as ligands,[2-5] and also the number of mesomorphic metal-free 1,10-phenanthrolines is limited.[3,6] The development of liquid-crystalline 1,10-phenanthrolines is hampered by synthetic difficulties. These are mainly solubility problems and the formation of unwanted side-products. We explored a published approach to functionalize 1,10-phenanthrolines, based on 2-arylimidazo*[4,5-f]*-1,10-phenanthroline heterocycles.[3,4,7] 2-Arylimidazo*[4,5-f]*-1,10-phenanthroline can easily be prepared in one step and the possibilities to vary the substitution pattern directly at the precursory benzaldehyde stage provide an easy access to a rich variety of building blocks. These ligands have been used in the past for complex formation with ruthenium(II)[8] and as a coligand in luminescent lanthanide(III) complexes. Recently Cardinaels reported on the influence of the transition metal ion and complex geometry, the substitution pattern, and alkoxy chain length on the mesomorphic properties of imidazo*[4,5-f]*-1,10-phenanthroline-based derivatives.[9] The structure and thermal behavior of these compounds is different from that of the related imidazo*[4,5-f]*-1,10-phenanthrolines bearing 4-cyanobiphenyl groups connected via a long alkyl spacer on which Cardinaels et al. reported previously.[3]

In this chapter, we discuss the influence of the lanthanide ion on the mesomorphic properties of the imidazo*[4,5-f]*-1,10-phenanthroline, 1:2 metal-to-ligand ratio, trivalent lanthanide complex. The complexes of the

ligands L_I, L_{II}, L_{III}, L_{IV}, L_V, L_{VI}, L_{VII}, L_{VIII} and L_{IX} with lanthanum(III) were prepared in order to examine the influence of the substitution pattern and alkoxy chain length on the thermal behavior of the metal complexes. Complexes of ligand L_{IX} with lanthanum(III), praseodymium(III), neodymium(III), samarium(III), europium(III), gadolinium(III), terbium(III), dysprosium(III) and holmium(III) were synthesized in order to study the influence of the lanthanide contraction on the thermal behavior of the metal complexes ($[LnCl_3(L_{IX})_2(H_2O)]$, Ln = La, Pr, Nd, Sm, Eu, Gd, Tb, Dy, Ho). The lanthanide contraction is the gradual decrease of the ionic radius of the trivalent lanthanide ion going along the lanthanide series.

3.2 Synthesis and characterization

3.2.1 Synthesis and characterization of the ligands

The 2-arylimidazo*[4,5-f]*-1,10-phenanthrolines were prepared by a condensation reaction between 1,10-phenanthroline-5,6-dione and an appropriate polyalkoxy benzaldehyde in the presence of ammonium acetate and glacial acetic acid. The synthetic route is similar to the method of Steck and Day for the preparation of 2-substituted phenanthrimidazoles.[10] 1,10-Phenanthroline is oxidized to 1,10-phenanthroline-5,6-dione according to a method described by Hiort et al.[8] Structure variations include the choice of different chain substitution patterns for the benzaldehyde as well as the variation of the alkoxy chain length. 4-Hydroxybenzaldehyde, 3,4-dihydroxybenzaldehyde, 3,5-dihydroxy-benzaldehyde, 2,3,4-trihydroxybenzaldehyde, 2,4,5-trihydroxybenzaldehyde and 3,4,5-trihydroxybenzaldehyde were used as starting products. They were all prepared as their tetradecyloxy polyether homologues (**L$_{IV}$, L$_{VI}$, L$_{VII}$, L$_{VIII}$, L$_{IX}$**) or as hexadecyloxy ether ones (**L$_I$**). The 3,4-dialkoxybenzaldehyde series was prepared with various chain lengths (OC_6H_{13}, $OC_{10}H_{21}$, $OC_{14}H_{29}$, $OC_{18}H_{37}$, **L$_{II}$, L$_{III}$, L$_{IV}$,** and **L$_V$**, respectively). The synthesis of the ligands is outlined in Scheme 3.1. An overview of the different ligands is given in Figure 3.1. All the imidazo*[4,5-f]*-1,10-phenanthrolines were characterized by CHN analysis, IR spectroscopy, ^{1}H and ^{13}C NMR spectroscopy and by mass spectrometry.
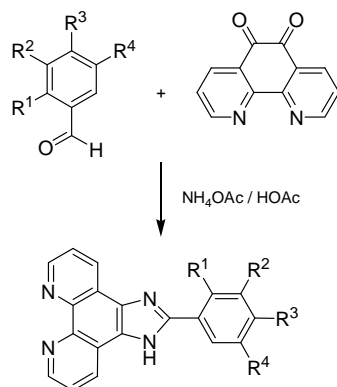
Scheme 3.1: Synthesis of the imidazo[4,5-f]*-1,10-phenanthroline ligands.*

The imidazo*[4,5-f]*-1,10-phenanthrolines containing aliphatic chains are soluble in diethyl ether, hexane and warm ethanol, besides to dichloromethane, chloroform, tetrahydrofuran and toluene.
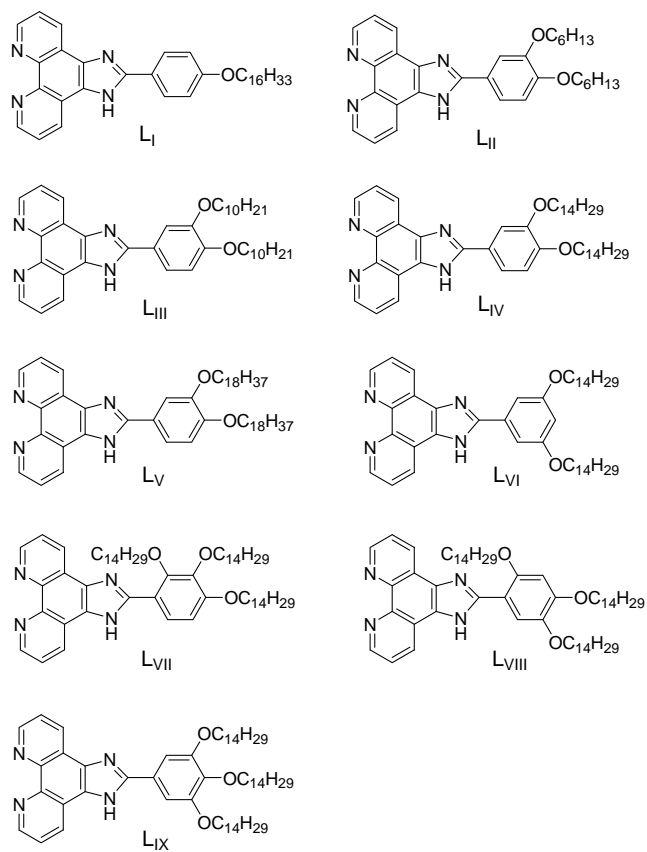
Figure 3.1: Overview of the imidazo[4,5-f]*-1,10-phenanthroline ligands.*

3.2.2 Synthesis and characterization of the lanthanide(III) complexes

The lanthanide(III) complexes were prepared by reaction between the corresponding ligand and $LnCl_3 \cdot xH_2O$ (2:1 molar ratio) (Ln = La, Pr, Nd, Sm, Eu, Gd, Tb, Dy, Ho) in ethanol, shown in Figure 3.2.
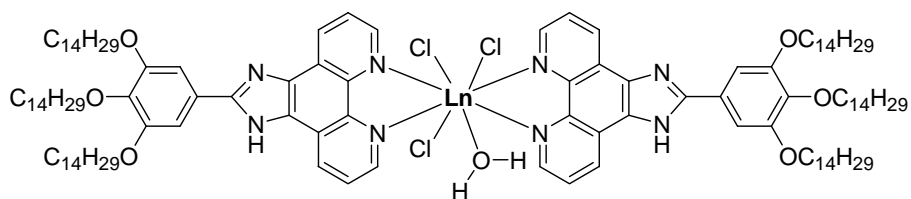
Figure 3.2: Lanthanide(III) chloride complex.

All the lanthanide complexes were characterized by CHN analysis and by mass spectrometry. All attempts to grow single crystals for the complexes failed. Actually, very few examples of crystal structures of imidazo*[4,5-f]*-1,10-phenanthrolines have been published. For these lanthanide(III) complexes, the reported structure with the closest similarity is that of $[LaCl_3(phen)_2(H_2O)] \cdot MeOH$.[11] In this compound, the lanthanum(III) ion is coordinated to three chloride ions, one water molecule and two 1,10-phenanthroline ligands. The two 1,10-phenanthroline rings are positioned at an approximately perpendicular position to each other. In the lanthanide(III) chloride complexes presented in this work, there is very likely one molecule of water directly coordinated to the lanthanide(III) ion. If there is no water molecule present in the first coordination sphere, the coordination number of the lanthanide(III) ion is only seven, which is rather low (the coordination number is usually eight or nine). Secondly, in the crystal structure of $[LaCl_3(phen)_2(H_2O)] \cdot MeOH$, there is also one water molecule present in the first coordination sphere.

3.3 Thermal behavior of the lanthanide(III) complexes

Complexes of the ligands L_I, L_{II}, L_{III}, L_{IV}, L_V, L_{VI}, L_{VII}, L_{VIII} and L_{IX} with lanthanum(III) were prepared in order to examine the influence of the substitution pattern and alkoxy chain length on the thermal behavior of the metal complexes ($[LaCl_3(L)_2(H_2O)]$, L = L_I, L_{II}, L_{III}, L_{IV}, L_V, L_{VI}, L_{VII}, L_{VIII}, L_{IX}). Except for the lanthanum(III) complex $[LaCl_3(L_{IX})_2(H_2O)]$, which exhibited a cubic phase (see below), none of the lanthanum(III) complexes were liquid-crystalline. The complexes of the ligands with a 2,3,4-trisubstitution pattern and a 2,4,5-trisubstitution pattern ($[LaCl_3(L_{VII})_2(H_2O)]$ and $[LaCl_3(L_{VIII})_2(H_2O)]$, respectively) melted directly to the isotropic liquid. The complexes of the ligands with less than three alkoxy chains ($[LaCl_3(L)_2(H_2O)]$, L = L_I, L_{II}, L_{III}, L_{IV}, L_V, L_{VI}) all decomposed before melting at temperatures above 300 °C. Comparing the thermal behavior of the complexes $[LaCl_3(L_{VII})_2(H_2O)]$, $[LaCl_3(L_{VIII})_2(H_2O)]$ and $[LaCl_3(L_{IX})_2(H_2O)]$, it is clear that the long tetradecyloxy chain in the 2-position prohibits the formation of a mesophase. The lateral alkoxy chain in the 2-position strongly reduces lateral interactions between the molecules and reduces microsegregation.

Complexes of ligand L_{IX} with lanthanum(III), praseodymium(III), neodymium(III), samarium(III), europium(III), gadolinium(III), terbium(III), dysprosium(III) and holmium(III) were synthesized in order to study the influence of the lanthanide contraction on the thermal behavior of the metal complexes ($[LnCl_3(L_{IX})_2(H_2O)]$, Ln = La, Pr, Nd, Sm, Eu, Gd, Tb, Dy, Ho). The lanthanide contraction is the gradual decrease of the ionic radius of the trivalent lanthanide ion going along the lanthanide series. The thermal behavior of the lanthanide(III) complexes is summarized in the phase diagram shown in Figure 3.3.
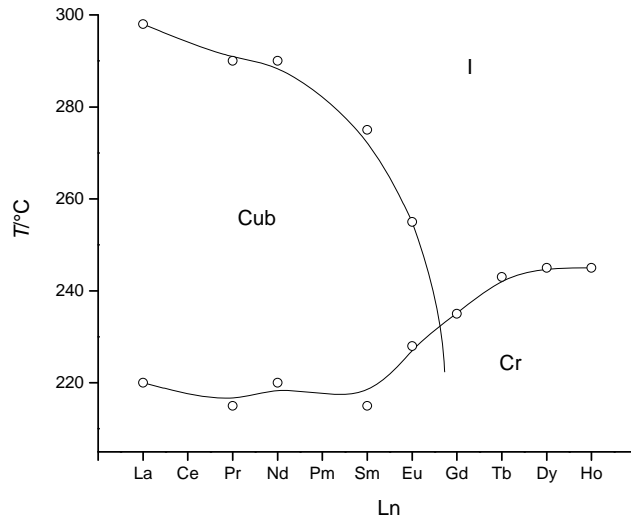
*Figure 3.3: Phase diagram of the lanthanide(III) complexes
[LnCl$_3$(L_{IX})$_2$(H$_2$O)] (Cr = crystalline phase, Cub = cubic phase, I =
isotropic liquid).*

Going from lanthanum(III) to holmium(III), there is a gradual increase
starting at Sm of the melting temperature and a strong decrease of the
clearing temperature. The La-Eu complexes form an enantiotropic cubic
mesophase, whereas the Gd-Ho complexes are not liquid-crystalline. A
monotropic (cubic) mesophase can be expected for the complexes of the
heavy lanthanides, but due to the fast crystallization of the complexes on
cooling from the isotropic liquid, such a monotropic mesophase could not
be observed. Thus, the lanthanide(III) ion has a great influence on the
thermodynamic stability of the mesophase, which decreases over the
lanthanide series until the complete loss of the liquid-crystalline properties
for complexes of lanthanide(III) ions with a smaller ionic radius than that of
europium(III). The strong effect of the lanthanide(III) ion on the transition
temperatures is in agreement with that observed for the lanthanide(III)

64

alkanoates,[12] and Schiff's base complexes with nitrate counterions for which either the mesophase stability was considerably decreased or the liquid-crystalline properties totally suppressed, going along the lanthanide series from lanthanum(III) to lutetium(III).[13]

Other polycatenar lanthanidomesogens were also reported to exhibit a cubic phase, with a *Im-3m* cubic space group.[14] In this case, the polycatenar ligand possessed a linear or bent shape, and upon complexation to $Ln(NO_3)_3$, the corresponding nitrate complexes $[Ln(Li)(NO_3)_3]$ adopted either a bent or a linear shape, respectively. They showed a lamellar mesophase (Ln = Pr, Nd for the bent complexes and Ln = Pr-Gd, Dy, Tm for the linear ones), a *Im-3m* cubic phase for Ln = Pr-Ho and a hexagonal columnar phase (Col_h) for Ln = Er-Lu. Thus, the mesomorphic behavior was also found to be sensitive to the lanthanide contraction, although in a more spectacular way than in the presently described lanthanidomesogens, as lamellar and cubic phases are favored in the light lanthanides in contrast to the heavier, for which a Col_h phase is induced. In the case of the $[LnCl_3(\mathbf{L_{IX}})_2(H_2O)]$ complexes, the thermal stability was considerably enhanced with respect to the $[Ln(Li)(NO_3)_3]$ complexes.

Cubic mesophases are rather uncommonly observed in thermotropic systems and difficult to detect and characterize.[14-22] No texture could be observed, only the formation of large black (optically isotropic) viscous areas. They are distinguished from the isotropic liquid because of their higher viscosity and often by the faceting of air bubbles having distorted polygonal shapes entrapped in the sample. In other cases, applying some pressure with a spatula on the cover slip induced light flashes, which immediately disappeared when the pressure was released. However, no precise structural information can be deduced from this technique only, and unequivocal mesophase assignment is achieved by X-ray diffraction. The Bragg reflections collected from the X-ray diffraction patterns of the cubic mesophases of all the lanthanide(III) complexes are listed in Table 3.1.

Table 3.1: Bragg reflections collected from the X-ray diffraction patterns of all the cubic lanthanide(III) complexes.

Compound	$d_{meas.}$/Å [a]	$h^2+k^2+l^2$	hkl [b]	I [c]	$d_{calc.}$/Å [a,d]	Parameters at T/°C [d]
[LaCl$_3$(**L$_{IX}$**)$_2$(H$_2$O)]	41.01	4	200	S	40.89	T = 260 °C
	36.43	5	210	VS	36.58	a = 81.78 Å
	33.41	6	211	S	33.39	Cub-
	25.88	10	310	W	25.86	Pm-3n
	8.25			br		N = 136.7
	4.6			br		
[PrCl$_3$(**L$_{IX}$**)$_2$(H$_2$O)]	41.15	4	200	M	41.18	T = 240 °C
	36.85	5	210	VS	36.83	a = 82.36 Å
	33.63	6	211	S	33.62	Cub-
	8.3			br		Pm-3n
	4.6			br		N = 139.7
[NdCl$_3$(**L$_{IX}$**)$_2$(H$_2$O)]	41.19	4	200	M	41.07	T = 240 °C
	36.68	5	210	VS	36.73	a = 82.14 Å
	33.49	6	211	S	33.53	Cub-
	8.25			br		Pm-3n
	4.6			br		N = 138.5
[SmCl$_3$(**L$_{IX}$**)$_2$(H$_2$O)]	40.12	4	200	S	40.0	T = 220 °C
	35.66	5	210	VS	35.78	a = 80.0 Å
	32.65	6	211	S	32.66	Cub-
	8.25			br		Pm-3n
	4.6			br		N = 128
[EuCl$_3$(**L$_{IX}$**)$_2$(H$_2$O)]	39.9	4	200	W	39.62	T = 230 °C
	35.42	5	210	VS	35.44	a = 79.25 Å
	32.14	6	211	VS	32.35	Cub-
	8.38			br		Pm-3n
	4.7			br		N = 124.5

[a] $d_{meas.}$ and $d_{calc.}$ are the measured and calculated diffraction spacing.
[b] hkl are the indexation of the reflections.

[c] I is the intensity of the reflections: VS, very strong; S, strong; M, medium; br stands for broad reflection.

[d] $d_{calc.}$ and the lattice parameter a are deduced from the following mathematical expression: $\langle d_{hkl} \rangle = a/N_{hkl}(\sum d_{hkl}.(h^2+k^2+l^2)^{\frac{1}{2}}$, where N_{hkl} is the number of hkl reflections. N is the number of molecules per cubic cell ($N = a^3/V_{mol}$), and $V_{mol} \sim 4000 \text{ Å}^3$.

The cubic structure of these mesophases was deduced from a set of three or four small-angle sharp reflections for which the reciprocal spacings were in the ratios $\sqrt{4}$, $\sqrt{5}$, $\sqrt{6}$, $\sqrt{10}$ (Ln = La) or $\sqrt{4}$, $\sqrt{5}$, $\sqrt{6}$ (Ln = Pr, Nd, Sm, Eu) (Table 2), although with such a small number of reflections, the determination of the cubic space group is difficult, and almost impossible. Along these sharp reflections, two broad scattering were observed, a weak one at 8.2-8.4 Å and a large one at 4.6-4.7 Å, corresponding to some weak intermolecular correlations and molten aliphatic chains respectively. Nevertheless, these reflections were indexed as (200), (210), (211) and (310) of a primitive cubic cell on the basis of the following analysis. For a body centered cubic lattice (*I*-type), the considered sequences in this case would be $\sqrt{8}$, $\sqrt{10}$, $\sqrt{12}$, $\sqrt{20}$ for Ln = La, and $\sqrt{8}$, $\sqrt{10}$, $\sqrt{12}$ for Ln = Pr, Nd, Sm, Eu, (the general condition for the (hkl) reflections is $h + k + l = 2n$), all compatible with this symmetry. These reflections can then be indexed as (220), (310), (222), and (420). However, quite a large number of reflections are missing (7) and these absences are not all explained by the reflection conditions (the only absence explained is the 200 reflection in the $I4_132$ goup). Amongst the 10 body-centered space groups, *Ia*-3 and *Ia*-3d are excluded because of the presence of the (310) reflex, and *I*-43*d* because that of (222), leaving 7 possible but unlikely space groups (*I*23, I2$_1$3, *Im*-3, *I*432, *I*4$_1$32, *I*-43*m*, *Im*-3*m*). In the case of a face-centered space group (*F*-type), the compatible sequence of reflections ratio ($\sqrt{16}$, $\sqrt{20}$, $\sqrt{24}$, $\sqrt{40}$; conditions $h + k$, $h + l$, $k + l = 2n$) allows the indexation of the reflections as (400), (420), (422), and (620). The presence of $\sqrt{20}$ excludes automatically the diamond structure. Only 6 out of 11 space groups are compatible, namely the *F*23, *Fm*-3, *F*432, *F*4$_1$32, *F*-43*m* and *Fm*-3*m* space groups. However, the

10 intermediate reflections that are missing and which cannot be explained by the reflection conditions of these 6 space groups (k, l = 2n for $0kl$, h = 2n for $h00$, and $h + l$ = 2n for hhl), are not favorable to the assignment of a face-centered space group. As far as the 15 primitive cubic space groups (*P*-type) are concerned, several could be immediately disregarded due to the presence of some particular reflections such as the (200) reflex eliminating the *P*4$_3$32 and *P*4$_1$32 space groups, the (210) reflection excluding the *Pn*-3, *Pn*-3*n*, and *Pn*-3*m* space groups and the (310) reflex the *Pa*-3 one. Amongst the 9 remaining primitive, the most probable space groups are *Pm*-3*n*, *P*-43*n*, since amongst the 5 absent reflections, 3 of them, namely (100), (300) and (221), are explained by the space groups conditions (h = 2n for $h00$ and l = 2n for hhl); the least probable space groups are *P*2$_1$3 and *P*4$_2$32 (h = 2n for $h00$), and *P*23, *Pm*-3, *P*432, *P*-43*m* and *Pm*-3*m* (no conditions). None of the space groups retained in this list have yet been found for a liquid-crystalline cubic phase, except the *Pm*-3*n* cubic space group (No. 223).[17-19]

Thus, we are left with 9 primitive, 7 centered and 6 face-centered (the least probable ones) space groups. An interesting evidence for considering primitive rather than body-centered space groups is the distribution of the intensity of reflections in the XRD pattern as a function of the diffraction angle. In essentially all reported body-centered cubic structures,[17-21] the intensity decreases progressively with increasing the diffraction angle in the corresponding X-ray patterns, whilst this is not the case for primitive cubic cells.[23] Here, we do not observe this progressive decrease of the reflection intensity with increasing the diffraction angle (Figure 3.4), the strongest reflection being always the (210) between the (200) and the (211). From these simple arguments (distribution of reflections intensity, unexplained absence by the space groups conditions), both the body-centred and face-centred symmetries were excluded, and thus we considered the most probable primitive cubic space group, namely the *Pm*-3*n* space group.
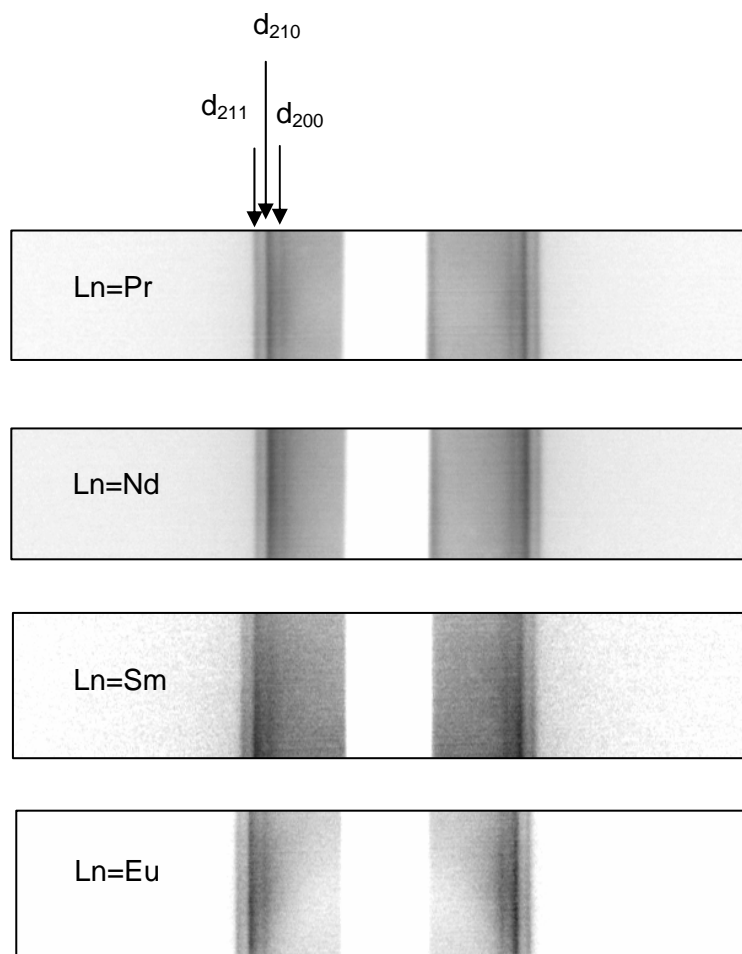
Figure 3.4: Small-angle X-ray patterns of four of the lanthanide(III) complexes, recorded at 240 °C (Ln = Pr, Nd), 230 °C (Ln = Sm), and 220 °C (Ln = Eu).

Recently, a model for the *Pm-3n* cubic phase, intermediate between micellar and bicontinuous topologies, was suggested and found to render account fairly well of the organization of semi-rigid dendrimers within this mesophase (Figure 3.5).[23] Such a model can be fully applied here and consists of the formation of an infinite 3D interlocking network of mutually perpendicular evenly pinched columns, compatible with the symmetry of the space group (3 pairs of column sites evenly spaced along the bisectors of the cubic cell faces and two interstitial sites at the centre and corners of the cubic lattice (Figure 3.5). This model imposes some constraints on the molecular disposition, which can be evidenced by the broad band at 8.2-8.4 Å.
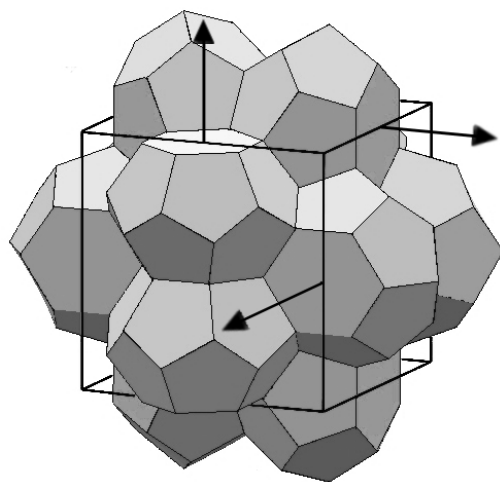
Figure 3.5: Schematic representation of the 3D interlocking pinched columns model lattice. The arrows indicate the growth direction of the evenly pinched columns.

3.4 Photophysical properties of the lanthanide(III) complexes

The europium(III), neodymium(III) and samarium(III) imidazo*[4,5-f]*-1,10-phenanthroline chloro complexes [LnCl$_3$(**L$_{IX}$**)$_2$(H$_2$O)] did show only a very weak luminescence. Excitation was done at 350 nm. The weak luminescence can be explained by the water molecule directly attached to the lanthanide ion, this water can easily quench the luminescence.

3.5 STM study of the lanthanide(III) complexes

Molecules with long alkyl chains are known to show a good affinity for highly oriented pyrolytic graphite. Upon their adsorption, scanning tunnelling microscopy (STM) often provides structural information with submolecular resolution. As an example, we have investigated the self-assembly of EuCl$_3$(**L$_{IX}$**)$_2$(H$_2$O) at the solid-liquid interface. Figure 3.*6* shows STM images of a self-assembled monolayer of EuCl$_3$(**L$_{IX}$**)$_2$(H$_2$O) formed at the 1-phenyloctane/graphite interface. A regular pattern of bright and dark areas is observed. In these current images, bright (dark) areas correlate with a high (low) tunnelling current. Generally, aromatic moieties are characterized by a relatively high tunnelling current while alkyl chains are typically less transmissive for tunnelling electrons. Thus in these images the bright features are attributed to the aromatic moieties of the ligands and the central ion while the darker areas correspond to the aliphatic chains. The high contrast of the central core of this molecule both results from the high electron density and specific morphology, since the **L$_{IX}$** ligands in the complex are not expected to be fully coplanar with the surface. The complex forms clusters and curved lamellae. The surface layer lacks long range order. The size of these clusters ranges from 3.3 nm to 5.5 nm,

suggesting they do not correspond to single molecules but are composed of 2 to 5 molecules. In some areas alkyl chains could be visualized.
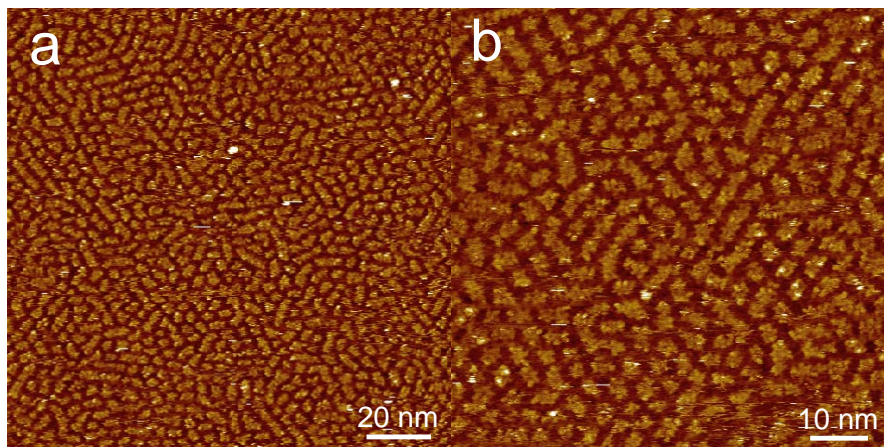
Figure 3.6: STM images of a self-assembled monolayer of EuCl3(L_{IX})2(H2O) at the phenyloctane/graphite interface. The bias voltage is -1.04 V, the setpoint tunnelling current is 258 pA.

In contrast, upon changing the solvent to 1-octanoic acid, a regular well-ordered pattern appears almost immediately (Figure 3.7). Rhombus-shaped bright features are visible: their long axis measures 4 nm and the short axis about 2 nm. After calibration *vs* the graphite lattice, the unit cell parameters of this two-dimensional crystal were determined to be $a = 4.8 \pm 0.2$ nm, $b = 5.0 \pm 0.2$ nm and $\theta = 55 \pm 3°$. From the high resolution image the aliphatic chains are resolved with near atomic resolution. Per bright rhombus there are sixteen alkyl chains, four of which run along the unit cell parameter a. This clearly indicates that the bright features are not single molecules. Considering the core size of the complex (nearly 2.5 nm in length and 1 nm in width) and the number of alkyl chains, the bright features are attributed to dimers of the complex. Four of the alkyl chains are considered to be coadsorbed solvent molecules. Co-adsorption is believed to be promoted by hydrogen bonding interactions between the carboxylic acid groups of the

72

solvent molecules with the nitrogen atoms of the aromatic ligands. These observations are in line with the lack of ordering observed at the 1-phenyloctane/graphite interface.
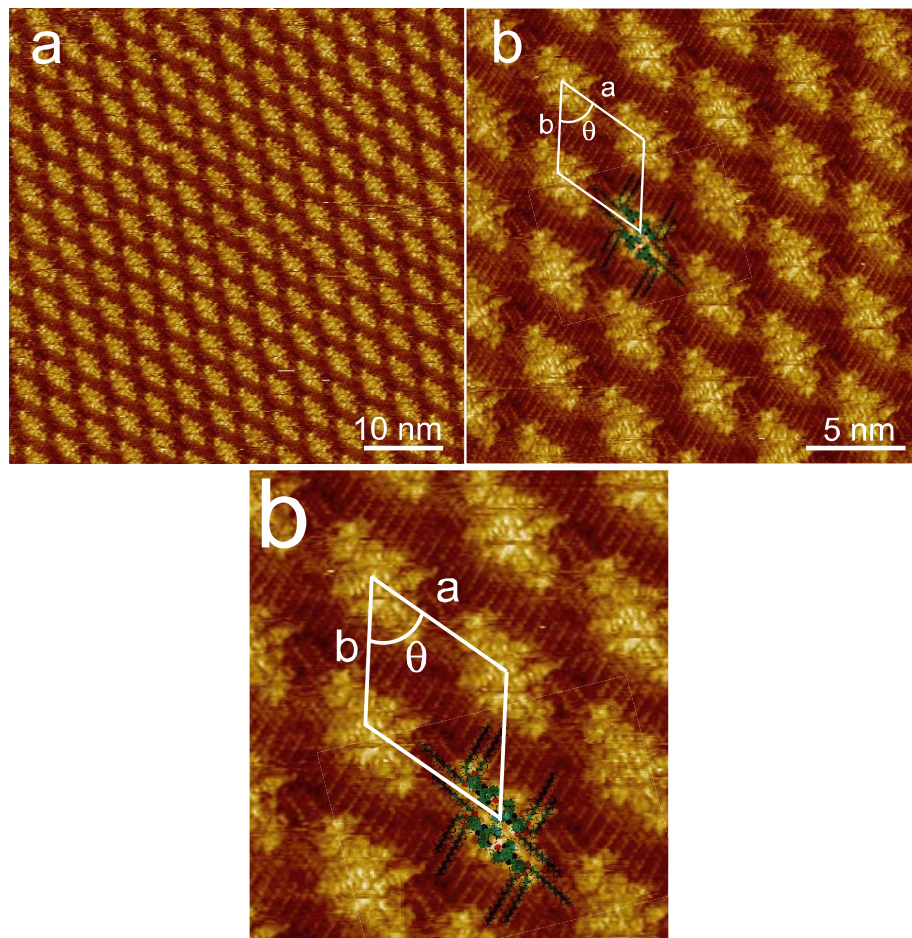
Figure 3.7: STM images of a self-assembled monolayer of $EuCl_3(\mathbf{L_{IX}})_2(H_2O)$ at the octanoic acid/graphite interface. A unit cell has been marked in the right image. A tentative molecular model of the dimer structure is indicated on top of the STM image. The bias voltage is -1.04 V, the setpoint tunnelling current is 258 pA.

3.6 Conclusion

Transformation of 1,10-phenanthroline into substituted 2-aryl-imidazo*[4,5-f]*-1,10-phenanthroline via condensation of 1,10-phenanthroline-5,6-dione with a substituted benzaldehyde in the presence of ammonium acetate is a facile route to functionalize 1,10-phenanthrolines. By a proper choice of the substitution pattern of the substituted benzaldehydes, it is possible to obtain lipophilic 1,10-phenanthroline ligands, which are useful for the design of metallomesogens. Although the ligands are not liquid-crystalline, the lanthanide complexes show a mesophase over a broad temperature range. The $EuCl_3(\mathbf{L_{IX}})_2(H_2O)$ complex forms self-assembled monolayers at the solution/graphite interface. A STM study indicates that the order of the monolayers strongly depends on the solvent. Whereas rather disordered monolayers were obtained on the 1-phenyloctane/graphite interface, well-ordered monolayers were observed at the 1-octanoic acid/graphite interface. The lanthanide(III) complexes of the type $[LnCl_3(\mathbf{L_{IX}})_2(H_2O)]$ (Ln = Nd, Sm and Eu) only showed a very weak photoluminescence in comparison to the europium(III) complexes with 2-thenoyltrifluoroacetonate or dibenzoylmethanate and imidazo*[4,5-f]*-1,10-phenanthroline.[9]

3.7 Experimental section

Characterization of the mesophases by X-ray diffraction and discussion was performed in cooperation with Dr. Bertrand Donnio and Dr. Daniel Guillon. The STM experiment and following discussion was performed in cooperation with Prof. Steven De Feyter.

3.7.1 Synthesis of precursors and ligands

(a) 1,10-Phenanthroline-5,6-dione (1)
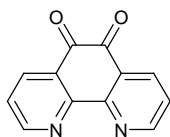
1,10-Phenanthroline monohydrate (**1**) (0.0504 mol, 10.00 g) was added in small portions under stirring to 60 mL of concentrated sulfuric acid in a round-bottom flask (500 mL) equipped with a reflux condenser. After the solid compound was dissolved, sodium bromide (0.0504 mol, 5.19 g) was added, followed by 30 mL of 70% nitric acid. The mixture was heated to 105 °C for 6 hours. The temperature was then lowered to 95 °C and the reflux condenser was removed to allow the bromine vapors to escape for a period of 16 hours. After being cooled to room temperature, the mixture was poured onto 800 g of ice and was carefully neutralized to pH 7 with about 300 mL of a 10 M solution of sodium hydroxide. The turbid solution was filtered and the solid residue was extracted with 5×200 mL of boiling water. The insoluble material was removed from the cooled extraction liquid by filtration and the combined aqueous solutions were extracted with dichloromethane, dried over anhydrous $MgSO_4$, and the solvent was removed under reduced pressure. The crude product was recrystallized from

toluene to obtain orange crystals. Yield: 30% (3.18 g). δ_H (300 MHz, CDCl$_3$): 7.58–7.62 (dd, 2H, H-aryl, J_o = 8.1 Hz, J_o = 4.8 Hz), 8.53 (dd, 2H, H-aryl, J_o = 8.1 Hz, J_m = 1.8 Hz), 9.12 (dd, 2H, H-aryl, J_o = 4.8 Hz, J_m = 1.8 Hz). Calcd. for C$_{12}$H$_6$N$_2$O$_2$·0.33H$_2$O: C 66.67, H 3.11, N 12.96. Found: C 67.25, H 2.77, N 12.99. M.p.: 257 °C (lit. m.p.: 258 °C[24]).

(b) Benzaldehydes

All the benzaldehydes **2 - 10** were prepared by adding the appropriate alkyl bromide (1.1, 2.2, or 3.3 eq.) to a solution of the corresponding mono-, di- or trihydroxybenzaldehyde (1 eq.) and potassium carbonate (1.1, 2.2 or 3.3 eq.) in DMF (100 mL). A catalytic amount of potassium iodide was added and the mixture was refluxed for 3 hours under a nitrogen atmosphere. Then the mixture was cooled to room temperature and poured into 300 mL of a H$_2$O/HCl (100:50) solution. The solution was extracted with dichloromethane and the combined organic layers were washed with brine. Then the organic layer was dried over anhydrous MgSO$_4$ and the solvent was removed under reduced pressure. The crude product was purified on a silica column with hexane/ethyl acetate (95:5) as the eluent. The product was recrystallized ethanol, methanol (4-hexadecyloxybenzaldehyde) or petroleum ether (2,4,5-Tritetradecyloxybenzaldehyde).

4-Hexadecyloxybenzaldehyde (2)
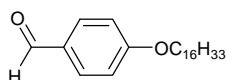
Yield: 60% (1.50 g). δ_H (300 MHz, CDCl$_3$): 0.88 (t, 3H, CH$_3$), 1.26–1.49 (m, 26H, CH$_2$), 1.79–1.84 (m, 2H, C**H**$_2$–CH$_2$–O), 4.04 (t, 2H, C**H**$_2$–O), 7.00 (d, 2H, H-aryl, J_o = 8.4 Hz), 7.81 (d, 2H, H-aryl, J_o = 8.4 Hz), 9.88 (s, 1H, CH=O). M.p.: 44 °C.

76

3,4-Dihexyloxybenzaldehyde (3)
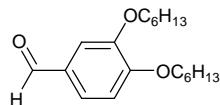
Yield: 78% (1.72g). δ_H (300 MHz, CDCl$_3$): 0.92 (t, 6H, CH$_3$), 1.27−1.58 (m, 10H, CH$_2$), 1.81−1.92 (m, 4H, C**H**$_2$–CH$_2$–O), 4.05–4.12 (m, 4H, C**H**$_2$–O), 6.95 (d, 1H, H-aryl, J_o = 8.0 Hz), 7.41−7.45 (m, 2H, H-aryl), 9.85 (s, 1H, CH=O). M.p.: 40 °C.

3,4-Didecyloxybenzaldehyde (4)
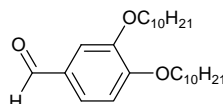
Yield: 69% (2.08 g). δ_H (300 MHz, CDCl$_3$): 0.91 (t, 6H, CH$_3$), 1.29−1.59 (m, 28H, CH$_2$), 1.81−1.90 (m, 4H, C**H**$_2$–CH$_2$–O), 4.04–4.11 (m, 4H, C**H**$_2$–O), 6.98 (d, 1H, H-aryl, J_o = 8.1 Hz), 7.41−7.45 (m, 2H, H-aryl), 9.84 (s, 1H, CH=O). M.p.: 62 °C (lit. m.p.: 65 °C[25]).

3,4-Ditetradecyloxybenzaldehyde (5)
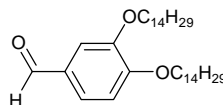
Yield: 69% (2.64 g). δ_H (300 MHz, CDCl$_3$): 0.89 (t, 6H, CH$_3$), 1.27−1.57 (m, 44H, CH$_2$), 1.81−1.90 (m, 4H, C**H**$_2$–CH$_2$–O), 4.01–4.11 (m, 4H, C**H**$_2$–O), 6.98 (d, 1H, H-aryl, J_o = 8.0 Hz), 7.40−7.45 (m, 2H, H-aryl), 9.84 (s, 1H, CH=O). M.p.: 72 °C (lit. m.p.: 78 °C[25]).

3,4-Dioctadecyloxybenzaldehyde (6)
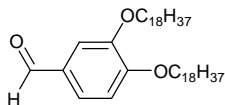
Yield: 82% (3.80 g). δ_H (300 MHz, CDCl$_3$): 0.89 (t, 6H, CH$_3$), 1.27–1.57 (m, 60H, CH$_2$), 1.81–1.89 (m, 4H, **CH$_2$**–CH$_2$–O), 4.04–4.11 (m, 4H, **CH$_2$**–O), 6.98 (d, 1H, H-aryl, J_o = 8.1 Hz), 7.41–7.45 (m, 2H, H-aryl), 9.85 (s, 1H, CH=O). M.p.: 83 °C.

3,5-Ditetradecyloxybenzaldehyde (7)
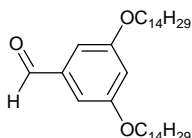
Yield: 77% (2.94 g). δ_H (300 MHz, CDCl$_3$): 0.89 (t, 6H, CH$_3$), 1.20–1.46 (m, 44H, CH$_2$), 1.76–1.83 (m, 4H, **CH$_2$**–CH$_2$–O), 3.98–4.02 (m, 4H, **CH$_2$**–O), 6.71 (s, 1H, H-aryl), 7.00 (s, 2H, H-aryl), 9.90 (s, 1H, CH=O). M.p.: 47 °C.

2,3,4-Tritetradecyloxybenzaldehyde (8)
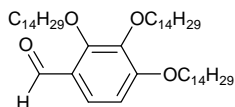
Yield: 55% (2.66 g). δ_H (300 MHz, CDCl$_3$): 0.89 (t, 9H, CH$_3$), 1.28–1.55 (m, 66H, CH$_2$), 1.76–1.88 (m, 6H, **CH$_2$**–CH$_2$–O), 3.99 (t, 2H, **CH$_2$**–O), 4.05 (t, 2H, **CH$_2$**–O), 4.18 (t, 2H, **CH$_2$**–O), 6.74 (d, 1H, H-aryl, J_o = 8.8 Hz), 7.57 (d, 1H, H-aryl, J_o = 8.8 Hz), 10.27 (s, 1H, CH=O). M.p.: 44 °C.

2,4,5-Tritetradecyloxybenzaldehyde (9)
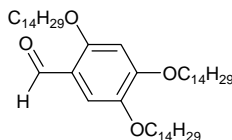
Yield: 51% (2.46 g δ_H (300 MHz, CDCl$_3$): 0.89 (t, 9H, CH$_3$), 1.28−1.53 (m, 66H, CH$_2$), 1.77−1.91 (m, 6H, C**H**$_2$–CH$_2$–O), 3.96–4.08 (m, 6H, C**H**$_2$–O), 6.46 (s, 1H, H-aryl), 7.33 (s, 1H, H-aryl), 10.34 (s, 1H, CH=O). M.p.: 79 °C.

3,4,5-Tritetradecyloxybenzaldehyde (10)
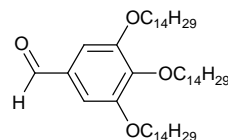
Yield: 41% (1.72 g). δ_H (300 MHz, CDCl$_3$): 0.89 (t, 9H, CH$_3$), 1.27−1.49 (m, 66H, CH$_2$), 1.72−1.88 (m, 6H, C**H**$_2$–CH$_2$–O), 4.02–4.17 (m, 6H, C**H**$_2$–O), 7.09 (s, 2H, H-aryl), 9.84 (s, 1H, CH=O). M.p.: 58 °C.

(c) Ligands

All the ligands were prepared by adding the appropriate alkyloxybenzaldehyde (1 eq.) to a warm solution of 1,10-phenanthroline-5,6-dione (**1**) (1 eq.) and ammonium acetate (8.5 eq.) in 20 mL of glacial acetic acid. The mixture was heated to 85 °C for 5 hours. After the reaction mixture was cooled to room temperature, it was poured into 100 mL of water and neutralized to pH 7 with an aqueous ammonia solution. The precipitate was filtered off, washed with distilled water and dried. The crude product was purified on a silica column with CHCl$_3$/hexane/MeOH (50:50:10) as the eluent. Since the compound holds solvents firmly, it was dried in a vacuum oven at 50 °C.

L$_I$
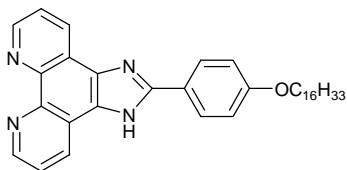
Yield: 62% (0.67 g). δ_H (400 MHz, 363 K, DMSO-d$_6$): 0.86 (t, 3H, CH$_3$), 1.26–1.52 (m, 26H, CH$_2$), 1.75–1.82 (m, 2H, **CH$_2$**–CH$_2$–O), 4.11 (t, 2H, **CH$_2$**–O), 7.14 (d, 2H, H-aryl, J_o = 8.8 Hz), 7.77–7.80 (b, m, 2H, H-aryl), 8.21 (d, 2H, H-aryl, J_o = 8.8 Hz), 8.95 (d, 2H, H-aryl, J_o = 8.00 Hz), 9.03 (b, s, 2H, H-aryl). δ_C (100 MHz, DMSO-d$_6$): 13.57, 21.86, 25.45, 28.51, 28.64, 28.74, 28.83, 28.89, 31.16, 115.19, 122.96, 127.98, 129.56, 143.52, 147.35, 151.07, 160.21. Calcd. for C$_{35}$H$_{44}$N$_4$O·0.5H$_2$O: C 77.03, H 8.31, N 10.27. Found: C 77.00, H 8.44, N 9.96. ESI-MS (methanol, m/z): 537.5, [M + H]$^+$. M.p.: 162 °C.

80

L$_{II}$
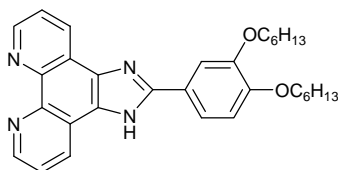
Yield: 68% (0.68 g). δ_H (300 MHz, THF-d$_8$): 0.83 (t, 3H, CH$_3$), 0.89 (t, 3H, CH$_3$), 1.12−1.37 (m, 8H, CH$_2$), 1.43−1.52 (m, 4H, CH$_2$), 1.72−1.88 (m, 4H, **CH$_2$**−CH$_2$−O), 3.51 (t, 2H, **CH$_2$**−O), 3.96 (t, 2H, **CH$_2$**−O), 6.93 (d, 1H, H-aryl, J_o = 6.2 Hz), 7.30 (b, m, 1H, H-aryl), 7.73 (b, m, 1H, H-aryl), 7.93−7.96 (m, 2H, H-aryl), 8.70− 8.73 (b, m, 2H, H-aryl), 8.95 (b, s, 1H, H-aryl), 9.12 (d, 1H, H-aryl, J_o = 5.7 Hz), 14.42 (b, s, 1H, N−H). δ_C (75 MHz, THF-d$_8$): 14.20, 23.27, 26.35, 26.50, 29.95, 30.10, 32.26, 32.35, 68.97, 69.45, 112.50, 114.08, 120.20, 121.03, 123.43, 123.98, 124.47, 125.75, 127.61, 130.62, 131.11, 137.57, 144.60, 144.88, 147.56, 148.11, 150.21, 151.27, 152.74. Calcd. for C$_{31}$H$_{36}$N$_4$O$_2$·0.5H$_2$O: C 73.63, H 7.38, N 11.08. Found: C 73.57, H 7.82, N 10.59. ESI-MS (methanol, m/z): 497.6, [M + H]$^+$. M.p.: 91 °C.

L$_{III}$
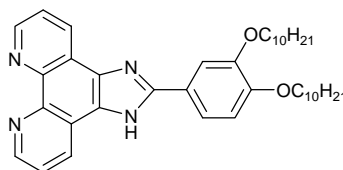
Yield: 41% (0.50 g). δ_H (400 MHz, THF-d$_8$): 0.83−0.87 (m, 6H, CH$_3$), 1.16−1.75 (m, 32H, CH$_2$), 3.43 (m, 2H, **CH$_2$**−O), 3.94 (m, 2H, **CH$_2$**−O), 6.91 (d, 1H, H-aryl, J_o = 8.4 Hz), 7.26 (b, m, 1H, H-aryl), 7.74 (b, m, 1H, H-

aryl), 7.92–7.99 (m, 2H, H-aryl), 8.67 (b, s, 1H, H-aryl), 8.76 (b, d, 1H, H-aryl), 8.95 (b, s, 1H, H-aryl), 9.16 (b, d, 1H, H-aryl), 14.68 (b, s, 1H, N–H). δ_C (100 MHz, THF-d_8): 14.20, 14.24, 23.34, 26.69, 30.02, 30.10, 30.15, 30.32, 30.40, 32.65, 32.70, 69.02, 69.55, 112.64, 114.27, 120.30, 121.10, 123.46, 123.98, 124.53, 125.82, 127.68, 130.80, 131.21, 137.59, 144.56, 144.84, 147.51, 148.06, 150.25, 151.29, 152.83. Calcd. for $C_{39}H_{52}N_4O_2 \cdot 0.5H_2O$: C 75.81, H 8.65, N 9.07. Found: C 76.08, H 8.99, N 8.73. ESI-MS (methanol, m/z): 609.7, $[M + H]^+$. M.p.: 60 °C.

L$_{IV}$
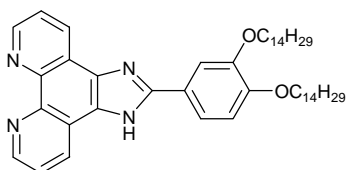
Yield: 69% (1.00 g). δ_H (400 MHz, THF-d_8): 0.85 (t, 6H, CH$_3$), 1.23−1.88 (m, 48H, CH$_2$), 3.57 (t, 2H, **CH**$_2$−O), 3.96 (t, 2H, **CH**$_2$−O), 6.94 (d, 1H, H-aryl, J_o = 8.0 Hz), 7.34 (b, s, 1H, H-aryl), 7.71 (b, s, 1H, H-aryl), 7.92−7.96 (m, 2H, H-aryl), 8.73 (b, s, 2H, H-aryl), 8.95 (b, s, 1H, H-aryl), 9.10 (b, s, 1H, H-aryl), 14.22 (b, s, 1H, N−H). δ_C (100 MHz, THF-d_8): 13.73, 22.86, 26.29, 26.37, 29.63, 29.71, 29.92, 29.97, 32.19, 68.80, 69.10, 78.89, 112.33, 113.79, 119.67, 120.38, 122.88, 123.29, 124.04, 125.12, 127.01, 129.83, 130.41, 144.37, 147.20, 147.66, 149.83, 150.92, 152.07. Calcd. for $C_{47}H_{68}N_4O_2 \cdot 0.5H_2O$: C 77.32, H 9.53, N 7.67. Found: C 77.82, H 9.77, N 7.23. ESI-MS (methanol, m/z): 721.8, $[M + H]^+$. M.p.: 64 °C.

82

L$_V$
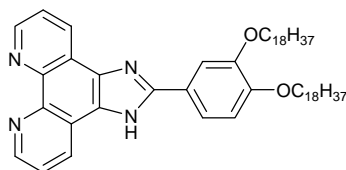
Yield: 30% (0.50 g). δ_H (400 MHz, THF-d$_8$): 0.87 (t, 6H, CH$_3$), 1.28–1.76 (m, 64H, CH$_2$), 3.52 (t, 2H, **CH$_2$**–O), 3.96 (t, 2H, **CH$_2$**–O), 6.93 (d, 1H, H-aryl, J_o = 8.4 Hz), 7.30 (b, m, 1H, H-aryl), 7.72 (b, m, 1H, H-aryl), 7.92–7.96 (m, 2H, H-aryl), 8.73 (b, m, 2H, H-aryl), 8.95 (b, s, 1H, H-aryl), 9.13 (b, d, 1H, H-aryl), 14.40 (b, s, 1H, N–H). δ_C (100 MHz, THF-d$_8$): 14.22, 23.34, 26.75, 26.86, 30.09, 30.11, 30.20, 30.39, 30.45, 30.47, 30.51, 30.54, 32.67, 69.17, 69.58, 112.75, 114.28, 120.23, 120.97, 123.37, 123.86, 124.56, 125.73, 127.57, 130.48, 131.04, 137.60, 144.70, 144.93, 147.61, 148.09,150.30, 151.36, 152.68. Calcd. for C$_{55}$H$_{84}$N$_4$O$_2$·0.5H$_2$O: C 78.43, H 10.17, N 6.65. Found: C 78.47, H 9.77, N 6.78. ESI-MS (methanol, m/z): 833.9, [M + H]$^+$. M.p.: 116 °C.

L$_{VI}$
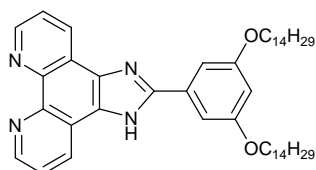
Yield: 34% (0.49 g). δ_H (300 MHz, THF-d$_8$): 0.87 (t, 6H, CH$_3$), 1.24 (m, 44H, CH$_2$), 1.55 (m, 4H, **CH$_2$**–CH$_2$–O), 3.57 (t, 4H, **CH$_2$**–O), 6.41 (s, 1H, H-aryl), 7.32 (b, m, 1H, H-aryl), 7.53 (s, 2H, H-aryl), 7.77 (b, m, 1H, H-aryl), 8.68 (b, s, 1H, H-aryl), 8.77 (b, d, 1H, H-aryl), 8.98 (b, m, 1H, H-

aryl), 9.15 (b, d, 1H, H-aryl), 14.70 (b, s, 1H, N−H). δ_C (75 MHz, THF-d$_8$): 14.33, 23.43, 26.84, 30.10, 30.20, 30.29, 30.53, 32.75, 68.39, 103.61, 105.34, 121.00, 123.68, 124.08, 125.78, 127.80, 130.84, 131.12, 133.13, 137.51, 145.04, 148.14, 148.30, 152.41, 161.52. Calcd. for $C_{47}H_{68}N_4O_2 \cdot 0.5H_2O$: C 77.32, H 9.53, N 7.67. Found: C 77.29, H 9.23, N 7.48. ESI-MS (methanol, m/z): 721.8, $[M + H]^+$. M.p.: 158 °C.

L$_{VII}$
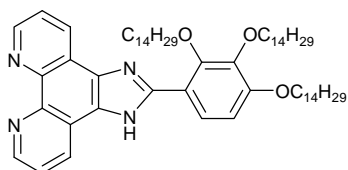
Yield: 42% (0.78 g). δ_H (400 MHz, CDCl$_3$): 0.85−0.89 (m, 9H, CH$_3$), 1.22−1.59 (m, 66H, CH$_2$), 1.82−1.96 (m, 6H, **CH**$_2$–CH$_2$–O), 4.07 (t, 4H, **CH**$_2$–O), 4.30 (t, 2H, **CH**$_2$–O), 6.88 (d, 1H, H-aryl, J_o = 8.8 Hz), 7.66 (dd, 1H, H-aryl, J_o = 8.2 Hz, J_m = 4.2 Hz), 7.70 (dd, 1H, H-aryl, J_o = 8.2 Hz, J_m = 4.2 Hz), 8.23 (d, 1H, H-aryl, J_o = 8.8 Hz), 8.28 (d, 1H, H-aryl, J_o = 8.2 Hz), 9.04 (d, 1H, H-aryl, , J_o = 8.2 Hz), 9.14 (s, 2H, H-aryl), 11.46 (s, 1H, N−H). δ_C (100 MHz, CDCl$_3$): 14.06, 22.66, 26.13, 26.19, 26.45, 29.33, 29.35, 29.41, 29.59, 29.62, 29.64, 29.69, 29.73, 30.40, 30.96, 31.91, 68.95, 73.92, 74.93, 109.29, 115.41, 118.90, 122.60, 123.19, 123.85, 124.28, 124.49, 127.86, 130.37, 136.10, 141.52, 144.35, 144.42, 148.04, 148.52, 149.19, 150.83, 155.02. Calcd. for $C_{61}H_{96}N_4O_3 \cdot 0.5H_2O$: C 77.74, H 10.37, N 5.94. Found: C 78.22, H 10.40, N 5.61. ESI-MS (methanol, m/z): 933.9, $[M + H]^+$. M.p.: 77 °C.

L$_{VIII}$
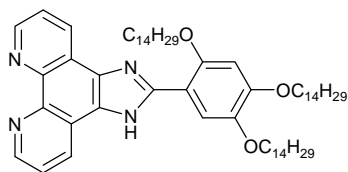
Yield: 45% (0.84 g). δ_H (300 MHz, THF-d$_8$): 0.86–0.88 (m, 9H, CH$_3$), 1.22–2.03 (m, 72H, CH$_2$), 4.06–4.10 (m, 4H, **CH**$_2$–O), 4.22 (t, 2H, **CH**$_2$–O), 6.76 (s, 1H, H-aryl), 7.58–7.67 (m, 2H, H-aryl), 8.09 (s, 1H, H-aryl), 8.51 (d, 1H, H-aryl, J_o = 7.8 Hz), 8.98–9.00 (m, 3H, H-aryl), 11.82 (s, 1H, N–H). δ_C (75 MHz, THF-d$_8$): 14.32, 23.44, 27.00, 27.05, 27.22, 30.22, 30.32, 30.51, 30.58, 32.76, 69.84, 70.59, 101.23, 111.64, 116.03, 120.01, 122.92, 123.38, 125.12, 125.73, 128.84, 130.30, 136.60, 144.86, 145.27, 145.43, 147.99, 148.39, 149.91, 152.12, 152.65. Calcd. for C$_{61}$H$_{96}$N$_4$O$_3$·0.5H$_2$O: C 77.74, H 10.37, N 5.94. Found: C 77.63, H 10.77, N 5.95. ESI-MS (methanol, m/z): 933.9, [M + H]$^+$. M.p.: 81 °C.

L_{IX}
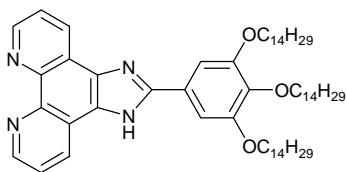
Yield: 55% (1.03 g). δ_H (300 MHz, THF-d$_8$): 0.87 (t, 9H, CH$_3$), 1.25−1.67 (m, 72H, CH$_2$), 3.57−3.62 (m, 4H, **CH**$_2$−O), 3.88 (t, 2H, **CH**$_2$−O), 7.30 (b, m, 1H, H-aryl), 7.68 (s, 2H, H-aryl), 7.74 (b, m, 1H, H-aryl), 8.66 (b, s, 1H, H-aryl), 8.80 (b, d, 1H, H-aryl), 8.97 (b, s, 1H, H-aryl), 9.19 (b, d, 1H, H-aryl), 14.82 (b, s, 1H, N−H). δ_C (75 MHz, THF-d$_8$): 14.36, 23.46, 26.91, 27.03, 30.23, 30.59, 31.26, 32.79, 69.25, 73.51, 105.86, 121.15, 123.68, 124.17, 125.88, 126.39, 127.92, 131.02, 131.42, 137.57, 140.35, 144.67, 144.94, 147.75, 148.24, 152.80, 154.24. Calcd. for C$_{61}$H$_{96}$N$_4$O$_3$·0.5H$_2$O: C 77.74, H 10.37, N 5.94. Found: C 78.24, H 10.59, N 5.44. ESI-MS (methanol, m/z): 933.9, [M + H]$^+$. M.p.: 83 °C.

3.7.2 Synthesis of lanthanide(III) complexes

All the lanthanide(III) complexes were prepared by adding slowly a solution of $LnCl_3 \cdot xH_2O$ (1 eq.) in ethanol to a solution of the appropriate ligand (2 eq.) in hot ethanol. The solution was stirred for 30 minutes at 65 °C. A yellow/orange precipitate was formed, filtered off, washed with ethanol and dried in a vacuum oven at 50 °C.

(a) $[LaCl_3(L_I)_2(H_2O)]$

Orange powder. Yield: 80%. Calcd. for $C_{70}H_{88}Cl_3LaN_8O_2 \cdot 4H_2O$: C 60.45, H 6.96, N 8.06. Found: C 60.68, H 6.90, N 8.00. The compound decomposes before melting (> 300 °C).

(b) $[LaCl_3(L_{II})_2(H_2O)]$

Orange powder. Yield: 84%. Calcd. for $C_{62}H_{72}Cl_3LaN_8O_4 \cdot 4H_2O$: C 56.82, H 6.15, N 8.55. Found: C 56.91, H 6.23, N 8.55. The compound decomposes before melting (> 300 °C).

(c) $[LaCl_3(L_{III})_2(H_2O)]$

Orange powder. Yield: 82%. Calcd. for $C_{78}H_{104}Cl_3LaN_8O_4 \cdot 3H_2O$: C 61.75, H 7.31, N 7.39. Found: C 61.82, H 7.19, N 7.01. The compound decomposes before melting (> 300 °C).

(d) [LaCl$_3$(L$_{IV}$)$_2$(H$_2$O)]

Orange powder. Yield: 88%. Calcd. for C$_{94}$H$_{136}$Cl$_3$LaN$_8$O$_4$·4H$_2$O: C 64.17, H 8.25, N 6.37. Found: C 64.16, H 8.25, N 5.98. The compound decomposes before melting (> 300 °C).

(e) [LaCl$_3$(L$_V$)$_2$(H$_2$O)]

Orange powder. Yield: 85%. Calcd. for C$_{110}$H$_{168}$Cl$_3$LaN$_8$O$_4$·3H$_2$O: C 67.21, H 8.92, N 5.70. Found: C 67.13, H 9.10, N 5.29. The compound decomposes before melting (> 300 °C).

(f) [LaCl$_3$(L$_{VI}$)$_2$(H$_2$O)]

Orange powder. Yield: 86%. Calcd. for C$_{94}$H$_{136}$Cl$_3$LaN$_8$O$_4$·H$_2$O: C 66.20, H 8.16, N 6.57. Found: C 66.18, H 8.16, N 6.24. The compound decomposes before melting (> 300 °C).

(g) [LaCl$_3$(L$_{VII}$)$_2$(H$_2$O)]

Orange powder. Yield: 80%. Calcd. for C$_{122}$H$_{192}$Cl$_3$LaN$_8$O$_6$·3H$_2$O: C 67.64, H 9.21, N 5.17. Found: C 67.32, H 9.05, N 4.81. M.p.: 234 °C.

(h) [LaCl$_3$(L$_{VIII}$)$_2$(H$_2$O)]

Orange powder. Yield: 81%. Calcd. for C$_{122}$H$_{192}$Cl$_3$LaN$_8$O$_6$·2H$_2$O: C 68.21, H 9.20, N 5.22. Found: C 68.26, H 9.31, N 5.18. M.p.: 242 °C.

(i) [LaCl$_3$(L$_{IX}$)$_2$(H$_2$O)]

Orange powder. Yield: 80%. Calcd. for C$_{122}$H$_{192}$Cl$_3$LaN$_8$O$_6$·2H$_2$O: C 68.21, H 9.20, N 5.22. Found: C 67.89, H 9.70, N 4.77. The compound is liquid-crystalline: Cr 220 Cub 298 I.

(j) [PrCl$_3$(L$_{IX}$)$_2$(H$_2$O)]

Orange powder. Yield: 95%. Calcd. for C$_{122}$H$_{192}$Cl$_3$PrN$_8$O$_6$·H$_2$O: C 68.72, H 9.17, N 5.26. Found: C 68.79, H 8.93, N 4.95. The compound is liquid-crystalline: Cr 215 Cub 290 I.

(k) [NdCl$_3$(L$_{IX}$)$_2$(H$_2$O)]

Orange powder. Yield: 92%. Calcd. for C$_{122}$H$_{192}$Cl$_3$NdN$_8$O$_6$·H$_2$O: C 68.62, H 9.16, N 5.25. Found: C 68.36, H 8.81, N 5.02. The compound is liquid-crystalline: Cr 220 Cub 290 I.

(l) [SmCl$_3$(L$_{IX}$)$_2$(H$_2$O)]

Yellow powder. Yield: 77%. Calcd. for C$_{122}$H$_{192}$Cl$_3$SmN$_8$O$_6$·2H$_2$O: C 67.85, H 9.15, N 5.19. Found: C 67.46, H 9.76, N 4.75. The compound is liquid-crystalline: Cr 215 Cub 275 I.

(m) [EuCl$_3$(L$_{IX}$)$_2$(H$_2$O)]

Orange powder. Yield: 80%. Calcd. for C$_{122}$H$_{192}$Cl$_3$EuN$_8$O$_6$·3H$_2$O: C 67.24, H 9.16, N 5.14. Found: C 67.18, H 9.11, N 4.82. The compound is liquid-crystalline: Cr 228 Cub 255 I.

(n) [GdCl$_3$(L$_{IX}$)$_2$(H$_2$O)]

Yellow powder. Yield: 93%. Calcd. for C$_{122}$H$_{192}$Cl$_3$GdN$_8$O$_6$·H$_2$O: C 68.20, H 9.10, N 5.22. Found: C 68.05, H 9.35, N 4.77. M.p.: 235 °C.

(o) [TbCl$_3$(L$_{IX}$)$_2$(H$_2$O)]

Orange powder. Yield: 89%. Calcd. for C$_{122}$H$_{192}$Cl$_3$TbN$_8$O$_6$·2H$_2$O: C 67.58, H 9.11, N 5.17. Found: C 67.63, H 8.91, N 4.87. M.p.: 243 °C.

(p) [DyCl$_3$(L$_{IX}$)$_2$(H$_2$O)]

Yellow powder. Yield: 89%. Calcd. for C$_{122}$H$_{192}$Cl$_3$DyN$_8$O$_6$·2H$_2$O: C 67.47, H 9.10, N 5.16. Found: C 67.48, H 9.10, N 4.91. M.p.: 245 °C.

(q) [HoCl$_3$(L$_{IX}$)$_2$(H$_2$O)]

Orange powder. Yield: 76%. Calcd. for C$_{122}$H$_{192}$Cl$_3$HoN$_8$O$_6$·3H$_2$O: C 66.84, H 9.10, N 5.11. Found: C 66.78, H 8.89, N 4.80. M.p.: 245 °C.

3.8 References

1. Sammes, P. G.; Yahioglu, G. *Chem. Soc. Rev.* **1994,** *23,* 327-334.

2. Date, R. W.; Iglesias, E. F.; Rowe, K. E.; Elliott, J. M.; Bruce, D. W. *Dalton Trans.* **2003,** 1914-1931.

3. Cardinaels, T.; Driesen, K.; Parac-Vogt, T. N.; Heinrich, B.; Bourgogne, C.; Guillon, D.; Donnio, B.; Binnemans, K. *Chem. Mater.* **2005,** *17,* 6589-6598.

4. Cardinaels, T.; Ramaekers, J.; Guillon, D.; Donnio, B.; Binnemans, K. *J. Am. Chem. Soc.* **2005,** *127,* 17602-17603.

5. Ziessel, R.; Pickaert, G.; Camerel, F.; Donnio, B.; Guillon, D.; Cesario, M.; Prange, T. *J. Am. Chem. Soc.* **2004,** *126,* 12403-12413.

6. Bousquet, S. J. P.; Bruce, D. W. *J. Mater. Chem.* **2001,** *11,* 1769-1771.

7. Bian, Z. Q.; Wang, K. Z.; Jin, L. P.; Gao, L. H. *Synth. Commun.* **2003,** *33,* 3477-3482.

8. Hiort, C.; Lincoln, P.; Norden, B. *J. Am. Chem. Soc.* **1993,** *115,* 3448-3454.

9. Cardinaels, T. Liquid-crystalline complexes of transition metals and rare earths with substituted 1,10-phenanthroline ligands. K.U.Leuven, 2006.

10. Steck, E. A.; Day, A. R. *J. Am. Chem. Soc.* **1943,** *65,* 452-456.

11. Mao, J.-G.; Jin, Z.-S.; Ni, J.-Z. *Chin. J. Struct. Chem.* **1994,** *13,* 377-381.

12. Binnemans, K.; Jongen, L.; Görller-Walrand, C.; D'Olieslager, W.; Hinz, D.; Meyer, G. *Eur. J. Inorg. Chem.* **2000,** 1429-1436.

13. Binnemans, K.; Van Deun, R.; Bruce, D. W.; Galyametdinov, Y. G. *Chem. Phys. Lett.* **1999,** *300,* 509-514.

14. Terazzi, E.; Torelli, S.; Bernardinelli, G.; Rivera, J. P.; Benech, J. M.; Bourgogne, C.; Donnio, B.; Guillon, D.; Imbert, D.; Bünzli, J. C. G.; Pinto, A.; Jeannerat, D.; Piguet, C. *J. Am. Chem. Soc.* **2005,** *127,* 888-903.

15. Piguet, C.; Bünzli, J. C. G.; Donnio, B.; Guillon, D. *Chem. Commun.* **2006,** 3755-3768.

16. Terazzi, E.; Suarez, S.; Torelli, S.; Nozary, H.; Imbert, D.; Mamula, O.; Rivera, J. P.; Guillet, E.; Benech, J. M.; Bernardinelli, G.; Scopelliti, R.; Donnio, B.; Guillon, D.; Bünzli, J. C. G.; Piguet, C. *Adv. Funct. Mater.* **2006,** *16,* 157-168.

17. Diele, S. *Curr. Opin. Colloid Interface Sci.* **2002,** *7,* 333-342.

18. Imperor-Clerc, M. *Curr. Opin. Colloid Interface Sci.* **2005,** *9,* 370-376.

19. Kutsumizu, S. *Curr. Opin. Solid State Mater. Sci.* **2002,** *6,* 537-543.

20. Tschierske, C. *Curr. Opin. Colloid Interface Sci.* **2002,** *7,* 69-80.

21. Diele, S.; Goring, P. Thermotropic Cubic Phases. In *Handbook of Liquid Crystals;* Demus, D.; Goodby, J. W.; Gray, G. W.; Spiess, H.-W.; Vill, V., Eds.; Wiley-VCH: Weinheim, 1998; pp 887-900.

22. Fazio, D.; Mongin, C.; Donnio, B.; Galerne, Y.; Guillon, D.; Bruce, D. W. *J. Mater. Chem.* **2001,** *11,* 2852-2863.

23. Bury, I.; Heinrich, B.; Bourgogne, C.; Guillon, D.; Donnio, B. *Chem. Eur. J.* **2006,** *12,* 8396-8413.

24. Dickeson, J. E.; Summers, L. A. *Australian Journal of Chemistry* **1970,** *23,* 1023-&.

25. Nguyen, H. T.; Destrade, C.; Malthete, J. *Liq. Cryst.* **1990,** *8,* 797-811.

Chapter 4: Promotion of liquid-crystalline behavior of metallomesogens by electrostatic interactions

4.1 Introduction

In the previous chapter, we introduced imidazo*[4,5-f]*-1,10-phenanthrolines as a class of ligands for the design of metallomesogens.[1] These imidazo*[4,5-f]*-1,10-phenanthrolines are versatile ligands because of their easy substitution and because they can coordinate to various metal ions, leading to complexes with different ligand-to-metal ratios. By attaching cyanobiphenyl groups via long alkyl spacers to the parent ligand, it was possible to design the first examples of nematogenic lanthanide(III) complexes. However, the results for the imidazo*[4,5-f]*-1,10-phenanthrolines with alkyl chains (without mesogenic groups attached) were rather disappointing, because none of the ligands and only few metal complexes showed liquid-crystalline behavior.[2] One of the most interesting metal complexes was the uranyl compound with three imidazo*[4,5-f]*-1,10-phenanthroline ligands and triflate counter ions, which exhibited a hexagonal columnar phase over a wide temperature range.[3] This lead us to the hypothesis that the mesophase-promoting effect was (at least partially) due to the electrostatic interactions between the anions and the large cationic cores. In this chapter, we present another example of promotion of liquid-crystalline behavior by electrostatic interactions. The neutral rhenium(I) complexes of the imidazo*[4,5-f]*-1,10-phenanthrolines and the similar pyrazino*[2,3-f]*-1,10-phenanthrolines are not liquid-crystalline, whereas the corresponding ionic ruthenium(II) complexes form a smectic A mesophase. A structural model of the mesophase is proposed on the basis of small-angle X-ray scattering using synchrotron radiation. The transition temperatures of the ionic metallomesogens could be tuned by changing the

counter ion. Examples of ruthenium(II)-containing thermotropic metallomesogens are scarce.[4-6] Lyotropic ruthenium(II) complexes have been studied, because they can act as a template for supported heterogeneous ruthenium catalysts.[7-10] Ruthenium(II) complexes are also of interest because of their excellent photophysical properties,[11-14] so that ruthenium(II)-containing metallomesogens form a class of luminescent liquid crystals. The luminescence properties of the new ionic liquid-crystalline ruthenium(II) complexes are also described.

4.2 Synthesis and characterization

4.2.1 Synthesis and characterization of the ligands

The synthesis of the ligands L_V and L_{X-XIII} is outlined in Scheme 4.1. The 2-substituted imidazo*[4,5-f]*-1,10-phenanthroline L_V was prepared by a condensation reaction between 1,10-phenanthroline-5,6-dione and 3,4-dioctadecyloxybenzaldehyde, following a literature procedure.[2] The pyrazino*[2,3-f]*-1,10-phenanthroline L_{X-XIII} were synthesized via two reaction steps. The first step consists of the condensation between 1,10-phenanthroline-5,6-dione and 4,5-dichlorobenzene-1,2-diamine to afford precursor **11**. The second step is the nucleophilic aromatic substitution of **11** by the corresponding 1-alkanethiolate.[15] A series was synthesized with various chain lengths (SC_6H_{13}, $SC_{10}H_{21}$, $SC_{14}H_{29}$, $SC_{18}H_{37}$, L_X, L_{XI}, L_{XII}, and L_{XIII}, respectively).
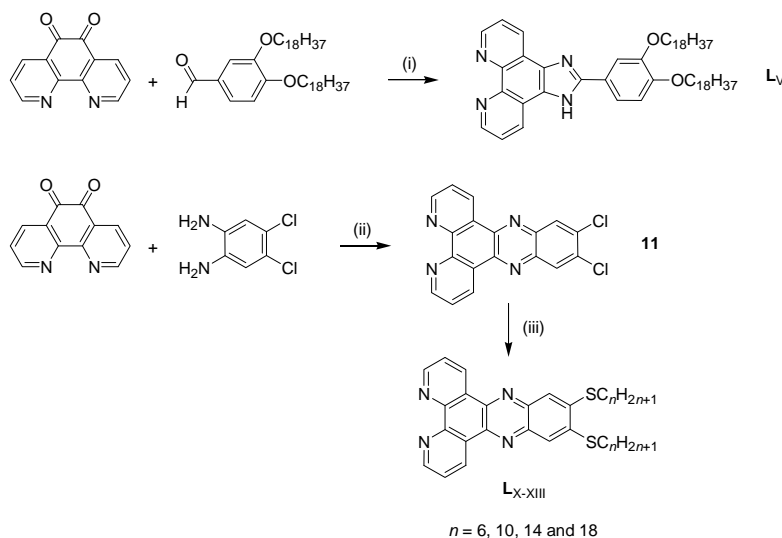
Scheme 4.1: (i) CH₃COOH, CH₃COONH₄, 85 °C; (ii) CH₃COOH, 100 °C; (iii) CₙH₂ₙ₊₁SH, K₂CO₃, DMF, 85 °C.

An overview of the different ligands is given in Figure 4.1. All the ligands were characterized by CHN analysis, ^{1}H NMR spectroscopy and by mass spectrometry.
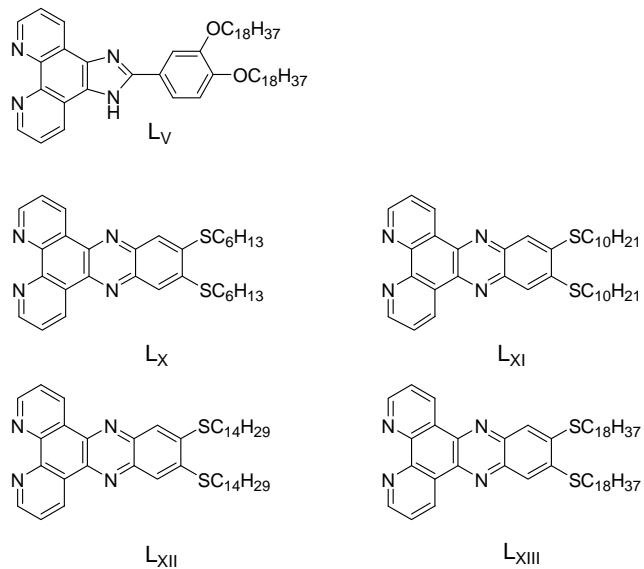
Figure 4.1: Overview of the pyrazino[2,3-f]-1,10-phenanthroline ligands.

4.2.2 Synthesis and characterization of the rhenium(I) complexes

The rhenium(I) complexes [ReBr(CO)$_3$**L$_{X-XIII}$**] were prepared by reaction between **L$_{X-XIII}$** and [ReBr(CO)$_5$] (1:1 molar ratio) in toluene. The molecular structure of [ReBr(CO)$_3$**L$_{X-XIII}$**] is presented in Figure 4.2.
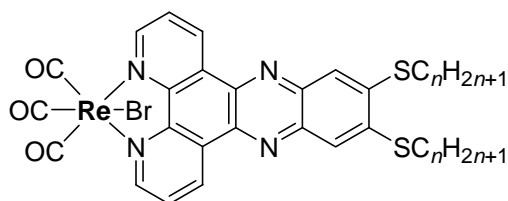
Figure 4.2: Molecular structure of [ReBr(CO)$_3$L$_{X-XII}$] complexes.

All the Rhenium(I) complexes were characterized by CHN analysis, ^{1}H NMR spectroscopy and by mass spectrometry.

4.2.3 Synthesis and characterization of the ruthenium(II) complexes

The molecular structure of the ruthenium(II) complexes is shown in Figure 4.3. Crude [Ru(bipy)$_2$L$_V$]Cl$_2$ and [Ru(bipy)$_2$L$_{XIII}$]Cl$_2$ were prepared by a reaction between L$_V$ and L$_{XIII}$, respectively, and *cis*-[RuCl$_2$(bipy)$_2$](**12**). Then, crude [Ru(bipy)$_2$L$_V$](PF$_6$)$_2$ and [Ru(bipy)$_2$L$_{XIII}$](PF$_6$)$_2$ were synthesized by a metathesis reaction between crude [Ru(bipy)$_2$L$_V$]Cl$_2$ and [Ru(bipy)$_2$L$_{XIII}$]Cl$_2$, respectively, and potassium hexafluorophosphate. [Ru(bipy)$_2$L$_V$](PF$_6$)$_2$ and [Ru(bipy)$_2$L$_{XIII}$](PF$_6$)$_2$ were purified by column chromatography on alumina. This synthetic sequence was used because it is not possible to purify [Ru(bipy)$_2$L$_V$]Cl$_2$ and [Ru(bipy)$_2$L$_{XIII}$]Cl$_2$ using column chromatography (these chloride complexes are too heavily adsorbed on alumina or silica). Pure [Ru(bipy)$_2$L$_V$]Cl$_2$ and [Ru(bipy)$_2$L$_{XIII}$]Cl$_2$ were prepared by a metathesis reaction between pure [Ru(bipy)$_2$L$_V$](PF$_6$)$_2$ and [Ru(bipy)$_2$L$_{XIII}$](PF$_6$)$_2$, respectively, and lithium chloride. [Ru(bipy)$_2$L$_V$](NTf$_2$)$_2$ and [Ru(bipy)$_2$L$_{XIII}$](NTf$_2$)$_2$ were synthesized by a metathesis reaction between [Ru(bipy)$_2$L$_V$]Cl$_2$ and [Ru(bipy)$_2$L$_{XIII}$]Cl$_2$, respectively, and lithium bis(trifluoromethylsulfonyl)imide (LiNTf$_2$).
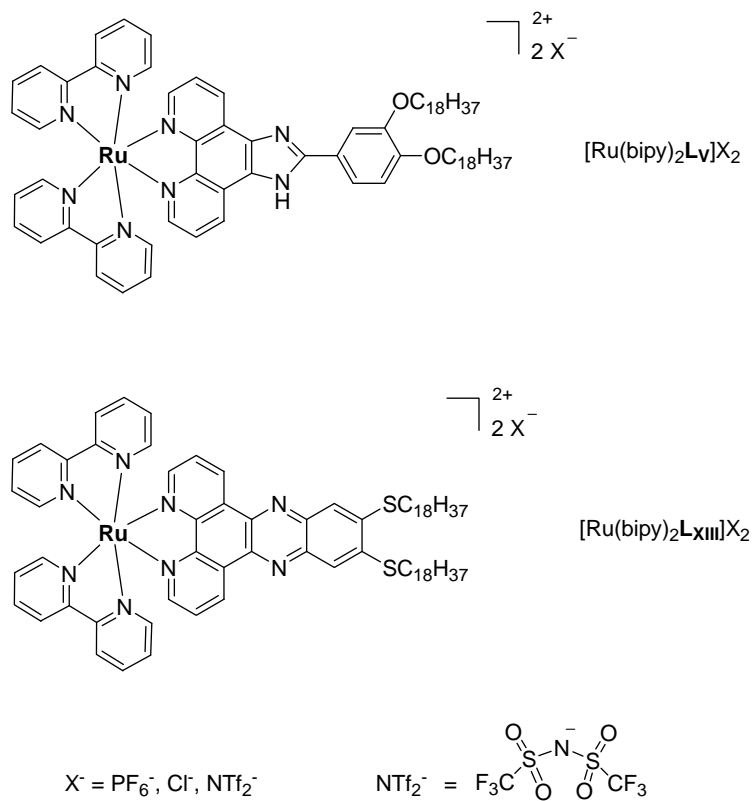
Figure 4.3: Molecular structure of the ruthenium(II) complexes.

All the Ruthenium(II) complexes were characterized by CHN analysis, ^{1}H NMR spectroscopy and by mass spectrometry.

4.3 Thermal behavior

4.3.1 Thermal behavior of the ligands

The thermal behavior of the imidazo*[4,5-f]*-1,10-phenanthroline **L$_V$** is already described in chapter 3.

The pyrazino*[2,3-f]*-1,10-phenanthroline **L$_{X-XIII}$** ligands were not liquid-crystalline and melted to the isotropic liquid at 157 °C, 133 °C, 122 °C and 119 °C. A typical decrease of the melting point by increasing chain length is shown (Figure 4.4).
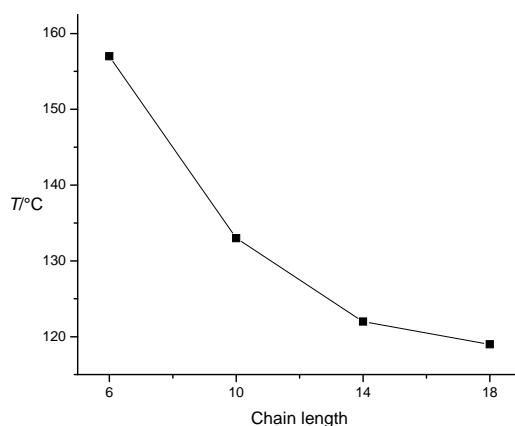
Figure 4.4: Melting temperature of the pyrazino[2,3-f]*-1,10-phenanthroline L$_{X-XIII}$ ligands as a function of the number of carbon atoms in the alkyl chain.*

4.3.2 Thermal behavior of the rhenium(I) complexes

The rhenium(I) complexes have a large dipole moment due to the polar Re-Br bond of the bulky [ReBr(CO)$_3$] fragment. This dipole is expected to influence the arrangement of the molecules in the mesophase and the solid

phase. The rhenium(I) complexes have a significant higher melting point than the corresponding ligands. None of the rhenium(I) complexes show liquid-crystalline behavior. The melting temperatures of the rhenium(I) complexes decreases by elongation of the substituted alkyl chains (Figure 4.5).
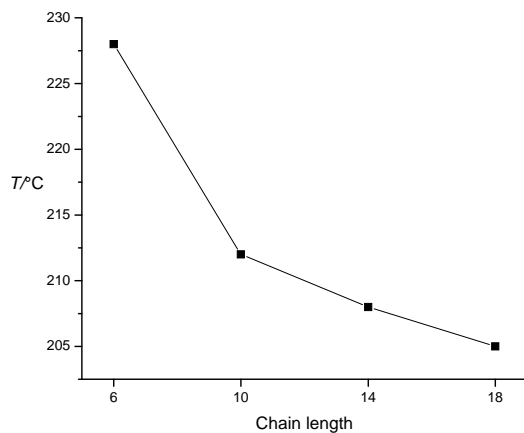
Figure 4.5: Melting temperatures of the rhenium(I)-complexes as a function of the number of carbon atoms in the alkyl chain.

4.3.3 Thermal behavior of the ruthenium(II) complexes

The thermal properties of all the ruthenium(II) complexes were examined by polarizing optical microscopy (POM), differential scanning calorimetry (DSC) and for some of them by X-ray diffraction on powder samples (see below). The thermal data for all the ruthenium(II) complexes are collected in Table 4.1.

Table 4.1: Thermal data for the ruthenium(II) complexes.

Compound	Thermal behavior[a,b]
$[Ru(bipy)_2\mathbf{L_V}]Cl_2$	Cr 227 SmA dec ~ 250
$[Ru(bipy)_2\mathbf{L_{XIII}}]Cl_2$	Cr 197 SmA dec ~ 250
$[Ru(bipy)_2\mathbf{L_V}](PF_6)_2$	Cr 185 SmA dec ~ 300
$[Ru(bipy)_2\mathbf{L_{XIII}}](PF_6)_2$	Cr 173 SmA dec ~ 300
$[Ru(bipy)_2\mathbf{L_V}](NTf_2)_2$	Cr 76 SmA 188 I
$[Ru(bipy)_2\mathbf{L_{XIII}}](NTf_2)_2$	Cr 53 I

[a] Abbreviations: Cr = crystalline or partially crystalline phase; SmA = smectic A phase; I = isotropic liquid; dec = decomposition.
[b] All the transition temperatures listed in this table are those observed by POM.

A typical DSC trace of $[Ru(bipy)_2\mathbf{L_V}](NTf_2)_2$ is shown in Figure 4.6. Except for $[Ru(bipy)_2\mathbf{L_{XIII}}](NTf_2)_2$, all the ruthenium(II) complexes showed enantiotropic SmA phases, which were identified by their optical textures, observed by polarizing optical microscopy. The SmA phases were recognized by the formation of bâtonnets on cooling from the isotropic liquid. On further cooling, an oily streak texture containing homeotropic domains (Figure 4.7 - left) or a focal conic texture (Figure 4.7 - right) was formed.

103
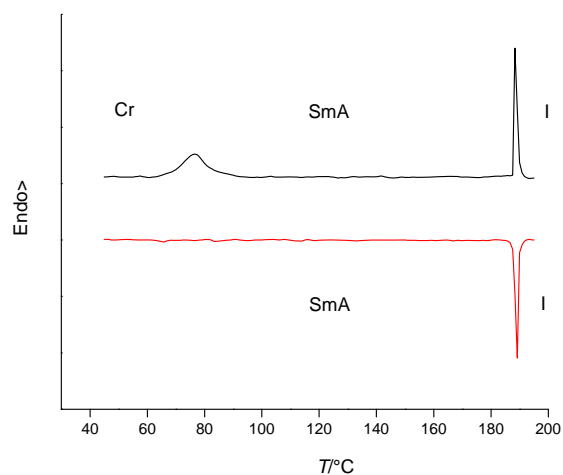
*Figure 4.6: DSC trace of [Ru(bipy)$_2$**L$_V$**](NTf$_2$)$_2$ (first heating/cooling run; heating/cooling rate of 10 °C min^{-1}). The heating run is shown in black whereas the cooling run is shown in red. Abbreviations: Cr = crystalline or partially crystalline phase; SmA = smectic A phase; I = isotropic liquid.*

*Figure 4.7: Left: oily streak texture of the SmA phase of [Ru(bipy)$_2$**L$_V$**](NTf$_2$)$_2$ at 178 °C (200× magnification). Right: focal conic texture of the SmA phase of [Ru(bipy)$_2$**L$_V$**](NTf$_2$)$_2$ at 165 °C (200× magnification).*

The observation of SmA phases could be expected. Indeed, lamellar mesophases are most commonly observed for ionic (metal-containing) liquid crystals.[16] The strong, isotropic electrostatic forces between neigboring ruthenium(II) complexes stabilize a lamellar arrangement.

The lack of mesomorphism observed for $[Ru(bipy)_2\mathbf{L_{XIII}}](NTf_2)_2$ was very surprising because the analogous bistriflimide complex $[Ru(bipy)_2\mathbf{L_V}](NTf_2)_2$ did show a smectic A phase. In addition, the transition temperatures of the ruthenium(II) complexes containing the same counterions are similar (although slightly lower for the ruthenium(II) complexes of $\mathbf{L_{XIII}}$). A possible reason for this is that in the case of $[Ru(bipy)_2\mathbf{L_{XIII}}](NTf_2)_2$, $\mathbf{L_{XIII}}$ is rigid and cannot form any hydrogen bonds with neigboring ruthenium(II) complexes. On the contrary, in the case of $[Ru(bipy)_2\mathbf{L_V}](NTf_2)_2$, $\mathbf{L_V}$ is flexible (because of the single bond between the imidazole ring and the terminal phenyl ring) and can form hydrogen bonds with neigboring ruthenium(II) complexes via the N-H group of the imidazole ring. Indeed, in the crystal structure of an analogous ligand of $\mathbf{L_V}$ (containing one hexyloxy chain instead of two octadecyloxy chains), it is clear that these ligands form strong hydrogen bonds.[2]

The influence of the type of counterion (PF_6-, Cl- and NTf_2-) is straightforward but large. The highest transition temperatures were observed for the ruthenium(II) complexes containing (small) chloride anions ($[Ru(bipy)_2\mathbf{L_V}]Cl_2$ and $[Ru(bipy)_2\mathbf{L_{XIII}}]Cl_2$) whereas the lowest transition temperatures were observed for the ruthenium(II) complexes containing (large) bistriflimide anions ($[Ru(bipy)_2\mathbf{L_V}](NTf_2)_2$ and $[Ru(bipy)_2\mathbf{L_{XIII}}](NTf_2)_2$). Introduction of bistriflimide anions lowered the transition temperatures by more than 100 °C! $[Ru(bipy)_2\mathbf{L_V}](NTf_2)_2$ and $[Ru(bipy)_2\mathbf{L_{XIII}}](NTf_2)_2$ melted below 100 °C and consequently are ionic liquids. Unfortunately, except for $[Ru(bipy)_2\mathbf{L_V}](NTf_2)_2$, all the mesomorphic ruthenium(II) complexes decompose before reaching the clearing point and the chloride complexes ($[Ru(bipy)_2\mathbf{L_V}]Cl_2$ and $[Ru(bipy)_2\mathbf{L_{XIII}}]Cl_2$) were thermally less stable than the

hexafluorophosphate complexes ($[Ru(bipy)_2\mathbf{L_V}](PF_6)_2$ and $[Ru(bipy)_2\mathbf{L_{XIII}}](PF_6)_2$).

All the mesomorphic ruthenium(II) complexes were studied by small-angle X-ray scattering (SAXS) on powder samples. The data collected from the SAXS patterns are presented in Table 4.2. The nature of the smectic A phases of $[Ru(bipy)_2\mathbf{L_V}](PF_6)_2$, $[Ru(bipy)_2\mathbf{L_{XIII}}](PF_6)_2$, $[Ru(bipy)_2\mathbf{L_V}]Cl_2$, $[Ru(bipy)_2\mathbf{L_{XIII}}]Cl_2$ and $[Ru(bipy)_2\mathbf{L_V}](NTf_2)_2$ were confirmed by SAXS. SAXS patterns typical for smectic phases were recorded (Figure 4.8 shows a typical SAXS pattern of $[Ru(bipy)_2\mathbf{L_V}](NTf_2)_2$). Several sharp reflections in the reciprocal spacing ratio 1:2:3 or 1:3 were observed (Table 2), corresponding to the lamellar periodicity (layer thickness) $d = 52.52$ Å, 46.79 Å, 53.61 Å, 49.39 Å, and 51.05 Å for $Ru(bipy)_2\mathbf{L_I}](PF_6)_2$, $[Ru(bipy)_2\mathbf{L_{XIII}}](PF_6)_2$, $[Ru(bipy)_2\mathbf{L_V}]Cl_2$, $[Ru(bipy)_2\mathbf{L_{XIII}}]Cl_2$ and $[Ru(bipy)_2\mathbf{L_V}](NTf_2)_2$, respectively. The relative intensities of these reflections depend on the internal (electron density) structure of the stacked layers.
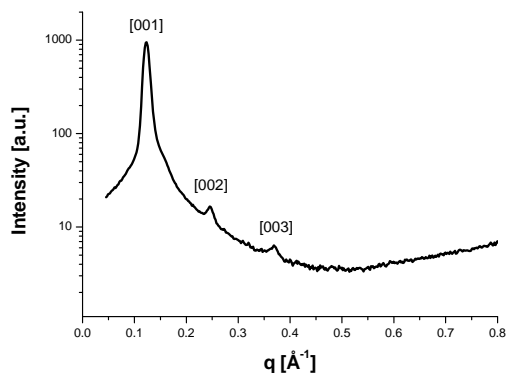
*Figure 4.8: SAXS pattern of [Ru(bipy)₂**L**ᵥ](NTf₂)₂ showing the smectic phase.*

Table 4.2: Bragg reflections collected from the SAXS patterns of all the mesomorphic ruthenium(II) complexes.

Compound	$T/°C$	$d_{exp}/Å$ [a]	$[hkl]$ [b]	I [c]	$d_{theo}/Å$ [a,d]	Parameters [d]
[Ru(bipy)$_2$**L$_V$**] (PF$_6$)$_2$	200	52.38	001	VS (sh)	52.52	SmA
		17.55	003	W (sh)	17.51	$d = 52.52$ Å
						$V_{mol} = 2885$ Å^3
						$A_M = 109.86$ Å^2
						$A_{CH} = 27.47$ Å^2
[Ru(bipy)$_2$**L$_{XIII}$**] (PF$_6$)$_2$	200	46.72	001	VS (sh)	46.79	SmA
		23.36	002	W (sh)	23.39	$d = 46.79$ Å
		15.64	003	W (sh)	15.60	$V_{mol} = 2919$ Å^3
						$A_M = 124.77$ Å^2
						$A_{CH} = 31.19$ Å^2
[Ru(bipy)$_2$**L$_V$**] Cl$_2$	240	53.60	001	VS (sh)	53.61	SmA
		17.87	003	W (sh)	17.87	$d = 53.61$ Å
						$V_{mol} = 2540$ Å^3
						$A_M = 94.76$ Å^2
						$A_{CH} = 23.69$ Å^2
[Ru(bipy)$_2$**L$_{XIII}$**] Cl$_2$	240	49.39	001	VS (sh)	49.39	SmA
		16.46	003	W (sh)	16.46	$d = 49.39$ Å
						$V_{mol} = 2575$ Å^3
						$A_M = 104.27$ Å^2
						$A_{CH} = 26.07$ Å^2
[Ru(bipy)$_2$**L$_V$**] (NTf$_2$)$_2$	140	50.84	001	VS (sh)	51.05	SmA
		25.61	002	W (sh)	25.53	$d = 51.05$ Å
		17.03	003	W (sh)	17.02	$V_{mol} = 3259$ Å^3
						$A_M = 127.68$ Å^2
						$A_{CH} = 31.92$ Å^2

[a] d_{exp} and d_{theo} are the experimentally measured and theoretical diffraction spacings. The distances are given in Å. [b] [*hkl*] are the Miller indices of the reflections. [c] Intensity of the reflections: VS: very strong, W: weak; sh stands for sharp reflections. [d] d_{theo} and the mesophases parameters d and A_M are deduced from the following mathematical expressions: $d = <d_{001}> = [\Sigma_l d_{00l}.l]/N_{00l}$ where N_{00l} is the number of *00l* reflections, the molecular area $A_M = 2V_{mol}/d$ and $A_{CH} = A_M/4$. V_{mol} is the molecular volume: $V_{mol} = M/0.6022\rho$, where $\rho = 27.0673/V_{CH2}$ and M is the molecular weight (g mol^{-1}) ($V_{CH2} = 26.5616 + 0.02023T$ (T in °C)). Abbreviations: SmA = smectic A phase.

Because the layer thickness d is approximately 1.2×L (L is the molecular length), a molecular model is proposed in which the molecules are arranged head-to-head, leading to a microphase separation between ionic parts and aliphatic chains (Figure 4.9). In this way, the molecular area of two ionic fragments $A_M = 2V_{mol}/d$ is found to be 95-128 Å^2 (V_{mol} is calculated using the relation $V_{mol} = (M/0.6022)f$, where M is the molecular mass (g mol^{-1}) and f is a temperature correcting factor ($f = 0.9813 + 7.474.10^{-4}T$; T in °C). Moreover, such a large molecular area has to be counterbalanced by four aliphatic chains, resulting in a molecular cross-sectional area per aliphatic chain of $A_{CH} = A_M/4 = 24$-32 Å^2. This can only be achieved by a complete interdigitation of the aliphatic chains, wich is supported by the fact that d is only 1.2×L. The molecular area of the ionic fragments depends on the size of the anions but also on the ligand type. When comparing [Ru(bipy)$_2$**L$_V$**]Cl$_2$ and [Ru(bipy)$_2$**L$_V$**](NTf$_2$)$_2$, the molecular area of the ionic fragment of [Ru(bipy)$_2$**L$_V$**]Cl$_2$ ($A_M = 94.76$ Å^2) is much smaller than that of [Ru(bipy)$_2$**L$_V$**](NTf$_2$)$_2$ ($A_M = 127.68$ Å^2). The larger molecular area in the case of [Ru(bipy)$_2$**L$_V$**](NTf$_2$)$_2$ (caused by the larger NTf$_2$$^-$ ions) is counterbalanced by folding of the aliphatic chains: $A_{CH} = 31.92$ Å^2 for [Ru(bipy)$_2$**L$_V$**](NTf$_2$)$_2$ while $A_{CH} = 23.69$ Å^2 for [Ru(bipy)$_2$**L$_V$**]Cl$_2$. In addition, the layer spacing in the case of [Ru(bipy)$_2$**L$_V$**]Cl$_2$ is larger ($d = 53.61$ Å) than the layer spacing in the case of [Ru(bipy)$_2$**L$_V$**](NTf$_2$)$_2$ ($d = 51.05$ Å). When comparing [Ru(bipy)$_2$**L$_V$**](PF$_6$)$_2$ and [Ru(bipy)$_2$**L$_{XIII}$**](PF$_6$)$_2$, the molecular area of the ionic fragment of [Ru(bipy)$_2$**L$_V$**](PF$_6$)$_2$ ($A_M =$

109.86 $Å^2$) is smaller than that of [Ru(bipy)$_2$**L$_{XIII}$**](PF$_6$)$_2$ (A_M = 124.77 $Å^2$). Again, the larger molecular area in the case of [Ru(bipy)$_2$**L$_{XIII}$**](PF$_6$)$_2$ (caused by the different molecular structure of **L$_{XIII}$**) is counterbalanced by folding of the aliphatic chains: A_{CH} = 31.19 $Å^2$ and d = 46.79 Å for [Ru(bipy)$_2$**L$_{XIII}$**](PF$_6$)$_2$, while A_{CH} = 27.47 $Å^2$ and d = 52.52 Å for [Ru(bipy)$_2$**L$_V$**](PF$_6$)$_2$.

L$_I$, L$_{II}$ =

PF$_6^-$, Cl$^-$, NTf$_2^-$ =   ○

Figure 4.9: Model representing the molecular arrangement in the SmA phase of the mesomorphic ruthenium(II) complexes. The anions represented by blue solid lines lie in the plane of the cations (red). The anions represented by blue dotted lines lie below the plane of the cations (red).

4.4 Lyotropic mesomorphism

The imidazo*[4,5-f]*-1,10-phenanthroline ligand L_V and the corresponding ruthenium(II) complex [Ru(bipy)$_2$$L_V$]Cl$_2$ showed lyotropic mesophase behavior in lactic acid and acetic acid. The compounds were investigated with Lawrence penetration experiments.[17] The surfactant and the solvent are mixed between glass cover slips in such a way that a concentration gradient is established. This provides us a snapshot of the binary phase diagram. The method of this experiment is quite simple: a small amount of surfactant (Figure 4.10-3) is placed on a glass cover slip (Figure 4.10-1) and heated until the surfactant melts. Then a smaller glass cover slip (Figure 4.10-2) is gently placed on top. The cover slips with the surfactant in between are allowed to cool to room temperature. Then, the penetration cell is placed on the hot-stage of a polarizing optical microscope and a droplet of solvent (Figure 4.10-4) is allowed to migrate between the two glass cover slips and the surfactant will slowly dissolve into the solvent.
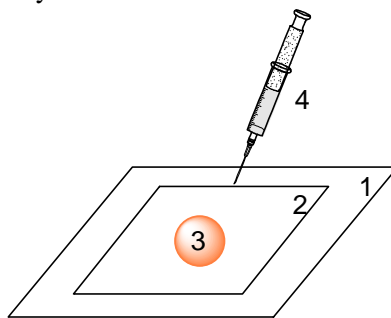
Figure 4.10: Experimental setup of the Lawrence penetration experiment (1 and 2 glass cover slips, 3 sample and 4 solvent).

Eventually a concentration gradient is formed: the concentration varies from 100% of (solid) surfactant in the center of the penetration cell to 100% of solvent at the edges of the penetration cell (Figure 4.11).

110

100% surfactant / 0% solvent

0% surfactant / 100% solvent
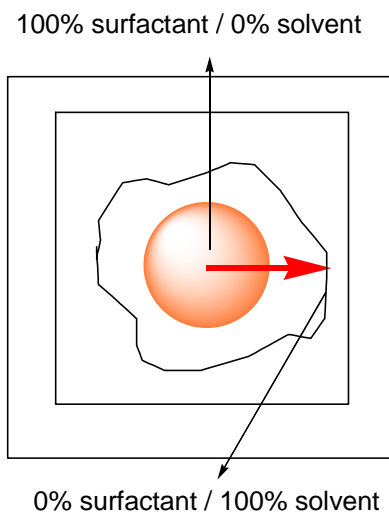
Figure 4.11: Representation of the concentration gradient in a Lawrence experiment.

In Figure 4.12, the optical textures of the lyotropic mesophases, obtained via Lawrence penetration experiments, are shown. Different textures appear in function of the concentration of surfactant. In Figure 4.12a, a penetration cell of L_V in acetic acid is shown. Three phase regions are formed: a lamellar phase (right), a columnar phase (left), and in between a cubic phase, which is optically isotropic. Figure 4.12b shows a penetration cell of L_V in lactic acid. Again, three phase regions are formed: a lamellar phase (right), a columnar phase (left), and the region in between is most likely a two-phase region (lamellar/columnar). A penetration cell of $[Ru(bipy)_2L_V]Cl_2$ in acetic acid is shown in Figure 4.12c. Only one phase is formed, but based on its optical texture, it is impossible to identify the mesophase type. Figure 4.12d shows the penetration cell of $[Ru(bipy)_2L_V]Cl_2$ in lactic acid. Three phase regions are formed: a lamellar phase (bottom), a columnar phase (top), and in between a cubic phase, which is optically isotropic.
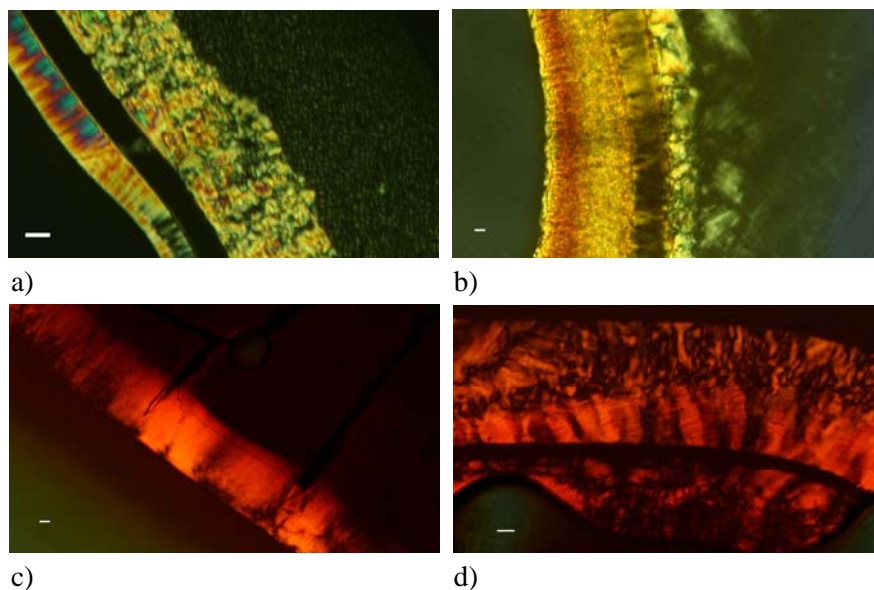
Figure 4.12: Textures of the lyotropic mesophases obtained via Lawrence penetration experiments: a) L_V in acetic acid at 80 °C; b) L_V in lactic acid at 80 °C; c) [Ru(bipy)$_2$$L_V$]Cl$_2$ in acetic acid at 70 °C; d) [Ru(bipy)$_2$$L_V$]Cl$_2$ in lactic acid at 110 °C, the white bar in the picture equals 100μ.

The isotropic region next to the columnar phase is the pure solvent and the isotropic region next to the lammelar phase is the pure solid compound.

Futher investigation of the lyotropic mesophases of L_V and [Ru(bipy)$_2$$L_V$]Cl$_2$ is necessary to unequivocally determine the mesophase type. This will be carried out via X-ray diffraction experiments using synchrotron radiation at ESRF (Grenoble).

4.5 Conclusion

It is commonly thought that the introduction of a bulky metal-containing fragment in liquid-crystalline ligand destabilizes the mesophases and often leads to non-mesomorphic metal complexes. This chapter shows that electrostatic interactions stabilize the mesophases in high coordination number metallomesogens. This is illustrated for imidazo*[4,5-f]*-1,10-phenanthroline and pyrazino*[2,3-f]*-1,10-phenanthroline ligands, which do not exhibit liquid-crystalline phases. Complex formation of these ligands with the $Re(CO)_3Br$ unit does not lead to liquid-crystalline metal complexes. However, the ionic $[Ru(bipy)_2\mathbf{L}]^{2+}$ complexes are liquid-crystalline and the transition temperatures strongly depend on the counter anions. In all cases, a smectic A phase was observed. The ionic character of these complexes leads to the formation of layered structures in the molten state and thus to the formation of mesophases.

4.6 Experimental section

Characterization of the mesophases by X-ray diffraction and discussion was performed in cooperation with Prof. Bart Goderis.

4.6.1 Synthesis of precursors and ligands

(a) Precursor (11)
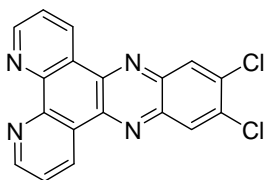
1,10-Phenanthroline-5,6-dione (0.0024 mol, 0.50 g) and 4,5-dichlorobenzene-1,2-diamine (0.0048 mol, 0.85 g) were heated under reflux in glacial acetic acid for 2 hours. The resulting green precipitate was filtered off, washed with water, ethanol, acetone and diethyl ether, and dried in a vacuum oven at 50 °C. Yield: 80% (0.67 g). δ_H (300 MHz, CDCl$_3$): 7.76 (dd, 2H, H-aryl, J_o = 7.8 Hz, J_o = 4.1 Hz), 8.38 (s, 2H, H-aryl), 9.26 (dd, 2H, H-aryl, J_o = 4.1 Hz, J_m = 1.6 Hz), 9.43 (dd, 2H, H-aryl, J_o = 7.8 Hz, J_m = 1.6 Hz). Calcd. for C$_{18}$H$_8$C$_{12}$N$_4$ (351.19): C 61.56, H 2.30, N 15.95. Found: C 61.49, H 2.65, N 15.68. ESI-MS (methanol, m/z): 351.4, [M + H]$^+$. M.p.: 355 °C.

(b) Cis-[RuCl$_2$(bipy)$_2$] (12)
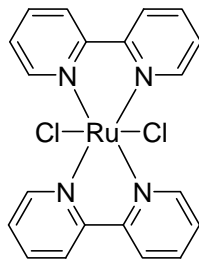
Cis-[RuCl$_2$(bipy)$_2$] was synthesized following a literature procedure:[2] a mixture of RuCl$_3$·3H$_2$O (0.0070 mol, 1.83 g), 2,2'-bipyridine (0.0140 mol, 2.20 g), LiCl (0.0470 mol, 2.00 g) and 20 mL of DMF was refluxed for 8 hours. Then the mixture was cooled and 150 mL of acetone was added. The precipitate was filtered off and washed 3 times with 25 mL of water and 3 times with 25 mL of diethyl ether. The dark green micro-crystalline product was dried under vacuum. Yield: 47% (1.61 g). Calcd. for C$_{20}$H$_{16}$Cl$_2$N$_4$Ru·0.5H$_2$O (484.34): C 48.69, H 3.47, N 11.36. Found: C 48.88, H 3.65, N 11.49. ESI-MS (methanol, m/z): 485.1, [M + H]$^+$.

(c) Ligand L$_X$
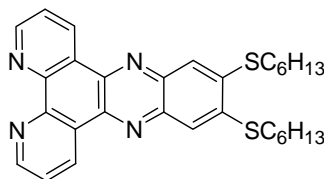
1-Hexanethiol (0.0112 mol, 1.32 g) and potassium carbonate (0.0036 mol, 5.07 g) were added to a solution of **11** (0.0028 mol, 0.99 g) in 100 mL of DMF. The mixture was heated to 85 °C and stirred for 5 days. Then, the reaction mixture was poured into water and the resulting yellow precipitate was filtered off, washed with water and dried. The crude product was

purified on a silica column with CH_2Cl_2/MeOH (95:5) as the eluent. Yield: 72% (1.04 g) δ_H (300 MHz, CDCl$_3$): 0.93 (b, t, 6H, CH$_3$), 1.32-1.44 (m, 8H, CH$_2$), 1.55-1.64 (m, 4H, CH$_2$), 1.85-1.94 (m, 4H, C**H**$_2$-CH$_2$-O), 3.24 (t, 4H, CH$_2$-O, J = 6.4 Hz), 7.76-7.79 (m, 2H, H-aryl), 7.98 (s, 2H, H-aryl), 9.25 (d, 2H, H-aryl, J_o = 1.9 Hz), 9.57 (d, 2H, H-aryl, J_o = 8.3 Hz). Calcd. for $C_{30}H_{34}N_4S_2$ (514.75): C 70.00, H 6.66, N 10.88. Found: C 69.72, H 6.36, N 10.35. ESI-MS (methanol, m/z): 515.8, $[M + H]^+$. M.p.: 157 °C.

(d) Ligand L$_{XII}$
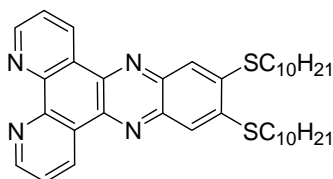
1-Decanethiol (0.0056 mol, 0.98 g) and potassium carbonate (0.0018 mol, 2.53 g) were added to a solution of **11** (0.0014 mol, 0.49 g) in 100 mL of DMF. The mixture was heated to 85 °C and stirred for 5 days. Then, the reaction mixture was poured into water and the resulting yellow precipitate was filtered off, washed with water and dried. The crude product was purified on a silica column with CH_2Cl_2/MeOH (95:5) as the eluent. Yield: 65% (0.57 g). δ_H (300 MHz, CDCl$_3$): 0.87 (b, t, 6H, CH$_3$), 1.25-1.38 (m, 24H, CH$_2$), 1.55-1.59 (m, 4H, CH$_2$), 1.86-1.94 (m, 4H, C**H**$_2$-CH$_2$-O), 3.24 (b, t, 4H, CH$_2$-O), 7.74-7.80 (m, 2H, H-aryl), 8.02 (s, 2H, H-aryl), 9.25 (b, d, 2H, H-aryl), 9.61 (d, 2H, H-aryl, J_o = 8.4 Hz). Calcd. for $C_{38}H_{50}N_4S_2$ (626.96): C 72.80, H 8.04, N 8.94. Found: C 72.48, H 8.40, N 8.55. ESI-MS (methanol, m/z): 628.0, $[M + H]^+$. M.p.: 133 °C.

(e) Ligand L$_{XII}$
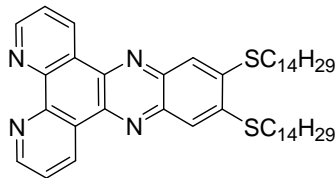
1-Tetradecanethiol (0.0056 mol, 1.29 g) and potassium carbonate (0.0018 mol, 2.53 g) were added to a solution of **11** (0.0014 mol, 0.49 g) in 100 mL of DMF. The mixture was heated to 85 °C and stirred for 5 days. Then, the reaction mixture was poured into water and the resulting yellow precipitate was filtered off, washed with water and dried. The crude product was purified on a silica column with CH$_2$Cl$_2$/MeOH (95:5) as the eluent. Yield: 67% (0.89 g). δ_H (300 MHz, CDCl$_3$): 0.87 (b, t, 6H, CH$_3$), 1.26-1.39 (m, 40H, CH$_2$), 1.58 (m, 4H, CH$_2$), 1.85-1.94 (m, 4H, C**H**$_2$-CH$_2$-O), 3.23 (t, 4H, CH$_2$-O, J = 7.2 Hz), 7.76-7.81 (m, 2H, H-aryl), 8.00 (s, 2H, H-aryl), 9.26 (d, 2H, H-aryl, J_o = 2.8 Hz), 9.59 (d, 2H, H-aryl, J_o = 7.6 Hz). Calcd. for C$_{46}$H$_{66}$N$_4$S$_2$ (739.17): C 74.74, H 9.00, N 7.58. Found: C 74.78, H 8.52, N 7.25. ESI-MS (methanol, m/z): 740.0, [M + H]$^+$. M.p.: 122 °C.

(f) Ligand L$_{XIII}$
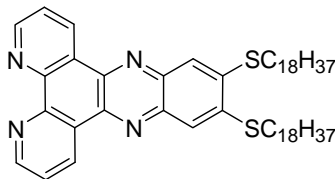
Octadecanethiol (0.0056 mol, 1.60 g) and potassium carbonate (0.0018 mol, 2.53 g) were added to a solution of **11** (0.0014 mol, 0.49 g) in 100 mL of DMF. The mixture was heated to 85 °C and stirred for 5 days. Then, the reaction mixture was poured into water and the resulting yellow precipitate was filtered off, washed with water and dried. The crude product was

purified on a silica column with CH_2Cl_2/MeOH (95:5) as the eluent. Yield: 60% (0.72 g). δ_H (300 MHz, $CDCl_3$): 0.87 (b, t, 6H, CH_3), 1.25-1.39 (m, 56H, CH_2), 1.55-1.59 (m, 4H, CH_2), 1.86-1.96 (m, 4H, CH_2-CH_2-O), 3.25 (t, 4H, CH_2-O, J = 7.6 Hz), 7.77-7.82 (m, 2H, H-aryl), 8.02 (s, 2H, H-aryl), 9.27 (d, 2H, H-aryl, J_o = 4.3 Hz), 9.61 (d, 2H, H-aryl, J_o = 8.3 Hz). Calcd. for $C_{54}H_{82}N_4S_2$·$0.5H_2O$ (851.39): C 75.38, H 9.72, N 6.51. Found: C 75.20, H 10.21, N 6.28. ESI-MS (methanol, m/z): 852.3, $[M + H]^+$. M.p.: 119 °C.

4.6.2 Synthesis of the rhenium(I) complexes

All the rhenium(I) complexes were prepared following the same procedure: rhenium(I) pentacarbonyl bromide (1 eq.) was added to a solution of L_{X-XIII} (1 eq.) in toluene and the mixture was refluxed for 3 hours. Then the solvent was removed under reduced pressure and the crude product was purified on a silica column with $CHCl_3$/hexane (50:50) as the eluent. The complex was dissolved in a minimum amount of $CHCl_3$ and precipitated in methanol. The yellow precipitate was filtered off and dried in a vacuum oven at 50 °C.

(a) $Re(CO)_3Br·L_X$
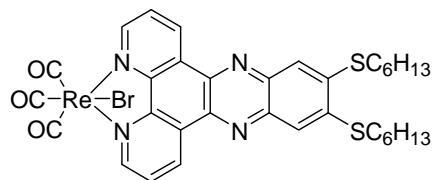
Orange product. Yield: 70%. δ_H (300 MHz, $CDCl_3$): 0.94 (t, 6H, CH_3, J = 7.2 Hz), 1.38-1.44 (m, 8H, CH_2), 1.59-1.67 (m, 4H, CH_2), 1.88-1.98 (m, 4H, CH_2-CH_2-O), 3.27 (t, 4H, CH_2-O, J = 7.3 Hz), 7.95-7.99 (m, 4H, H-aryl), 9.44 (d, 2H, H-aryl, J_o = 5.3 Hz), 9.74 (d, 2H, H-aryl, J_o = 8.1 Hz). Calcd.

for $C_{33}H_{34}BrN_4O_3ReS_2$ (864.89): C 45.83, H 3.96, N 6.48. Found: C 45.59, H 4.01, N 6.1. ESI-MS (methanol, m/z): 887.3, $[M + Na]^+$. M.p.: 228 °C.

(b) Re(CO)$_3$Br·L$_{XI}$
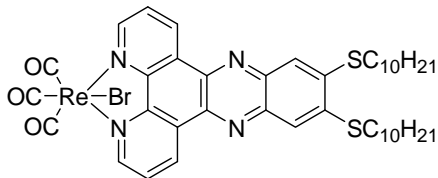
Orange product. Yield: 62%. δ_H (300 MHz, CDCl$_3$): 0.88 (t, 6H, CH$_3$, $J = 6.1$ Hz), 1.29-1.45 (m, 24H, CH$_2$), 1.57-1.67 (m, 4H, CH$_2$), 1.89-1.98 (m, 4H, **CH**$_2$-CH$_2$-O), 3.26 (t, 4H, CH$_2$-O, $J = 7.2$ Hz), 7.90-7.96 (m, 4H, H-aryl), 9.42 (d, 2H, H-aryl, $J_o = 4.4$ Hz), 9.59 (d, 2H, H-aryl, $J_o = 8.2$ Hz). Calcd. for $C_{41}H_{50}BrN_4O_3ReS_2$ (977.10): C 50.40, H 5.16, N 5.73. Found: C 50.16, H 5.50, N 5.30. ESI-MS (methanol, m/z): 977.5, $[M + H]^+$. M.p.: 212 °C.

(c) Re(CO)$_3$Br·L$_{XII}$
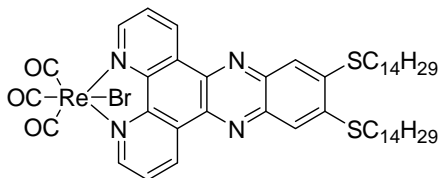
Orange product. Yield: 58%. δ_H (300 MHz, CDCl$_3$): 0.88 (t, 6H, CH$_3$, $J = 6.06$ Hz), 1.26-1.45 (m, 40H, CH$_2$), 1.59-1.66 (m, 4H, CH$_2$), 1.88-1.98 (m, 4H, **CH**$_2$-CH$_2$-O), 3.26 (t, 4H, CH$_2$-O, $J = 7.20$ Hz), 7.93-7.97 (m, 4H, H-aryl), 9.44 (d, 2H, H-aryl, $J_o = 4.74$ Hz), 9.66 (d, 2H, H-aryl, $J_o = 8.13$ Hz). Calcd. for $C_{49}H_{66}BrN_4O_3ReS_2$ (1089.31): C 54.03, H 6.11, N 5.14. Found: C 54.08, H 6.02, N 4.82. ESI-MS (methanol, m/z): 1090.4, $[M + H]^+$. M.p.: 208 °C.

119

(d) Re(CO)₃Br·L_XIII
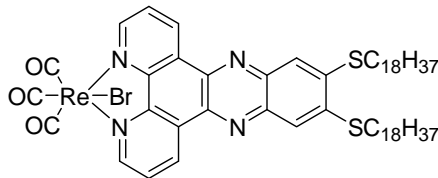
Orange product. Yield: 64%. δ_H (300 MHz, CDCl₃): 0.88 (t, 6H, C**H**₃, J = 6.39 Hz), 1.26-1.44 (m, 52H, C**H**₂), 1.52-1.66 (m, 8H, C**H**₂), 1.88-1.98 (m, 4H, C**H**₂-CH₂-O), 3.27 (t, 4H, C**H**₂-O, J = 7.23 Hz), 7.95-7.99 (m, 4H, H-aryl), 9.44 (d, 2H, H-aryl, J_o = 5.46 Hz), 9.73 (d, 2H, H-aryl, J_o = 8.16 Hz). Calcd. for C₅₇H₈₂BrN₄O₃ReS₂ (1201.53): C 56.98, H 6.88, N 4.66. Found: C 57.06, H 7.20, N 4.40. ESI-MS (methanol, m/z): 1223.4, [M + Na]⁺. M.p.: 205 °C.

4.6.3 Synthesis of the ruthenium(II) complexes

(a) [Ru(bipy)₂L_V](PF₆)₂
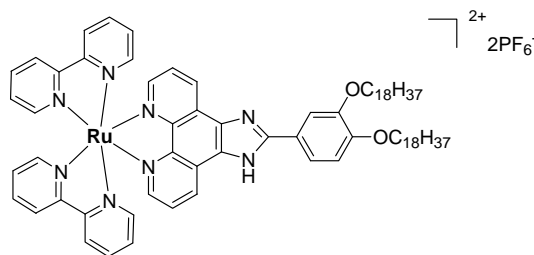
Cis-[RuCl₂(bipy)₂] (0.0015 mol, 0.73 g) was dissolved in 100 mL of a warm ethanol/water (7:3, v/v) mixture under a nitrogen atmosphere and the solution was stirred for one hour at 80 °C. Then **L_V** (0.0015 mol, 1.22) was added and the mixture was refluxed overnight under a nitrogen atmosphere after which the solution became clearly red. Ethanol was removed under

120

reduced pressure and a saturated solution of KPF$_6$ in water was added. A red precipitate was formed, filtered off and washed with water. The crude product was purified on an alumina column with acetonitrile/toluene (2:1, v/v) as the eluent. The product was dissolved in a minimum amount of ethanol and precipitated in hexane. The red precipitate was filtered off and dried in a vacuum oven at 50 °C. Yield: 79% (1.76 g). δ_H (300 MHz, CDCl$_3$): 0.85-0.89 (m, 6H, CH$_3$), 1.24-1.25 (m, 56H, CH$_2$), 1.42-1.49 (m, 4H, CH$_2$), 1.81 (b, m, 4H, **CH**$_2$-CH$_2$-O), 3.99 (b, t, 2H, CH$_2$-O), 4.10 (b, t, 2H, CH$_2$-O), 6.94 (d, 1H, H-aryl, J_o = 6.1 Hz), 7.16-7.24 (m, 2H, H-aryl), 7.37-7.46 (m, 3H, H-aryl), 7.53-7.60 (m, 2H, H-aryl), 7.73-7.77 (m, 3H, H-aryl), 7.84-7.97 (m, 8H, H-aryl), 8.37-8.43 (m, 4H, H-aryl), 9.04-9.09 (m, 2H, H-aryl), 11.95 (b, s, 1H, N-H). Calcd. for C$_{75}$H$_{100}$F$_{12}$N$_8$O$_2$P$_2$Ru (1536.65): C 58.62, H 6.56, N 7.29. Found: C 58.47, H 6.82, N 7.01. ESI-MS (methanol, m/z): 623.7, [M − 2PF$_6$]$^{2+}$.

(b) [Ru(bipy)$_2$L$_{XIII}$](PF$_6$)$_2$
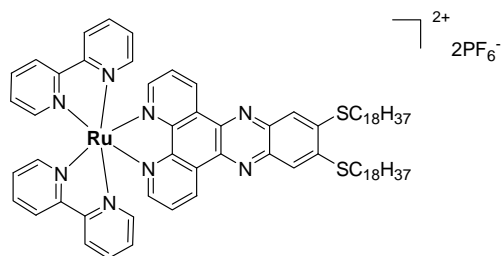
[Ru(bipy)$_2$**L$_{XIII}$**](PF$_6$)$_2$ was prepared starting from *Cis*-[RuCl$_2$(bipy)$_2$] (0.0006 mol, 0.30 g) and **L$_{XIII}$** (0.0006 mmol, 0.53 g) using the same procedure as described for [Ru(bipy)$_2$**L$_V$**](PF$_6$)$_2$ to yield the product as a red powder. Yield: 74% (1.30 g). δ_H (400 MHz, CDCl$_3$): 0.87 (t, 6H, CH$_3$, J = 6.8 Hz), 1.25-1.42 (m, 56H, CH$_2$), 1.55-1.62 (m, 4H, CH$_2$), 1.86-1.93 (m, 4H, **CH**$_2$-CH$_2$-O), 3.24 (t, 4H, CH$_2$-O, J = 7.2 Hz), 7.35 (t, 2H, H-aryl, J = 6.5 Hz), 7.52 (t, 2H, H-aryl, J = 6.4Hz), 7.74 (d, 2H, H-aryl, J_o = 5.3 Hz), 7.87 (d, 2H, H-aryl, J_o = 5.2 Hz), , 7.90-7.95 (m, 4H, H-aryl), 7.97 (s, 2H,

H-aryl), 8.02 (t, 2H, H-aryl, J = 7.76 Hz), 8.17 (d, 2H, H-aryl, J_o = 4.88 Hz), 8.41-8.46 (m, 4H, H-aryl), 9.60 (d, 2H, H-aryl, J_o = 8.1 Hz). Calcd. for $C_{74}H_{98}F_{12}N_8P_2RuS_2$ (1554.75): C 57.17, H 6.35, N 7.21. Found: C 56.98, H 6.50, N 6.95. ESI-MS (methanol, m/z): 1409.6, $[M - PF_6]^+$.

(c) [Ru(bipy)$_2$L$_V$]Cl$_2$
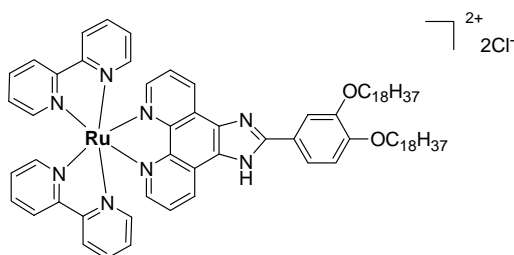
A saturated solution of LiCl in acetone was added to a solution of [Ru(bipy)$_2$**L$_V$**](PF$_6$)$_2$ (0.0008 mol, 1.21 g) in 20 mL of acetone. An orange precipitate was formed, filtered off, washed with acetone and dried in a vacuum oven at 50 °C. Yield: 98% (1.01 g). δ_H (300 MHz, CDCl$_3$): 0.87 (t, 6H, CH$_3$, J = 6.3 Hz), 1.25-1.56 (m, 60H, CH$_2$), 1.79-1.92 (m, 4H, **CH$_2$**-CH$_2$-O), 4.05 (t, 2H, CH$_2$-O, J = 6.5 Hz), 4.28 (t, 2H, CH$_2$-O, J = 6.4 Hz), 7.00 (d, 1H, H-aryl, J_o = 8.5 Hz), 7.23-7.34 (m, 2H, H-aryl), 7.46-7.47 (m, 1H, H-aryl), 7.52-7.65 (m, 4H, H-aryl), 7.74-7.89 (m, 5H, H-aryl), 8.01-8.06 (m, 2H, H-aryl), 8.10-8.19 (m, 2H, H-aryl), 8.24-8.25 (m, 1H, H-aryl), 8.33 (d, 1H, H-aryl, J_o = 7.9 Hz), 8.86-8.92 (m, 2H, H-aryl), 9.04 (d, 1H, H-aryl, J_o = 7.9 Hz), 9.10 (d, 1H, H-aryl, J_o = 7.8 Hz), 9.18 (d, 1H, H-aryl, J_o = 8.1 Hz), 10.38 (d, 1H, H-aryl, J_o = 8.0 Hz), 15.43 (b, s, 1H, N-H). ESI-MS (methanol, m/z): 623.4, $[M - 2Cl]^{2+}$.

(d) [Ru(bipy)$_2$L$_{XIII}$]Cl$_2$
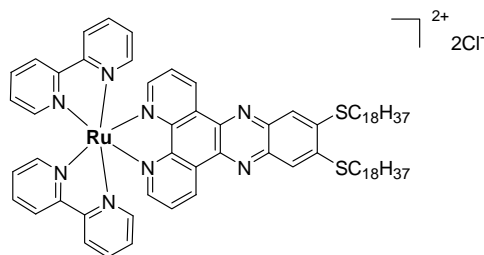
[Ru(bipy)$_2$**L$_{XIII}$**]Cl$_2$ was prepared starting from [Ru(bipy)$_2$**L$_{XIII}$**](PF$_6$)$_2$ (0.0003 mol, 0.40 g) using the same procedure as described for [Ru(bipy)$_2$**L$_V$**]Cl$_2$ to yield the product as a red powder. Yield: 91% (0.31 g). δ_H (400 MHz, CDCl$_3$): 0.87 (t, 6H, CH$_3$, J = 6.8 Hz), 1.25-1.45 (m, 56H, CH$_2$), 1.56-1.63 (m, 4H, CH$_2$), 1.87-1.95 (m, 4H, C**H**$_2$-CH$_2$-O), 3.26 (t, 4H, CH$_2$-O, J = 6.8 Hz), 7.42 (t, 2H, H-aryl, J = 6,1 Hz), 7.63 (t, 2H, H-aryl, J = 5.9 Hz), 7.86 (d, 2H, H-aryl, J_o = 4.8 Hz), 7.97-8.11 (m, 8H, H-aryl), 8,16 (t, 2H, H-aryl, J = 7.44 Hz), 8.40 (d, 2H, H-aryl, J_o = 3.6 Hz), 8.91-8.96 (m, 4H, H-aryl), 9.65 (d, 2H, H-aryl, J_o = 7.9 Hz). ESI-MS (methanol, m/z): 632.6, [M – 2Cl]$^{2+}$.

(e) [Ru(bipy)$_2$L$_V$](NTf$_2$)$_2$
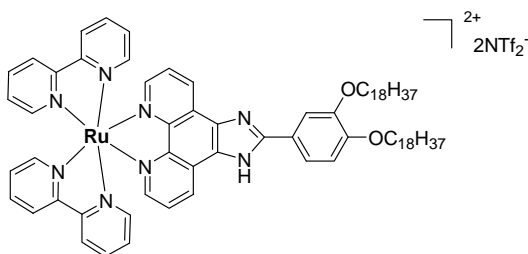
A saturated solution of LiNTf$_2$ (lithiumbis(trifluoromethylsulfonyl)imide) in water was added to a solution of [Ru(bipy)$_2$**L$_V$**]Cl$_2$ (0.0006 mol, 0.78 g) in 50 mL of a warm ethanol/water (1:5, v/v) mixture. A red precipitate was

123

formed, filtered off, washed with water and dried in a vacuum oven at 50 °C. Yield: 82% (0.87 g). δ_H (300 MHz, CDCl$_3$): 0.87 (t, 6H, CH$_3$, J = 6.3 Hz), 1.25-1.48 (m, 60H, CH$_2$), 1.79-1.89 (m, 4H, C**H**$_2$-CH$_2$-O), 4.04 (t, 2H, CH$_2$-O, J = 6.4 Hz), 4.12 (t, 2H, CH$_2$-O, J = 6.2 Hz), 6.99 (d, 1H, H-aryl, J_o = 8.4 Hz), 7.22-7.28 (m, 2H, H-aryl), 7.44-7.55 (m, 4H, H-aryl), 7.72-8.07 (m, 12H, H-aryl), 8.44-8.50 (m, 4H, H-aryl), 9.15 (d, 2H, H-aryl, J_o = 8.2 Hz), 12.13 (b, s, 1H, N-H). Calcd. for C$_{79}$H$_{100}$F$_{12}$N$_{10}$O$_{10}$RuS$_4$ (1807.01): C 52.51, H 5.58, N 7.75. Found: C 52.41, H 5.15, N 7.49. ESI-MS (methanol, m/z): 1526.3, [M – NTf$_2$]$^+$.

(f) [Ru(bipy)$_2$L$_{XIII}$](NTf$_2$)$_2$
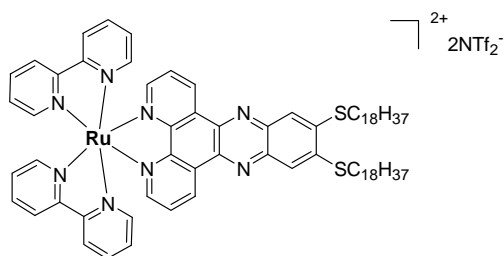
[Ru(bipy)$_2$**L$_{XIII}$**](NTf$_2$)$_2$ was prepared starting from [Ru(bipy)$_2$**L$_{XIII}$**]Cl$_2$ (0.0001 mmol, 0.15 g) using the same procedure as described for [Ru(bipy)$_2$**L$_V$**](NTf$_2$)$_2$ to yield the product as a red powder. Yield: 90% (0.18 g). δ_H (300 MHz, CDCl$_3$): 0.87 (t, 6H, CH$_3$, J = 6.5 Hz), 1.25-1.45 (m, 56H, CH$_2$), 1.52-1.62 (m, 4H, CH$_2$), 1.87-1.94 (m, 4H, C**H**$_2$-CH$_2$-O), 3.27 (t, 4H, CH$_2$-O, J = 7.3 Hz), 7.36-7.40 (m, 2H, H-aryl), 7.57-7.61 (m, 2H, H-aryl), 7.79 (d, 2H, H-aryl, J_o = 5.3 Hz), 7.93-8.12 (m, 10H, H-aryl), 8.24 (d, 2H, H-aryl, J_o = 4.8 Hz), 8.39-8.45 (m, 4H, H-aryl), 9.67 (d, 2H, H-aryl, J_o = 8.1 Hz). Calcd. for C$_{78}$H$_{98}$F$_{12}$N$_{10}$O$_8$RuS$_6$ (1825.12): C 51.33, H 5.41, N 7.67. Found: C 50.86, H 5.53, N 7.20. ESI-MS (methanol, m/z): 1544.6, [M – NTf$_2$]$^+$.

4.7 References

1. Cardinaels, T.; Driesen, K.; Parac-Vogt, T. N.; Heinrich, B.; Bourgogne, C.; Guillon, D.; Donnio, B.; Binnemans, K. *Chem. Mater.* **2005,** *17,* 6589-6598.

2. Cardinaels, T.; Ramaekers, J.; Nockemann, P.; Driesen, K.; Van Hecke, K.; Van Meervelt, L.; Lei, S.; De Feyter, S.; Guillon, D.; Donnio, B.; Binnemans, K. *Chem. Mater.* **2008** (DOI: 10.1021/cm070637i).

3. Cardinaels, T.; Ramaekers, J.; Guillon, D.; Donnio, B.; Binnemans, K. *J. Am. Chem. Soc.* **2005,** *127,* 17602-17603.

4. Barral, M. C.; Jimenez-Aparicio, R.; Priego, J. L.; Royer, E. C.; Torres, M. R.; Urbanos, F. A. *Inorg. Chem. Commun.* **1999,** *2,* 153-155.

5. Bonnet, L.; Cukiernik, F. D.; Maldivi, P.; Giroudgodquin, A. M.; Marchon, J. C.; Ibnelhaj, M.; Guillon, D.; Skoulios, A. *Chem. Mater.* **1994,** *6,* 31-38.

6. Caplan, J. F.; Murphy, C. A.; Swansburg, S.; Lemieux, R. P.; Cameron, T. S.; Aquino, M. A. S. *Can. J. Chem.* **1998,** *76,* 1520-1523.

7. Bruce, D. W.; Holbrey, J. D.; Tajbakhsh, A. R.; Tiddy, G. J. T. *J. Mater. Chem.* **1993,** *3,* 905-906.

8. Danks, M. J.; Jervis, H. B.; Nowotny, M.; Zhou, W. Z.; Maschmeyer, T. A.; Bruce, D. W. *Catal. Lett.* **2002,** *82,* 95-98.

9. Holbrey, J. D.; Tiddy, G. J. T.; Bruce, D. W. *J. Chem. Soc. , Dalton Trans.* **1995,** 1769-1774.

10. Jervis, H. B.; Raimondi, M. E.; Raja, R.; Maschmeyer, T.; Seddon, J. M.; Bruce, D. W. *Chem. Commun.* **1999,** 2031-2032.

11. Balzani, V.; Barigelletti, F.; Decola, L. *Top. Curr. Chem.* **1990,** *158,* 31-71.

12. Balzani, V.; Ceroni, P.; Juris, A.; Venturi, M.; Campagna, S.; Puntoriero, F.; Serroni, S. *Coord. Chem. Rev.* **2001,** *219,* 545-572.

13. Nakamaru, K. *Bull. Chem. Soc. Jpn.* **1982,** *55,* 2697-2705.

14. Sauvage, J. P.; Collin, J. P.; Chambron, J. C.; Guillerez, S.; Coudret, C.; Balzani, V.; Barigelletti, F.; Decola, L.; Flamigni, L. *Chem. Rev.* **1994,** *94,* 993-1019.

15. Kestemont, G.; de Halleux, V.; Lehmann, M.; Ivanov, D. A.; Watson, M. D.; Geerts, Y. H. *Chem. Commun.* **2001,** 2074-2075.

16. Binnemans, K. *Chem. Rev.* **2005,** *105,* 4148-4204.

17. Lawrence A.S.C. *Liq. Cryst. 2,* ed. G. H. Brown, Gordon and Breach, London, 1969, part 1, p. 1.

Chapter 5: Tetracatenars

5.1 Introduction

In this chapter, we report on a rigid extended tetracatenar system derived from 1,10-phenanthroline. The 1,10-phenanthroline unit is extended in the 3- and 8-positions using acetylene linking groups. The mesophase behavior of these ligands and their corresponding rhenium(I) complexes was investigated as a function of the alkoxy chain length. Self-assembled monolayers of the ligands and corresponding rhenium(I) complexes are studied by scanning tunneling microscopy (STM). Also the photophysical properties of the ligands and corresponding rhenium(I) complexes are investigated.

5.2 Synthesis and characterization

5.2.1 Synthesis and characterization of the ligands

For the synthesis of the 1,10-phenanthroline ligands **L$_{XIV}$ - L$_{XVIII}$**, a convergent methodology based on two successive Sonogashira couplings between appropriate aryl halides and phenyl acetylenes was developed (Scheme 5.1).[1,2] In the first step, 3,4-dihydroxybenzaldehyde was *O*-alkylated to give the appropriate benzaldehydes **14a-e**. Then, the benzaldehydes **14a-e** were converted by the Corey-Fuchs procedure[3] into the corresponding dibromo vinylic compounds **15a-e**, following published experimental conditions.[4] The dibromo vinylic compounds **15a-e** were transformed subsequently into the acetylenes **16a-e** by the Grignard reagent, EtMgBr. The first Sonogashira coupling between the acetylenes **16a-e** and
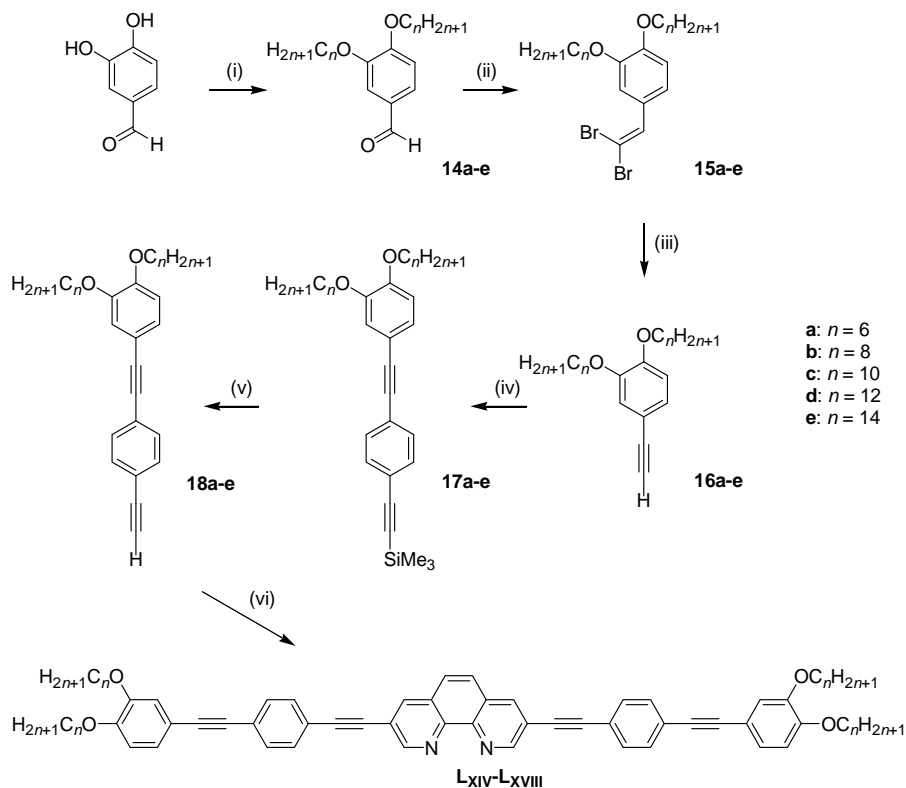
Scheme 5.1: Synthesis of the 1,10-phenanthroline ligands: (i) $C_nH_{2n+1}Br$, K_2CO_3, KI, DMF, reflux; (ii) CBr_4, PPh_3, NEt_3, CH_2Cl_2, 0 °C; (iii) (a) EtMgBr, THF, rt; (b) NH_4Cl, rt; (iv) 4-trimethylsilylethynylbromobenzene, [Pd(PPh₃)₄], piperidine, 60 °C; (v) (a) Bu_4NF, THF, -55 °C; (b) H_2O, -30 °C/ rt; (vi) 3,8-dibromo-1,10-phenanthroline, [PdCl₂(PPh₃)₂], CuI, diisopropylamine, DMF, 82 °C.

4-(trimethylsilyl)ethynylbromobenzene gave the alkynes **17a-e**, which were transformed into the acetylenes **18a-e** by reaction with Bu₄NF. Finally, the acetylenes **18a-e** and 3,8-dibromo-1,10-phenanthroline **13** (synthesized according to the method of Yamamoto and co-workers[5] and which was further purified by a method described by Meunier and co-workers[6]) were

coupled via a second Sonogashira reaction to give the 1,10-phenanthroline ligands **L$_{XIV}$** - **L$_{XVIII}$**. The structure and purity of the final compounds **L$_{XIV}$** - **L$_{XVIII}$** was confirmed by ^{1}H and ^{13}C NMR spectroscopy, elemental analysis and, in one case, single-crystal X-ray analysis.[7]

The X-ray single crystal structure of **L$_{XIV}$** (Figure 5.1 and Figure 5.2) shows the non-planarity of the whole molecule in the solid state. The phenyl rings adjacent to the 1,10-phenanthroline ring are out of plane with the latter (dihedral angles are 25.1(1)° and 56.1(1)°, respectively and in turn, the outer phenyl rings are out of plane with respect to the phenyl rings (37.6(1)° and 45.3(2)°, respectively). The molecules are arranged in antiparallel pairs by an offset, intermolecular π-π-stacking (smallest distance between the centroids of two of the 1,10-phenanthroline rings is 3.660(2) Å); only two rings of the 1,10-phenanthroline moiety are involved in the stacking. Additionally, intermolecular, edge-to-face C(-H)-π -interactions (ca 3.8 Å) are observed between phenyl rings next to the 1,10-phenanthroline core. Interdimeric H-bonds (ca. 2.65 Å), resulting in a staircase arrangement of the pairs, help in the stabilization of the crystalline phase.
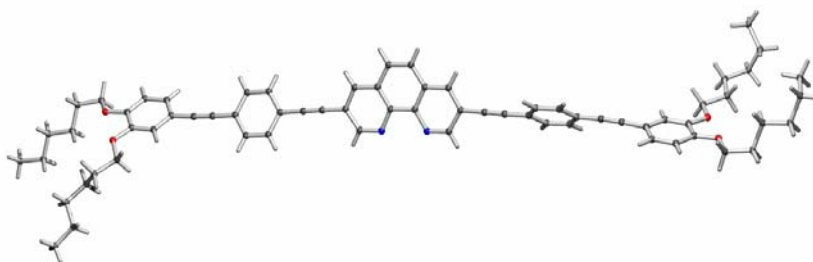
Figure 5.1: Molecular structure of L$_{XIV}$, determined by single-crystal X-ray diffraction.[7]

129
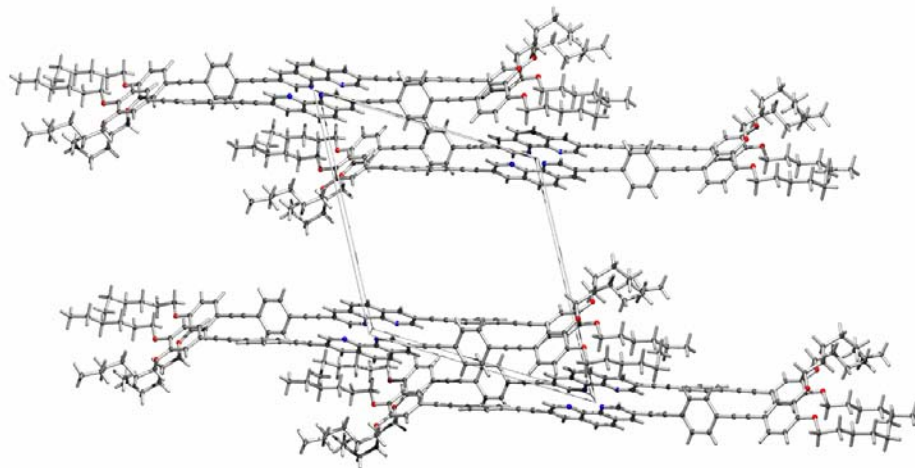
*Figure 5.2: Packing of molecules of **L$_{XIV}$** in the crystal structure.[7]*

5.2.2 Synthesis and characterization of the rhenium(I) complexes

The rhenium(I) complexes ReBr(CO)$_3$**L$_{XIV}$ - L$_{XVIII}$** were synthesized by reaction between the corresponding ligand **L$_{XIV}$ - L$_{XVIII}$** and [ReBr(CO)$_5$] (1:1 molar ratio) in toluene. All the rhenium(I) complexes were characterized by CHN analysis, ^{1}H and ^{13}C NMR, and IR spectroscopy. The structure of the rhenium(I) complexes is shown in Figure 5.3.

a: $n = 6$
b: $n = 8$
c: $n = 10$
d: $n = 12$
e: $n = 14$
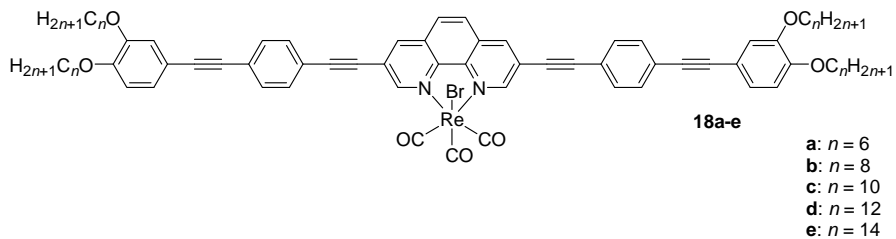
Figure 5.3: Structure of the rhenium(I) complexes.

130

5.3 Results

5.3.1 Thermal behavior of the ligands

The transition temperatures and thermal data for the ligands are collected in Table 5.1. The phase behavior of the ligands is summarized in the phase diagram shown in Figure 5.4.

Table 5.1: Transition temperatures and thermal data for the 1,10-phenanthroline ligands.

Compound	n	Transition[a]	$T/°C$	ΔH/kJ mol^{-1}	ΔS/J K^{-1} mol^{-1}
L$_{XIV}$	6	Cr-SmC	162	64.7	149
		SmC-Cub	237	2.0	4
		Cub-I	253	1.8	3
L$_{XV}$	8	Cr-SmC	151	24.8	58
		SmC-Cub	211	3.6	7
		Cub-I	237	1.6	3
L$_{XVI}$	10	Cr-SmC	133	24.4	60
		SmC-Cub	191	4.4	9
		(I-Col$_h$)	200	-[b]	-[b]

		Cub-I	214	0.7	1
L_{XVII}	12	Cr-Col_r	132	21.5	53
		Col_r-Col_h	165	1.8	4
		Col_h-I	206	1.6	3
L_{XVIII}	14	Cr-Col_r	134	39.3	97
		Col_r-Col_h	178	4.1	9
		Col_h-I	219	2.7	5

[a] Abbreviations: Cr = crystalline phase; SmC = smectic C phase; Cub = cubic phase; Col_h = hexagonal columnar phase; Col_r = rectangular columnar phase; I = isotropic liquid.
[b] Not detected by DSC.
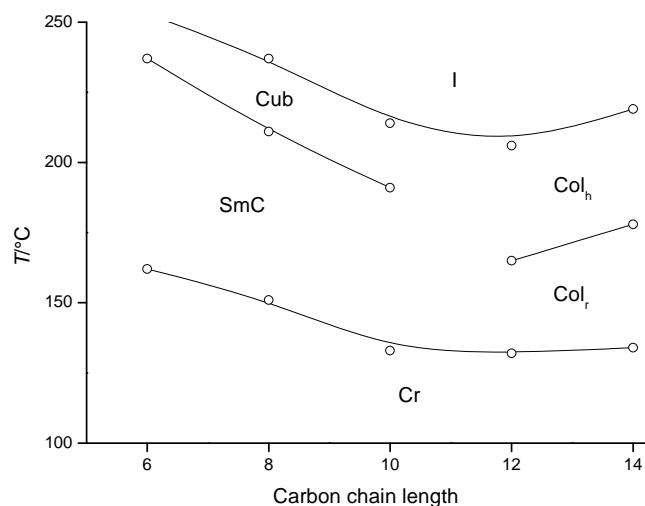
Figure 5.4: Phase diagram of the 1,10-phenanthroline ligands.

On examining the ligands by polarizing optical microscopy (POM), a small change in color (from yellow to yellow-brown) was noted and the appearance of some small isotropic regions occurred after some time. This color change and the formation of isotropic regions is due probably to some degradation of the ligands, which indicates that they are not stable to extended periods of illumination at high temperatures. The ligands L_{XIV} and L_{XV} (n = 6 and 8, respectively) exhibited two mesophases: a SmC phase at lower temperatures and a cubic phase at higher temperatures. The mesophases were identified by their optical textures. For the SmC phase, a broken fan texture (Figure 5.5) or a schlieren texture with only four brushes (Figure 5.6) was observed. When the sample was investigated without a glass cover slip on top of it, a "fingerprint-like" texture was seen (Figure 5.7).
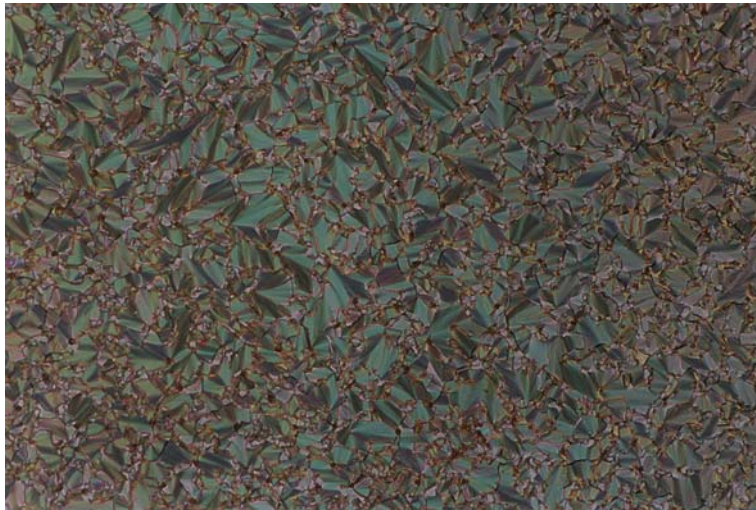
*Figure 5.5: Broken fan texture of **L_{XIV}** at 180 °C (200× magnification).*
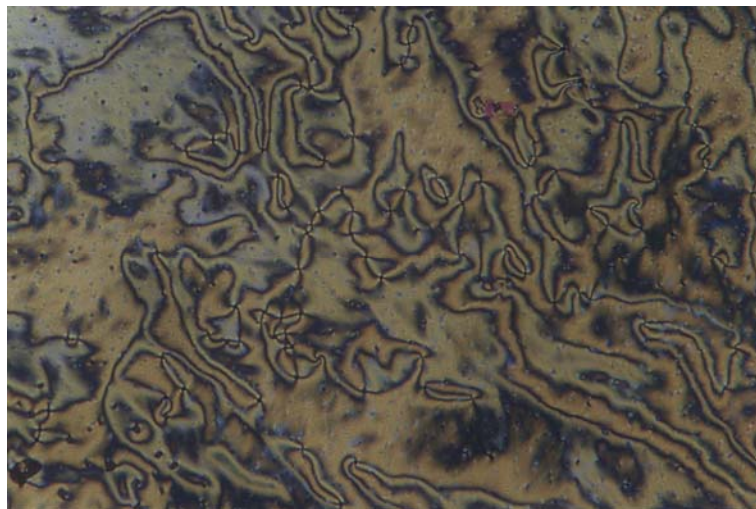
*Figure 5.6: Schlieren texture of **L_{XIV}** at 190 °C (500× magnification).*
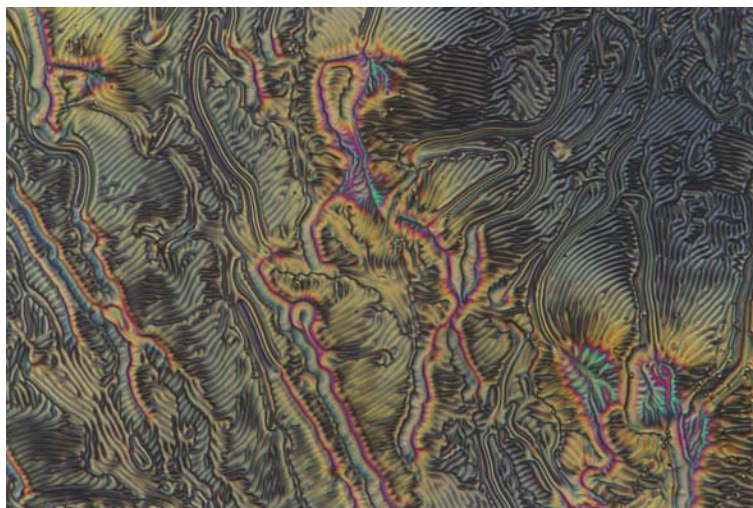
*Figure 5.7: "Fingerprint-like" texture of **L$_{XIV}$** at 165 °C (500×
magnification).*

The cubic phase was deduced on the basis of the extinction of the birefringence (optically isotropic material), its high viscosity, its slow formation kinetics and the presence of distorted air bubbles. Ligand **L$_{XVI}$** (*n* = 10) showed three mesophases: a low temperature SmC phase, a high temperature cubic phase, and a monotropic hexagonal columnar phase. On cooling from the isotropic liquid, the hexagonal columnar phase was formed at first, which on further cooling transformed into the cubic phase. The hexagonal columnar phase was identified on the basis of its fern-like texture on cooling from the isotropic liquid (Figure 5.8) and the presence of some homeotropic areas, which confirmed the uniaxial nature of the phase. The position of the Col$_h$ phase in this phase sequence requires comment, as it is the phase seen first on cooling from the isotropic phase yet it does not appear on heating. It is well established in tetracatenar mesogens that the phase progression SmC → Cub → Col$_h$ can occur as a function of chain length and on temperature.[8] Here, the cubic phase forms as a phase

intermediate between the flat, lamellar structure of the SmC phase and the curved interfaces of the Col_h phase.[9] This can be understood by enhancement of the amphiphilic character by the increase of the aliphatic volume fraction, either by temperature, chain-length, or chain-number. Considering the ideal sequence of mesophase, first the rigid core will tilt to compensate the chain-area increase, until a point where tilt is no more sufficient, and undulations occur. Such undulations allow to accommodate this chain-area increase, resulting in transitions to either Cub bicontinuous or Col phases. Transitions into and out of cubic phases are known to be slow on account of the rather substantial structural re-arrangements that occur, resulting in the formation of some kind of "kinetic domain". For example, such a "kinetic domain" accounted successfully for the appearance of a cooling sequence: I $\rightarrow$ N $\rightarrow$ SmC $\rightarrow$ Cub $\rightarrow$ SmC against the heating sequence of: SmC $\rightarrow$ Cub $\rightarrow$ N $\rightarrow$ I.[8] Schematic plots of free energy, G, versus temperature show the thermodynamic situation. In the present case, it is likely that close to the Cub-I transition, the free energies of Cub, Col_h and isotropic phases are very similar with the free energy of Col_h slightly below that of Cub. On cooling, however, the I-Cub transition supercools due to its slow kinetics allowing the Col_h phase to be seen. However, the Col_h is unstable thermodynamically with respect to the cubic phase, which is seen on further cooling.

*Figure 5.8: Fern-like texture of **L**$_{XVI}$ at 196 °C (200× magnification).*

Ligands **L**$_{XVII}$ and **L**$_{XVIII}$ (n = 12 and 14, respectively) showed two mesophases, a low temperature phase with a rectangular symmetry and a high temperature hexagonal columnar phase. The hexagonal columnar phase could be assigned using polarizing optical microscopy by the formation of a fern-like texture on cooling from the isotropic liquid. On further cooling, a mosaic texture or a fan-like texture was formed together with some homeotropic areas (Figure 5.9).
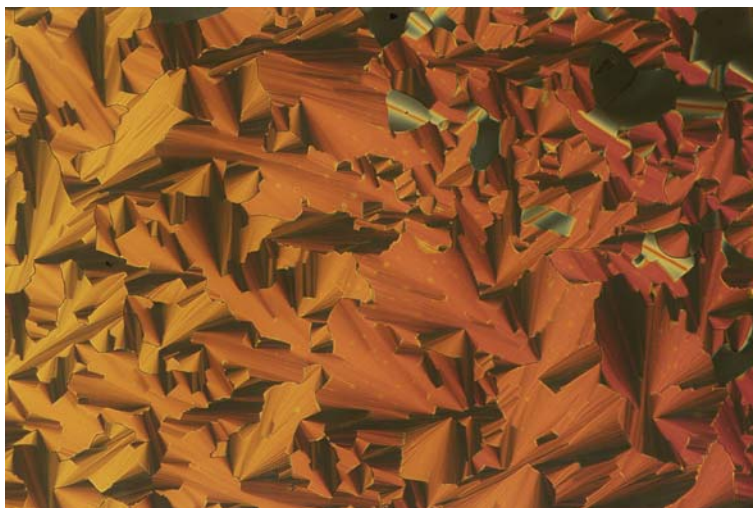
*Figure 5.9: Fan-like texture of **L_{XVIII}** at 190 °C (200× magnification).*

When cooling the hexagonal columnar phase, a change in the fan-like texture and the gradual disappearance of the homeotropic areas indicated the occurrence of a phase transition (Figure 5.10). However, on the basis of only the polarizing optical microscopy observations, the lower temperature phase could not be identified unequivocally.
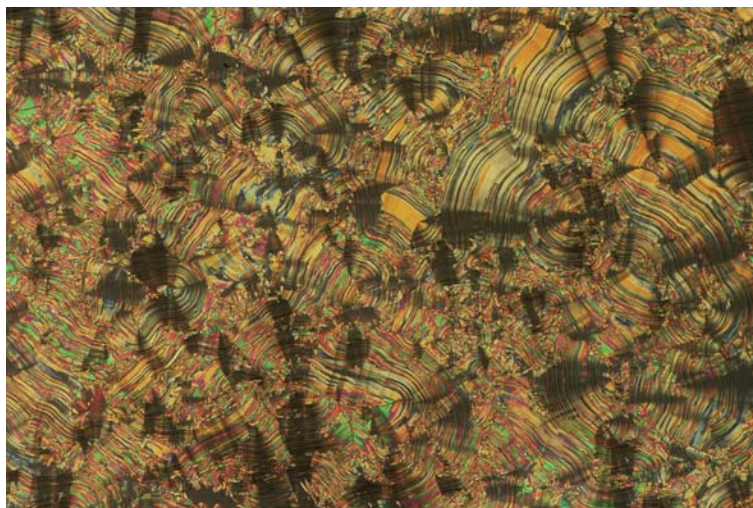
Figure 5.10: Phase transition Col_h-Col_r of L_{XVIII} at 166 °C on cooling (200× magnification).

X-ray measurements were undertaken to elucidate the nature and symmetry of all the mesophases exhibited by compounds L_{XIV}-L_{XVIII}, except for the monotropic phase of L_{XVI}, which could not be stabilized for long enough to give a diffraction pattern.

Two, equidistant and sharp reflections in the 1:2 ratio were observed in the diffractograms for the low-temperature mesophase of L_{XIV} and L_{XV} (Table 5.2) indicative of a lamellar ordering of the molecules. Indexation was as $00l$ reflections with $l = 1, 2$. As for the low-temperature phase of L_{XVI}, only one sharp reflection was obtained, although on the basis of the spacing (which is in the same range as that of L_{XIV} and L_{XV}) and on the optical texture (birefringent and homogeneous domains, but not absolutely characteristic), the phase was also assigned as smectic. To complete this description, two broad and diffuse scattering halos, corresponding to short-range order interactions, were detected at *ca* 4.5 Å (h_{CH}), associated with the molten chains, and at *ca* 8.5 ± 0.5 Å (h_{mol}), possibly due to some weak, lateral interactions.

Table 5.2: Bragg reflections collected from the X-ray diffraction patterns of all the 1,10-phenanthroline ligands.

Compds	T/°C	d_{exp}/Å [a]	[hkl] [b]	I [c]	d_{theo}/Å [a,d]	Parameters [d]
L$_{XIV}$	180	31.65	001	VS (sh)	31.63	SmC
		15.81	002	S (sh)	15.82	$d = 31.63$ Å
($n = 6$)		8.5	h_{mol}	W (br)		$V_{mol} = 1520$ Å^3
		4.5	h_{CH}	VS (br)		$A_M = 48.05$ Å^2
	200	32.1	001	VS (sh)	32.18	SmC
		16.13	002	S (sh)	16.09	$d = 32.18$ Å
		8.5	h_{mol}	W (br)		$V_{mol} = 1530$ Å^3
		4.6	h_{CH}	VS (br)		$A_M = 47.5$ Å^2
	240	42.09	211	VS (sh)	42.30	Cub-*Im3m*
		36.51	220	S (sh)	36.64	$a = 103.6$ Å
		33.05	310	W (br)	32.77	$V_{mol} = 1550$ Å^3
		4.6	h_{CH}	VS (br)		$V_{cub} = 1.11 \times 10^6$ Å^3
						$Z = 720$
L$_{XV}$	180	34.85	001	VS (sh)	-	SmC
		8.6	h_{mol}	W (br)		$d = 34.85$ Å
($n = 8$)		4.6	h_{CH}	VS (br)		$V_{mol} = 1760$ Å^3
						$A_M = 50.5$ Å^2
	215	45.05	211	VS (sh)	-	Cub-*Im3m*
		8.5	h_{mol}	W (br)		$a = 110.35$
		4.5	h_{CH}	VS (br)		$V_{mol} = 1785$ Å^3
						$V_{cub} = 1.34 \times 10^6$ Å^3
						$Z = 753$
L$_{XVI}$	160	35.66	001	VS (sh)	-	SmC
		8.6	h_{mol}	W (br)		$d = 35.66$ Å
($n = 10$)		4.5	h_{CH}	VS (br)		$V_{mol} = 1990$ Å^3
						$A_M = 55.7$ Å^2

	200	57.9	220	M (sh)	57.94	Cub-*Im3m*
		52.8	310	M (sh)	51.82	a = 115.88 Å
		47.2	222	VS (sh)	47.31	V_{mol} = 2020 Å^3
		43.51	321	VS (sh)	43.80	V_{cub} = 1.55×10^6 Å^3
		38.5	411/330	M (sh)	38.63	Z = 770
		36.43	420	M (sh)	36.65	
		8.5	h_{mol}	W (br)		
		4.6	h_{CH}	VS (br)		
L$_{XVII}$	140	45.98	01	VS (sh)	45.44	Col$_r$-*p2mm*
		38.32	11	S (sh)	38.32	a = 71.32 Å
(*n* = 12)		35.66	20	S (sh)	35.66	b = 45.44 Å
		21.82	12	W (sh)	21.65	S = 3240 Å^2
		8.3	h_{mol}	W (br)		V_{mol} = 2205 Å^3
		4.6	h_{CH}	VS (br)		h = 0.68Z
	180	46.12	10	VS (sh)	46.07	Col$_h$-*p6mm*
		26.56	11	W (sh)	26.60	a = 53.2 Å
		23.05	20	W (sh)	23.03	S = 2450 Å^2
		8.5	h_{mol}	W (br)		V_{mol} = 2245 Å^3
		4.6	h_{CH}	VS (br)		h = 0.91Z
L$_{XVIII}$	150	47.54	01	VS (sh)	48.15	Col$_r$-*p2mm*
		39.91	11	S (sh)	39.91	a = 71.32 Å
(*n* = 14)		35.66	20	S (sh)	35.66	b = 48.15 Å
		8.3	h_{mol}	W (br)		S = 3435 Å^2
		4.6	h_{CH}	VS (br)		V_{mol} = 2450 Å^3
						h = 0.71Z
	200	47.25	10	VS (sh)	47.15	Col$_h$-*p6mm*
		27.03	11	W (sh)	27.22	a = 54.44 Å
		23.7	20	M (sh)	23.58	S = 2567 Å^2
		8.5	h_{mol}	W (br)		V_{mol} = 2510 Å^3
		4.6	h_{CH}	VS (br)		h = 0.98Z

210	46.97	10	VS (sh)	-	Col_h-$p6mm$
	8.5	h_{mol}	W (br)		$a = 54.24$ Å
	4.6	h_{CH}	VS (br)		$S = 2547$ Å^2
					$V_{mol} = 2520$ Å^3
					$h = 0.99Z$

[a] d_{exp} and d_{theo} are the experimentally measured and theoretical diffraction spacings. The distances are given in Å. [b] [hkl] are the Miller indices of the reflections, and h and h_{CH} are the various short-range periodicities determined by XRD corresponding to some molecular (lateral) interactions (h_{mol}) and to the liquid-like order of the molten chains (h_{CH}). [c] Intensity of the reflections: VS: very strong, S: strong, M: medium, W: weak, VW: very weak; br and sh stand for broad and sharp reflections, respectively. [d] d_{theo} and the mesophases parameters d, a, b, A_M, S, V_{cub} are deduced from the following mathematical expressions. For the smectic phase, $d = <d_{001}> = [\Sigma_l d_{00l}.l]/N_{00l}$ and the molecular area $A_{mol} = V_{mol}/d$. For the Col_h phase, the lattice parameter $a = 2[\Sigma_{hk} d_{hk}.(h^2+k^2+hk)^{1/2}]/\sqrt{3}N_{hk}$ where N_{hk} is the number of hk reflections, and the lattice area (i.e. columnar cross-section) $S = a^2 3^{1/2}/2$. For the Col_r phase, $<d_{hk}> = 1/[(h^2/a^2+k^2/b^2)^{1/2}]$, the lattice area $S = a \times b$. For the cubic phase, $a = [\Sigma d_{hkl}.(h^2+k^2+l^2)^{1/2}]/N_{hkl}$, where N_{hkl} is the number of hkl reflections. Z is the number of molecules. For the columnar phases, it is defined as $Z = h.S/V_{mol}$ and for the cubic phases as $Z = a^3/V_{mol}$. [e] V_{mol} is the molecular volume: $V_{mol} = V_{Ar} + 4(nV_{CH2})$, where $V_{Ar} = 795$Å^3 and $V_{CH2} = 26.5616 + 0.02023T$ (T in °C); h is the intracolumnar repeating distance, deduced directly from the measured molecular volume and the columnar cross-section according to $h = ZV_{mol}/S$.

The interlayer periodicity, d, is almost invariant with temperature, and increases concomitantly with chain length. From the estimated molecular volume, the molecular area ($A_M = V_{mol}/d$) could be determined. The value calculated is about twice the cross-sectional area of a single aliphatic chain extended normal to the smectic layer (*ca* 22 to 24 Å^2, as in the SmA phase), which is consistent with the two chains grafted onto each extremity of the core. This agrees with the assignment as a smectic C phase in which the chains and the cores are segregated in sub-layers. In this arrangement, the chains are packed orthogonally in a compact manner, and the mesogenic cores are tilted with respect to the layer normal in order to compensate for the increase in the area that the chains project onto the core-chain interface.[10] The presence of the halo, referred to as h_{mol}, suggests the possibility of some sort of dimer formation, and it is possible that the anti-parallel arrangement present in the crystalline structure may suggest a model for this organization.

On heating, a transition into another phase was detected for the three compounds, consistent with the observations from optical microscopy, and a cubic mesophase with *Im*-3*m* symmetry was eventually deduced by SAXS measurements. The presence of three (**L$_{XIV}$**) or of six (**L$_{XVI}$**) low-angle reflections for which the reciprocal d-spacings are in the ratios √3:√4:√5 (**L$_{XIV}$**) or √4:√5:√6:√7:√9:√10 (**L$_{XVI}$**) indeed point to cubic organization [$(h^2+k^2+l^2)^{1/2} = a/d_{hkl}$)]; only one reflection was obtained for **L$_{XV}$**. The intense and broad diffraction peak centered at *ca* 4.5 Å (h_{CH}) corresponding to the molten alkyl chains, confirmed the fluid nature of the mesophase; the 8.5 Å (h_{mol}) reflection was also present.

The complete space group determination of mobile thermotropic cubic phases is difficult, but is nonetheless important in understanding the molecular organization. The large initial number of theoretical possibilities (36) can be reduced with a logical analysis of the data, as now shown. In our standard diffraction experiment, all non-centro-symmetric groups (groups with the 23, 432 and –43*m* Laue classes) can be disregarded due to the Friedel's law, thus leaving only 17 cubic space groups to consider.[11]

However, the number of possibilities as far as L_{XIV} is concerned, for which only three reflections were observed, still remains important, since 11 groups can still account for the phase symmetry and satisfy the reflection conditions (three primitive - *Pm*-3, *Pa*-3, *Pm*-3*m* -, 2 body-centered - *Im*-3, *Im*-3*m* -, and six face-centered space groups - *Fm*-3, *Fm*-3*m*, *Fm*-3c, *Fd*-3, *Fd*-3*c*, *Fd*-3*m*). However, assuming that both L_{XIV} and L_{XVI} (and *a fortiori* L_{XV}) exhibit the same cubic phase symmetry and molecular self-organization, the possibilities are much reduced. Thus, the ratio sequence for the reflections observed for L_{XVI} is not compatible with a face-centered network (*F*) nor with a primitive Bravais lattice (*P*). The symmetry of the cubic phase is thus characterized by a body-centered cubic network (*I*). The reflections were, therefore, indexed successfully as (211), (220) and (310) for L_{XIV} and (220), (310), (222), (321), (411/330), (420) for L_{XVI}, and all satisfied the reflection conditions [*0kl*:*k+l = 2n*, *hhl*:*l = 2n*, *h00*:*h = 2n*]. Only the space groups *Im*-3 or *Im*-3*m* are theoretically compatible with this set of reflections. Aggregation into the highest symmetry is generally assumed and, accordingly, the *Im*-3*m* space group is finally chosen.[12-15] The indexation of the single reflection of L_{XV} is, of course, impossible, however, one may expect that the phase lattice parameter of the cubic phase is intermediate between those of L_{XIV} and L_{XVI}, and we tentatively indexed the reflection as (211).

Cubic phases with the *Im*-3*m* space group are rare in thermotropic liquid crystals,[12-16] and their structure not well understood, contrary to situation with their lyotropic analogues. As deduced from the estimated molecular volume ($\rho \sim 1.0$ g cm^{-3}), the elementary cell of the cubic phase (a^3) contains about 700 to 800 molecules. A discontinuous model in which the phase is formed by two, independent and rigorously identical micelles (or multi-layer vesicles) with an aggregation number of 350 to 400 molecules, is almost certainly unrealistic in the present situation (*Z* is too elevated to allow such supramolecular objects to be formed).[16,17] However, another alternative and more appropriate description of the three-dimensional organization would be to consider multicontinuous cubic structures made of

two or three interwoven, infinite, interconnected columnar networks (*Im*-3*m* (*P*) and *Im*-3*m* (*I*), respectively), each separated by lipophilic films (minimal surfaces).[18,19] We believe that the most likely structure would be the triple interpenetrated *Im*-3*m* (*I*) network model due to the huge number of molecules per lattice and to the fact that the (321) reflection is one of the dominant reflections in the powder X-ray pattern of **L$_{XVI}$**. This is consistent with another study where the structure was confirmed by direct Fourier reconstruction of the electron density profile.[20] Despite this elegant work, a fully comprehensive explanation of the supramolecular organization is still not yet possible. The network models and the associated infinite periodic minimal surfaces of the *Im*-3*m* (*P*) and *Im*-3*m* (*I*) structures are represented in Figure 5.11.
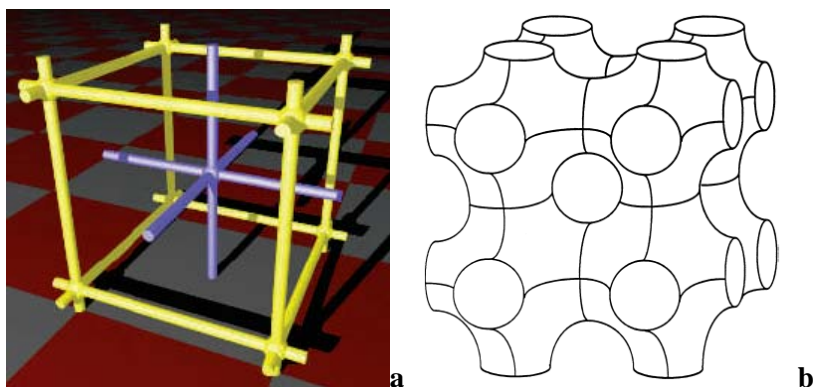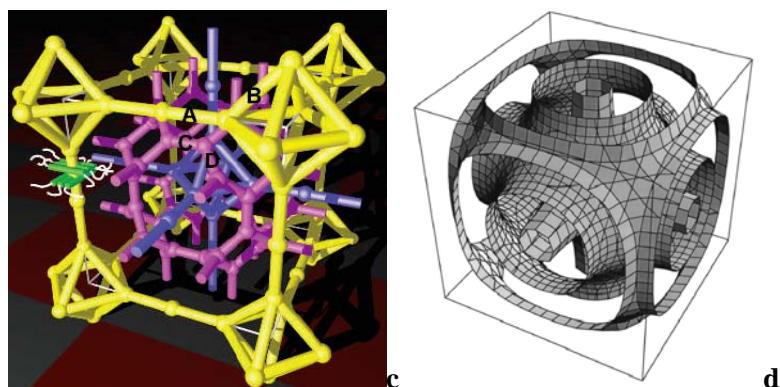
Figure 5.11: a) Network model of the Im-3m (P) bicontinuous cubic phase (the two interpenetrating networks are coloured blue and yellow) and b) associated infinite periodic minimal surface (Schwartz's P-surface). Model of the cubic unit cell with two layers made of alkyl chains separated by three core regions. c) Triple network representation of the Im-3m (I) structure (the three interpenetrating continuous networks are coloured purple, pink and yellow; the purple and yellow networks are identical but mutually displaced by (x/2,y/2,z/2)) and d) associated infinite periodic minimal surfaces based on the P Schwartz surface (central surface). Model of the cubic unit cell with three layers made of alkyl chains separated by four core regions. [20]

Finally, both ligands L_{XVII} and L_{XVIII} exhibit columnar mesophases as confirmed by XRD. The XRD patterns recorded for L_{XVII} and L_{XVIII} on cooling from the isotropic liquid down to *ca* 160 and 180 °C, respectively, are characterized by the presence of three, sharp, small-angle reflections, with reciprocal spacings in the ratio $1:\sqrt{3}:2$. These features are most readily assigned as the (10), (11), and (20) reflections of a hexagonal lattice (plane group *p6* or *p6mm*) with a lattice parameter, *a*, almost temperature- and chain length-independent ($a \sim 53$ Å for L_{XVII} and 54.3 Å for L_{XVIII}). The presence of the broad halo at 4.6 Å (h_{CH}) confirmed the fluid nature of the

mesophase, while the broad reflection at 8.5 Å (h_{mol}) is once more interpreted in terms of possible dimer formation. On further cooling, the phase symmetry changes from hexagonal into a simple rectangular lattice. The diffractograms of both compounds showed four (**L$_{XVII}$**) or three (**L$_{XVIII}$**) sharp and intense reflections that could be indexed as the (01), (11), (20) and (12) reflections of a simple rectangular lattice with plane group symmetry *p2mm* (or *pm*). Such symmetry for a rectangular lattice has been observed only rarely, the only examples to our knowledge being reported by Percec and co-workers in some dendritic materials.[21-23] Both wider-angle halos were again observed.

The formation of columnar mesophases in polycatenar systems is a consequence of the increasing volume of the terminal chains (caused either by increased temperature or by increasing chain length) not being accommodated by an increasing tilt of the molecular core, thus limiting long-range lateral molecular ordering and so breaking the layers.[24,25] Providing the correct repeating distance along the column is known, the effective number of molecules (*Z*) per repeat distance can be determined by the relationship between the columnar cross-section area (*S*) and the molecular volume (V_{mol}), according to $h.S = Z.V_{mol}$. If h_{mol} is considered as being the main periodicity along the column, then for the Col$_r$ phase, the equivalent of about 12 mesogens are found in a slice that is about 8.3 Å-thick (Figure 5.12). In the Col$_h$ phase, this figure goes down to 8-9 for the same periodicity, in agreement with a strong diminution of the column cross-section area (*ca* 25 %). The transition between these two mesophases likely occur by an increase of the average tilt angle of the bundles (and thus of the molecular axis) out of the symmetry plane, without destroying the internal structure of the column, in order that the cross-section achieves the nearly circular shape required to induce the 6-fold symmetry of the Col$_h$ phase (Figure 5.13).[24]
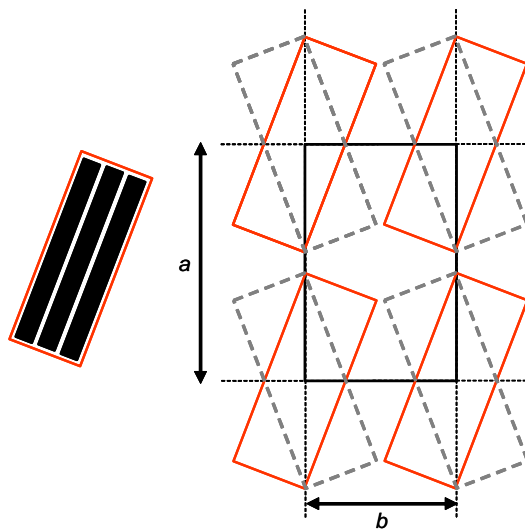
Figure 5.12: Schematic representation of the p2mm lattice of the rectangular phase, and possible molecular arrangement of the ligands in a bundle, and their stacking into columns (the black lines correspond to a dimer, and only one layer is shown). Solid line: bundles of the upper layer, and dotted lines: bundles in the lower level, each distant of 8.3 Å.

p2mm   *p6mm*
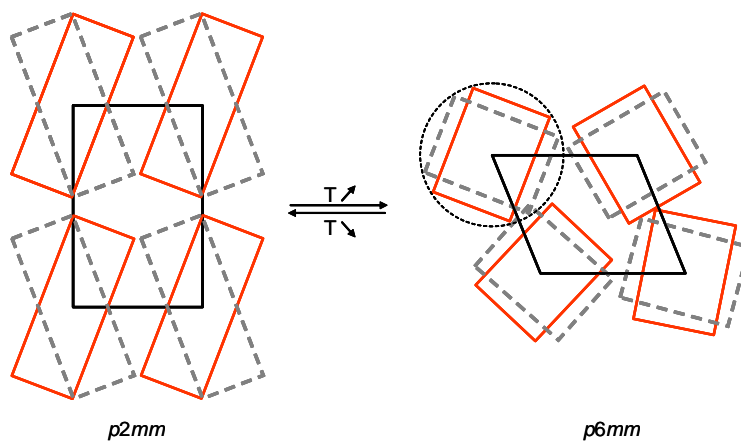
Figure 5.13: Schematic representation of the Col_r-p2mm and the Col_h-p6mm phase transition.

5.3.2 Thermal behavior of the rhenium(I) complexes

The transition temperatures and thermal data for all the rhenium(I) complexes are collected in Table 5.3. None of the rhenium(I) complexes were liquid-crystalline and, except for the rhenium(I) complex $ReBr(CO)_3L_{XIV}$ ($n = 6$), which decomposed before melting, all melted to the isotropic liquid on heating.

Table 5.3: Transition temperatures and thermal data for the rhenium(I) complexes.

Compound	n	Transition[a]	$T/°C$	ΔH/kJ mol^{-1}	ΔS/J K^{-1} mol^{-1}
Re(I)-L_{XIV}	6	Cr-I	>300	-[b]	-[b]
Re(I)-L_{XV}	8	Cr-I	303	29.3	51
Re(I)-L_{XVI}	10	Cr-I	288	9.8	17
Re(I)-L_{XVII}	12	Cr-I	276	67.8	123
Re(I)-L_{XVIII}	14	Cr-I	259	55.5	104

[a] Abbreviations: Cr = crystalline phase; I = isotropic liquid.

[b] Not detected by DSC.

5.3.3 Photophysical properties of the ligand L_{XVI}

Ligand L_{XVI} absorbs radiation at 300 nm (ε = 62600 dm^3 mol^{-1} cm^{-1}) and 370 nm (ε = 103000 dm^3 mol^{-1} cm^{-1}). Excitation at 370 nm results in a strong, white-blue fluorescence caused by a broadband emission at 475 nm, even in ambient light for diluted solutions. The absorption and emission spectra in chloroform are shown in Figure 5.14. Two absorption bands are also observed for the corresponding rhenium complex Re(I)Br(CO)$_3$$L_{XVI}$ (n = 10), shifted towards lower energies (λ_{max} = 415 nm, ε = 54700 dm^3 mol^{-1} cm^{-1} and 325 nm, ε = 63500 dm^3 mol^{-1} cm^{-1}). The strong, ligand emission is quenched in the complex and is replaced by two weaker emission bands when the rhenium complex is excited at 390 nm in chloroform. The first emission band is situated at the same position as the ligand emission and therefore can originate from the ligand itself, while a new emission band appears around 640 nm. Usually, emission from charge-transfer states (MLCT or LLCT) is observed for rhenium(I) carbonyl-diimine complexes with bromide ligands, but when the α-diimine ligand has an extensively delocalised π system, a low intraligand excited state is also plausible.[26]

Figure 5.14: Room-temperature absorbance and emission spectra for ligand L_{XVI} (black line) and rhenium complex Re(I)Br(CO)$_3$$L_{XVI}$ (grey line) in chloroform; excitation at 370 and 390 nm respectively.
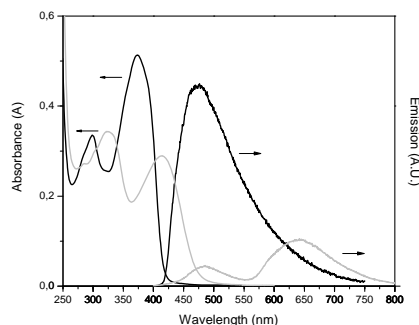
5.3.3 STM study of ligands and complexes

The self-assembly of the ligands L_{XV} and L_{XVIII} (n = 8 and 14, respectively), and the rhenium(I) complexes $ReBr(CO)_3L_{XV}$ and $ReBr(CO)_3L_{XVIII}$ (n = 8 and 14, respectively) on a highly oriented pyrolytic graphite surface (HOPG) was investigated by STM. Monolayers of L_{XIV}, L_{XVIII} and $Re(I)Br(CO)_3L_{XVIII}$ were observed, though the self-assembly of $ReBr(CO)_3L_{XV}$ was not successful despite repeated trials.

Typical high-resolution STM images of L_{XVIII} and $ReBr(CO)_3L_{XVIII}$ at the 1,2,4-trichlorobenzene (TCB)-HOPG interface are shown in Figure 5.15. As is generally observed for π-electron-rich systems, the π-electron-rich parts appear as bright structures corresponding to high tunneling currents, whereas the alkyl chains are not well resolved and are represented by dark areas due to low tunneling efficiency. The unit cell vectors $\vec{a}$ and $\vec{b}$ for L_{XVIII} are 8.1±0.1 nm and 4.2±0.1 nm, respectively, and the angle between $\vec{a}$ and $\vec{b}$, γ is 78°±2°. The distance between the adjacent closely-packed backbones is 0.73±0.05 nm. The packing model of the molecules for L_{XVIII} is illustrated in Figure 5.15A. The molecules form dimers, though the unit cell contains two different types of dimers and is rather complex (plane group p1, four molecules per unit cell). *Yet* for $ReBr(CO)_3L_{XVIII}$, the molecules are arranged into closely-packed lamellae in which the π-conjugated backbones are packed side by side in a plane parallel to the graphite surface. The unit cell vectors $\vec{a}$ and $\vec{b}$ for $ReBr(CO)_3L_{XVIII}$ are 1.7±0.1 nm and 12.2±0.1 nm, respectively, and the angle between $\vec{a}$ and $\vec{b}$, γ is 70°±2°. The distance between the adjacent conjugated backbones along the lamella axis is 1.6±0.1 nm. The unit cell (plane group p1) contains one molecule. The alkyl chains of the molecules of adjacent lamellae are interdigitating. The packing model of the molecules for $ReBr(CO)_3L_{XVIII}$ on graphite is illustrated in Figure 5.15B.
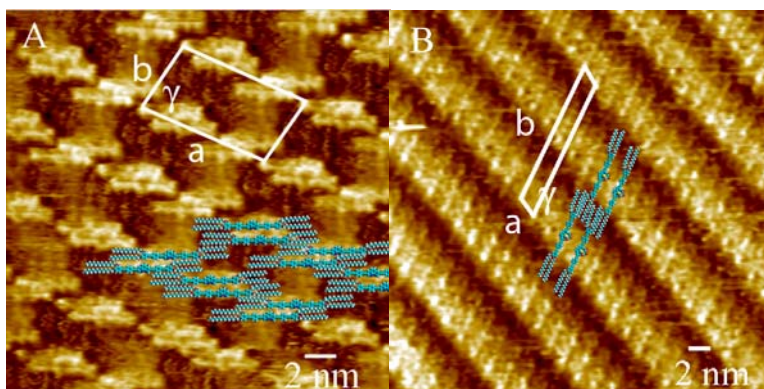
Figure 5.15: (A) STM image of a monolayer of L_{XVIII} at the TCB-HOPG interface (1mg/ml, I_{set} = 0.03 nA, V_{bias} = 1 V); (B) STM image of a monolayer of ReBr(CO)$_3$$L_{XVIII}$ at the TCB-HOPG interface (1mg/ml, I_{set} = 0.03 nA, V_{bias} = 1 V).

Interestingly, the self-assembly behavior of the compounds in octanoic acid is very different, compared to that in TCB. A possible reason is protonation of the nitrogen atoms of the phenanthroline core. Typical high-resolution STM images of L_{XV}, L_{XVIII} and ReBr(CO)$_3$$L_{XVIII}$ at the octanoic acid-HOPG interface are shown in Figure 5.16. All the compounds show lamellar structures and the packing molecules for L_{XV}, L_{XVIII} and ReBr(CO)$_3$$L_{XVIII}$ are depicted in the Figure 5.16A, B and C, respectively. At the octanoic acid-HOPG interface, the alkyl chains of the molecules of adjacent lamellae are not interdigitating, in contrast to the organization observed at the TCB - HOPG interface. The unit cell vectors $\vec{a}$ and $\vec{b}$ for L_{XVIII} are 0.92±0.05 nm and 7.1±0.1 nm, respectively, and the angle between $\vec{a}$ and $\vec{b}$, γ is 87°±2° (plane group $p1$, one molecule per unit cell). The vector $\vec{b}$, the mean width of a lamella, corresponds to the length of a molecule. The unit cell vectors $\vec{a}$ and $\vec{b}$ for ReBr(CO)$_3$$L_{XVIII}$ are 1.07±0.05 nm and 7.0±0.1 nm, respectively, and the angle between $\vec{a}$ and

152

$\vec{b}$, γ is 82°±2°. The distance between the adjacent molecules of ReBr(CO)$_3$**L$_{XVIII}$** along the lamella is longer than that of **L$_{XVIII}$**, which is caused by the metal complexation. Here, not only the conjugated backbone but also the alkyl chains of ReBr(CO)$_3$**L$_{XVIII}$** can be clearly identified (Figure 5.16B). For **L$_{XV}$**, the molecules are arranged into rows, in which two closely-packed molecules and one isolated molecule are arranged alternatively. The conjugated backbone is in particular well-resolved: each phenyl group and the central complexed unit are clearly distinguishable. The distance between the adjacent closely-packed backbones along the lamella is 0.6±0.05 nm and that between the closely-packed backbone and the isolated one is about 1.1±0.05 nm. The unit cell vectors $\vec{a}$ and $\vec{b}$ for **L$_{XV}$** are 5.6±0.1 nm and 5.5±0.1 nm, respectively, and the angle between $\vec{a}$ and $\vec{b}$, γ is 35°±2° (plane group $p1$, three molecules per unit cell). Note that the crystallinity is not perfect though as dimers and monomers do not always alternate.
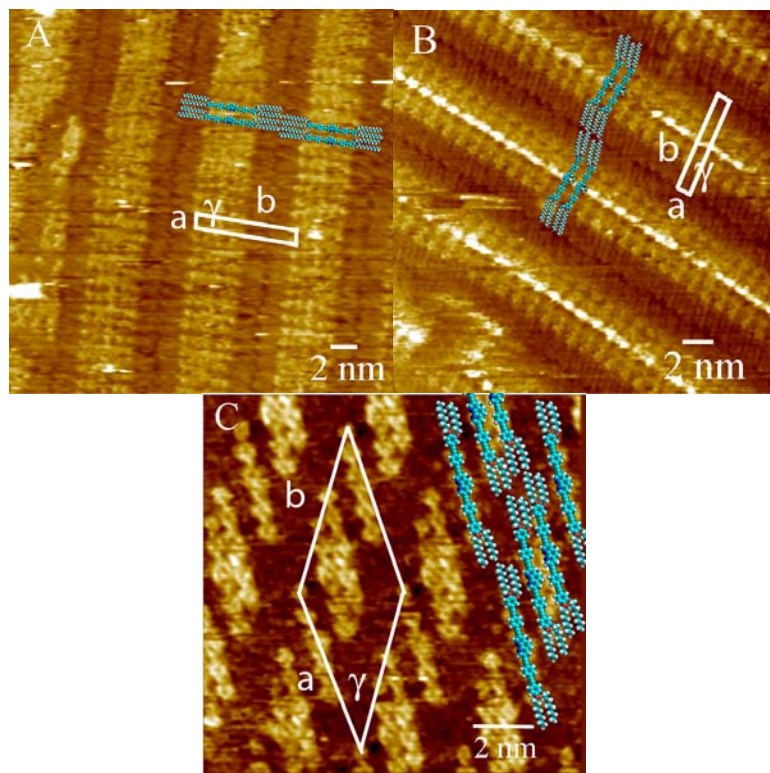
Figure 5.16: (A) STM image of a monolayer of L_{XVIII} at the octanoic acid-HOPG interface (1mg/ml, I_{set} = 0.03 nA, V_{bias} = 1 V); (B) STM image of a monolayer of ReBr(CO)$_3L_{XVIII}$ at the octanoic acid-HOPG interface (1mg/ml, I_{set} = 0.03 nA, V_{bias} = 1 V); (C) STM image of a monolayer of L_{XV} at the octanoic acid-HOPG interface (1mg/ml, I_{set} = 0.03 nA, V_{bias} = 1 V).

5.4 Discussion and conclusions

The rich mesomorphism exhibited by this series of compounds is not untypical for tetracatenar systems, namely the observation of nematic and lamellar phases at short chain lengths and columnar phases at long chain lengths.[9] A very interesting feature of such tetracatenar materials is the change from the nematic/lamellar phases to the columnar phase as a function of chain length and/or temperature. The basic driving force for this change in mesomorphism relies essentially on the significant mismatch between the molecular area of the rigid core of the mesogen projected onto the core-chain interface when compared with a similar projection of the two, terminal chains.[9,27] This explains why a tilted lamellar phase (SmC) is observed (tilt increases the projection of the core onto the interface). As the chain length or temperature increases, the apparent volume occupied by the terminal chains increases which is matched by an increase in the SmC tilt angle. However, there comes a point where tilt alone cannot counter the increase in chain volume, so that further increases in chain volume lead in turn to undulations in the layer structure and finally to the formation of columns perpendicular to the tilt direction.

Such a mechanism accounts for a direct SmC-Col$_h$ phase transition as a function of temperature and can also explain why one homologue may show a SmC phase while the next exhibits a columnar phase. Further, with small modification to allow undulations to develop in two dimensions, the mechanism can be used to explain the phase behavior of systems in which either a SmC or a Col$_h$ phase are bordered by a cubic phase. However, the mechanism cannot explain why in some polycatenar metal complexes a lamello-columnar phase is found between the SmC and the Col$_h$ phase as a function of only chain length.[9]

Of course, the other thing the mechanism does not account for is why there are so many different ways of undergoing the 'transition' from lamellar to

columnar behavior. Thus, for example, the 2,2'-bipyridines described by Rowe and Bruce show a 'classical' progression from SmC through to Col_h *via* a cubic phase as a function of both chain length and temperature.[8,28] These molecules have a zero dipole moment at their core (*transoid* arrangement of the 2,2'-bipyridine group) and four ester groups generating dipole moments further out from the center and conferring a certain degree of flexibility. These new 1,10-phenanthroline mesogens have a substantial lateral dipole at the core but apolar acetylenic linking groups that are inflexible, yet the overall morphology of the two phase diagrams is not at all dissimilar. However, if we now turn to other polycatenar 1,10-phenanthrolines that contain both acetylenic and ester linking groups, not only does the cubic phase disappear, but now the situation is found where one homologue ($n = 11$) shows only a SmC phase while the next ($n = 12$) shows only a Col_h phase.[29] While the factors that can promote cubic phase formation in both polycatenar and calamitic mesogens have been well elucidated, it is clear that apparently necessary preconditions do not predicate the appearance of the phase. Nor is the appearance or otherwise of the cubic phase a determining factor in the crossover behavior, for there are examples in the literature of other tetracatenar mesogens that progress from lamellar to columnar mesophases where some homologues show both phases.[25,30,31]

The rhenium(I) complexes containing the bulky [ReBr(CO)$_3$] fragment have an appreciable dipole moment due to the polar Re-Br bond. This dipole was expected to influence the arrangement of the molecules in the mesophase and the solid phase. Complexation to rhenium(I) led to an increase of the melting temperatures. However, the lack of mesomorphism was not expected as the rhenium(I) complexes described by Date et al. showed a hexagonal columnar phase at long chain lengths.[29]

Tetracatenar liquid crystals were obtained by substituting 1,10-phenanthroline in the 3- and 8-positions. The ligands exhibited a rich mesophase behavior: lamellar, cubic and columnar phases were observed, depending on the alkoxy chain length. On the contrary, no mesomorphism

156

could be observed for the corresponding rhenium(I) complexes. Scanning tunnelling microscopy studies show that LXVIII and ReBr(CO)$_3$LXVIII can be self-assembled into monolayers at the TCB-graphite and octanoic acid-graphite interfaces, but the packing structures are different. The packing structures depend on both the alkoxy chain length and the solvent. The ligands and corresponding rhenium(I) complexes are luminescent. In the case of the ligands, the white-blue luminescence is very strong.

5.5 Experimental section

5.5.1 Synthesis of precursors and ligands

(a) 3,8-Dibromo-1,10-phenanthroline (13)
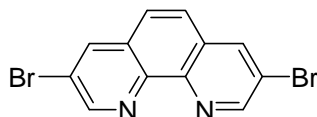
A stirred solution of 1-chlorobutane (200 ml) containing 1,10-phenanthroline (0.028 mol, 5.0 g), S_2Cl_2 (0.091 mol, 12.3 g), pyridine (0.090 mol, 7.1 g) and Br_2 (0.088 mol, 14.0 g) was heated under reflux for 16 h. After cooling to room temperature, the solid formed was separated and an aqueous solution of sodium hydroxide (excess) and chloroform (100 ml) was added. The organic layer was separated and washed with water. Then the organic layer was dried over $MgSO_4$ and the solvent was removed under reduced pressure. The crude product was purified on a silica column with chloroform/methanol (96:4) as the eluent to obtain a colorless solid. The product was crystallized from tetrachloroethylene (25 ml) and dried in a vacuum oven at 50 °C. Yield: 38% (3.6 g). δ_H (300 MHz, $CDCl_3$): 7.63 (s, 2H, H-aryl), 8.27 (s, 2H, H-aryl), 9.05 (s, 2H, H-aryl). Calcd. for $C_{12}H_6Br_2N_2 \cdot 0.25H_2O$: C 42.08, H 1.91, N 8.18. Found: C 42.01, H 1.47, N 8.00. M.p.: 281-283 °C (lit. m.p.: 270-273 °C)[32].

(b) Benzaldehydes (14)

All the benzaldehydes **14a-e** were prepared by adding the appropriate alkyl bromide (2.2 eq.) to a solution of 3,4-dihydroxybenzaldehyde (1 eq.) and potassium carbonate (2.2 eq.) in DMF (100 mL). A catalytic amount of potassium iodide was added and the mixture was refluxed for 3 hours under a nitrogen atmosphere. Then the mixture was cooled to room temperature and poured into 300 mL of a H_2O/HCl (100:50) solution. The solution was extracted with dichloromethane and the combined organic layers were washed with brine. Then the organic layer was dried over anhydrous $MgSO_4$ and the solvent was removed under reduced pressure. The crude product was purified on a silica column with hexane/ethyl acetate (95:5) as the eluent.

The characterization results of the ligands **14a**, **14b**, **14c** and **14e** are described in chapter 3.

Benzaldehyde 14d
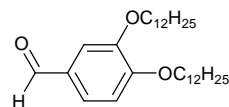
White solid. Yield: 82%. δ_H (300 MHz, $CDCl_3$): 0.88 (t, 6H, CH_3), 1.26-1.47 (m, 36H, CH_2), 1.82-1.88 (m, 4H, C**H**$_2$-CH_2-O), 4.03-4.10 (m, 4H, CH_2-O), 6.96 (d, 1H, H-aryl, J_o = 7.8 Hz), 7.40-7.43 (m, 2H, H-aryl), 9.83 (s, 1H, CH=O).

(c) Dibromo Vinylic Compounds (15)

All the dibromo vinylic compounds **15a-e** were prepared following the same procedure: a solution of triphenylphosphine (2.6 eq.) in CH_2Cl_2 (100 mL) was cooled in an ice bath. Then a solution of carbon tetrabromide (1.3 eq.) in CH_2Cl_2 (50 mL) was added at a rate to maintain the reaction temperature below 15 °C. The mixture was cooled to 0 °C and a solution of the appropriate benzaldehyde **14a-e** (1 eq.) and triethylamine (1 eq.) in CH_2Cl_2 (50 mL) was added dropwise. After stirring for 30 minutes, the reaction mixture was allowed to heat up to room temperature and the mixture was poured into hexane (200 mL). The mixture was filtered through Celite and the solid was washed with diethyl ether. The solvent was removed under reduced pressure and the compound was purified on a silica column with petroleumether/dichloromethane (50:50) as the eluent.

Dibromo Vinylic Compound 15a
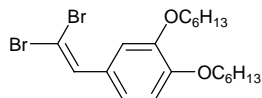
Yellow oil. Yield: 57%. δ_H (300 MHz, $CDCl_3$): 0.90 (t, 6H, CH_3), 1.26-1.49 (m, 12H, CH_2), 1.77-1.86 (m, 4H, C**H**$_2$-CH_2-O), 3.97-4.02 (m, 4H, CH_2-O), 6.85 (d, 1H, H-aryl, J_o = 8.3 Hz), 7.04 (dd, 1H, H-aryl, J_o = 8.3 Hz, J_m = 1.3 Hz), 7.18 (d, 1H, H-aryl, J_m = 1.3 Hz), 7.38 (s, 1H, $CH=CBr_2$).

Dibromo Vinylic Compound 15b
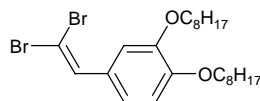
White solid. Yield: 61%. δ_H (300 MHz, CDCl$_3$): 0.88 (t, 6H, CH$_3$), 1.28-1.46 (m, 20H, CH$_2$), 1.76-1.86 (m, 4H, C**H**$_2$-CH$_2$-O), 3.97-4.01 (m, 4H, CH$_2$-O), 6.84 (d, 1H, H-aryl, J_o = 8.3 Hz), 7.04 (d, 1H, H-aryl, J_o = 8.3 Hz), 7.18 (s, 1H, H-aryl), 7.37 (s, 1H, CH=CBr$_2$).

Dibromo Vinylic Compound 15c
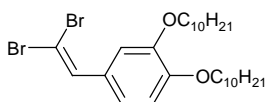
White solid. Yield: 62%. δ_H (300 MHz, CDCl$_3$): 0.88 (t, 6H, CH$_3$), 1.27-1.46 (m, 28H, CH$_2$), 1.76-1.83 (m, 4H, C**H**$_2$-CH$_2$-O), 3.97-4.01 (m, 4H, CH$_2$-O), 6.84 (d, 1H, H-aryl, J_o = 8.3 Hz), 7.04 (d, 1H, H-aryl, J_o = 8.3 Hz), 7.18 (d, 1H, H-aryl), 7.37 (s, 1H, CH=CBr$_2$).

Dibromo Vinylic Compound 15d
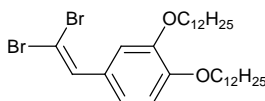
White solid. Yield: 55%. δ_H (300 MHz, CDCl$_3$): 0.88 (t, 6H, CH$_3$), 1.26-1.46 (m, 36H, CH$_2$), 1.77-1.86 (m, 4H, C**H**$_2$-CH$_2$-O), 3.97-4.02 (m, 4H, CH$_2$-O), 6.85 (d, 1H, H-aryl, J_o = 8.3 Hz), 7.04 (dd, 1H, H-aryl, J_o = 8.3 Hz, J_m = 1.3 Hz), 7.18 (s, 1H, H-aryl), 7.38 (s, 1H, CH=CBr$_2$).

161

Dibromo Vinylic Compound 15e
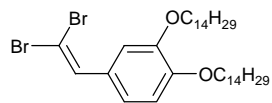
White solid. Yield: 59%. δ_H (300 MHz, CDCl$_3$): 0.88 (t, 6H, CH$_3$), 1.26-1.46 (m, 44H, CH$_2$), 1.77-1.86 (m, 4H, C**H**$_2$-CH$_2$-O), 3.97-4.02 (m, 4H, CH$_2$-O), 6.85 (d, 1H, H-aryl, J_o = 8.3 Hz), 7.04 (dd, 1H, H-aryl, J_o = 8.3 Hz, J_m = 1.2 Hz), 7.18 (d, 1H, H-aryl, J_m = 1.2 Hz), 7.38 (s, 1H, CH=CBr$_2$).

(d) Acetylenes (16)

All the acetylenes **16a-e** were prepared by slowly adding EtMgBr (2 eq., 1 M solution in THF) to a solution of the appropriate dibromo vinylic compound **15a-e** (1 eq.) in THF (100 mL) at a rate to maintain the reaction temperature between 25 and 30 °C. After stirring for 30 minutes, solid NH$_4$Cl was added and the mixture was poured into hexane (200 mL). The mixture was filtered and the solvent was evaporated under reduced pressure. The residue was purified on a silica column with petroleumether/dichloromethane (70:30) as the eluent.

Acetylene 16a
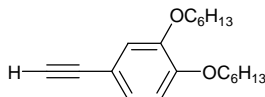
Yellow oil. Yield: 73%. δ_H (300 MHz, CDCl$_3$): 0.90 (t, 6H, CH$_3$), 1.33-1.48 (m, 12H, CH$_2$), 1.76-1.85 (m, 4H, C**H**$_2$-CH$_2$-O), 2.98 (s, 1H, C≡C-H), 3.95-4.01 (m, 4H, CH$_2$-O), 6.80 (d, 1H, H-aryl, J_o = 8.3 Hz), 6.99 (d, 1H, H-aryl, J_m = 1.3 Hz), 7.04 (dd, 1H, H-aryl, J_o = 8.3 Hz, J_m = 1.3 Hz).

Acetylene 16b
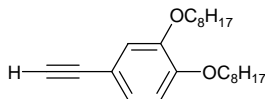
Brown solid. Yield: 76%. δ_H (300 MHz, CDCl$_3$): 0.88 (t, 6H, CH$_3$), 1.28-1.48 (m, 20H, CH$_2$), 1.76-1.85 (m, 4H, C**H**$_2$-CH$_2$-O), 2.97 (s, 1H, C≡C-H), 3.94-4.00 (m, 4H, CH$_2$-O), 6.79 (d, 1H, H-aryl, J_o = 8.3 Hz), 6.99 (d, 1H, H-aryl, J_m = 1.3 Hz), 7.04 (dd, 1H, H-aryl, J_o = 8.3 Hz, J_m = 1.3 Hz).

Acetylene 16c
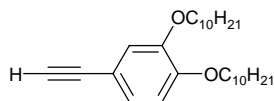
White solid. Yield: 69%. δ_H (300 MHz, CDCl$_3$): 0.88 (t, 6H, CH$_3$), 1.27-1.46 (m, 28H, CH$_2$), 1.76-1.83 (m, 4H, C**H**$_2$-CH$_2$-O), 2.98 (s, 1H, C≡C-H), 3.95-4.01 (m, 4H, CH$_2$-O), 6.80 (d, 1H, H-aryl, J_o = 8.3 Hz), 6.99 (d, 1H, H-aryl, J_m = 1.7 Hz), 7.04 (dd, 1H, H-aryl, J_o = 8.3 Hz, J_m = 1.7 Hz).

Acetylene 16d
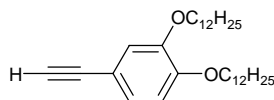
White solid. Yield: 71%. δ_H (300 MHz, CDCl$_3$): 0.88 (t, 6H, CH$_3$), 1.26-1.46 (m, 36H, CH$_2$), 1.76-1.85 (m, 4H, C**H**$_2$-CH$_2$-O), 2.98 (s, 1H, C≡C-H), 3.95-4.01 (m, 4H, CH$_2$-O), 6.80 (d, 1H, H-aryl, J_o = 8.2 Hz), 6.99 (s, 1H, H-aryl), 7.04 (d, 1H, H-aryl, J_o = 8.2 Hz).

Acetylene 16e
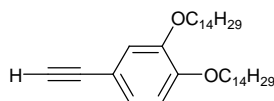
White solid. Yield: 79%. δ_H (300 MHz, CDCl$_3$): 0.89 (t, 6H, CH$_3$), 1.27-1.52 (m, 44H, CH$_2$), 1.77-1.86 (m, 4H, C**H**$_2$-CH$_2$-O), 2.99 (s, 1H, C≡C-H), 3.96-4.02 (m, 4H, CH$_2$-O), 6.81 (d, 1H, H-aryl, J_o = 8.2 Hz), 7.00 (d, 1H, H-aryl, J_m = 1.7 Hz), 7.05 (dd, 1H, H-aryl, J_o = 8.2 Hz, J_m = 1.7 Hz).

(e) Alkynes (17)

All the alkynes **17a-e** were prepared by adding 4-trimethylsilylbromobenzene (1 eq.) and [Pd(PPh$_3$)$_4$] (0.05 eq.) to a degassed solution of piperidine (40 mL). The solution was flushed with nitrogen and stirred for 20 minutes. Then the appropriate acetylene **16a-e** (1.2 eq.) was added. The mixture was flushed with nitrogen and heated to 60 °C for 24 hours. The mixture was poured into a saturated aqueous solution of ammonium chloride and extracted with diethyl ether. The organic layer was washed with water and brine, dried over MgSO$_4$ and the solvent was removed under reduced pressure. The crude product was purified on an alumina column with hexane/ethyl acetate (98:2) as the eluent.

Alkyne 17a
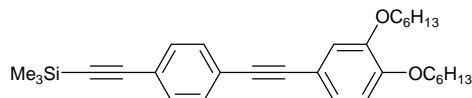
White powder. Yield: 55%. δ_H (300 MHz, CDCl$_3$): 0.27 (s, 9H, CH$_3$), 0.85-0.95 (m, 6H, CH$_3$), 1.36-1.49 (m, 12H, CH$_2$), 1.80-1.89 (m, 4H, C**H**$_2$-CH$_2$-O), 3.98-4.05 (m, 4H, CH$_2$-O), 6.86 (d, 1H, H-aryl, J_o = 8.3 Hz), 7.05 (d, 1H, H-aryl, J_m = 2.1 Hz), 7.09 (dd, 1H, H-aryl, J_o = 8.3 Hz, J_m = 2.1 Hz), 7.45 (s, 4H, H-aryl).

Alkyne 17b
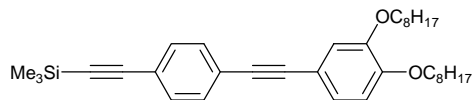
White powder. Yield: 67%. δ_H (300 MHz, CDCl$_3$): 0.25 (s, 9H, CH$_3$), 0.88-0.91 (m, 6H, CH$_3$), 1.29-1.47 (m, 20H, CH$_2$), 1.78-1.87 (m, 4H, C**H**$_2$-CH$_2$-O), 4.00 (t, 4H, CH$_2$-O), 6.84 (d, 1H, H-aryl, J_o = 8.2 Hz), 7.03 (s, 1H, H-aryl), 7.07 (d, 1H, H-aryl, J_o = 8.2 Hz), 7.43 (s, 4H, H-aryl).

165
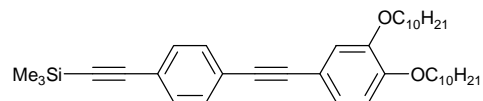
Alkyne 17c

White powder. Yield: 62%. δ_H (300 MHz, CDCl$_3$): 0.27 (s, 9H, CH$_3$), 0.88-0.92 (m, 6H, CH$_3$), 1.29-1.49 (m, 28H, CH$_2$), 1.80-1.89 (m, 4H, C**H**$_2$-CH$_2$-O), 4.00-4.04 (m, 4H, CH$_2$-O), 6.86 (d, 1H, H-aryl, J_o = 8.3 Hz), 7.04 (d, 1H, H-aryl, J_m = 1.8 Hz), 7.09 (dd, 1H, H-aryl, J_o = 8.3 Hz, J_m = 1.8 Hz), 7.45 (s, 4H, H-aryl).

Alkyne 17d
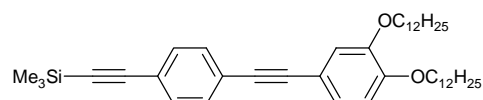
White powder. Yield: 61%. δ_H (300 MHz, CDCl$_3$): 0.25 (s, 9H, CH$_3$), 0.90 (t, 6H, CH$_3$), 1.26-1.47 (m, 36H, CH$_2$), 1.78-1.87 (m, 4H, C**H**$_2$-CH$_2$-O), 4.00 (t, 4H, CH$_2$-O), 6.84 (d, 1H, H-aryl, J_o = 8.3 Hz), 7.02 (s, 1H, H-aryl), 7.07 (d, 1H, H-aryl, J_o = 8.3 Hz), 7.42 (s, 4H, H-aryl).

Alkyne 17e
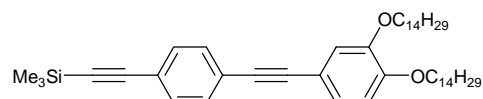
White powder. Yield: 69%. δ_H (300 MHz, CDCl$_3$): 0.25 (s, 9H, CH$_3$), 0.88 (t, 6H, CH$_3$), 1.26-1.47 (m, 44H, CH$_2$), 1.78-1.87 (m, 4H, C**H**$_2$-CH$_2$-O), 4.00 (t, 4H, CH$_2$-O), 6.84 (d, 1H, H-aryl, J_o = 8.3 Hz), 7.03 (s, 1H, H-aryl), 7.07 (d, 1H, H-aryl, J_o = 8.3 Hz), 7.45 (s, 4H, H-aryl).

(f) Acetylenes (18)

All the acetylenes **18a-e** were prepared by dissolving the appropriate alkyne **17a-e** (1 eq.) in dry THF (50 mL) and the solution was cooled to -55 °C. Bu_4NF (2.5 eq., 1 M solution in THF) was added and the reaction mixture was stirred for 1 hour. Then the solution was allowed to warm up to -30 °C at which point water was added (50 mL). The reaction mixture was allowed to warm up to room temperature and stirred for 16 hours under a nitrogen atmosphere. The solvent was evaporated and the resulting solid dissolved in dichloromethane and washed with water and brine. The organic layer was dried over $MgSO_4$ and the solvent was removed under reduced pressure. The crude product was purified on an alumina column with hexane/ethyl acetate (97:3) as the eluent.

Acetylene 18a
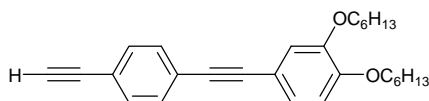
Yellow powder. Yield: 74%. δ_H (300 MHz, $CDCl_3$): 0.91 (t, 6H, CH_3), 1.34-1.50 (m, 12H, CH_2), 1.78-1.87 (m, 4H, CH_2-CH_2-O), 3.18 (s, 1H, C≡C-H), 4.01 (t, 4H, CH_2-O), 6.84 (d, 1H, H-aryl, J_o = 8.3 Hz), 7.03 (s, 1H, H-aryl), 7.08 (d, 1H, H-aryl, J_o = 8.3 Hz), 7.45 (s, 4H, H-aryl).

Acetylene 18b
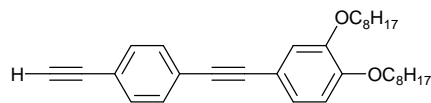
Yellow powder. Yield: 71%. δ_H (300 MHz, CDCl$_3$): 0.88-0.91 (m, 6H, CH$_3$), 1.29-1.47 (m, 20H, CH$_2$), 1.80-1.85 (m, 4H, CH$_2$-CH$_2$-O), 3.16 (s, 1H, C≡C-H), 4.00 (t, 4H, CH$_2$-O), 6.83 (d, 1H, H-aryl, J_o = 8.2 Hz), 7.03 (s, 1H, H-aryl), 7.07 (d, 1H, H-aryl, J_o = 8.2 Hz), 7.45 (s, 4H, H-aryl).

Acetylene 18c
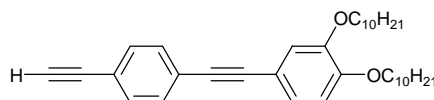
Yellow powder. Yield: 80%. δ_H (300 MHz, CDCl$_3$): 0.88 (t, 6H, CH$_3$), 1.28-1.47 (m, 28H, CH$_2$), 1.78-1.85 (m, 4H, CH$_2$-CH$_2$-O), 3.17 (s, 1H, C≡C-H), 4.01 (t, 4H, CH$_2$-O), 6.84 (d, 1H, H-aryl, J_o = 8.3 Hz), 7.03 (s, 1H, H-aryl), 7.08 (d, 1H, H-aryl, J_o = 8.3 Hz), 7.45 (s, 4H, H-aryl).

Acetylene 18d
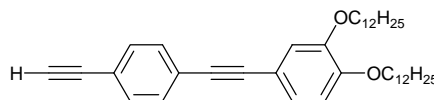
Yellow powder. Yield: 69%. δ_H (300 MHz, CDCl$_3$): 0.93 (t, 6H, CH$_3$), 1.31-1.50 (m, 36H, CH$_2$), 1.83-1.88 (m, 4H, CH$_2$-CH$_2$-O), 3.19 (s, 1H, C≡C-H), 4.03 (t, 4H, CH$_2$-O), 6.86 (d, 1H, H-aryl, J_o = 8.2 Hz), 7.07 (s, 1H, H-aryl), 7.11 (d, 1H, H-aryl, J_o = 8.2 Hz), 7.48 (s, 4H, H-aryl).

Acetylene 18e
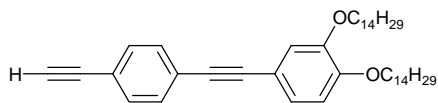
Yellow powder. Yield: 74%. δ_H (300 MHz, CDCl$_3$): 0.91 (t, 6H, CH$_3$), 1.29-1.49 (m, 44H, CH$_2$), 1.83-1.87 (m, 4H, CH$_2$-CH$_2$-O), 3.18 (s, 1H, C≡C-H), 4.03 (t, 4H, CH$_2$-O), 6.86 (d, 1H, H-aryl, J_o = 8.2 Hz), 7.06 (s, 1H, H-aryl), 7.10 (d, 1H, H-aryl, J_o = 8.2 Hz), 7.47 (s, 4H, H-aryl).

(g) Ligands L

All the ligands **L$_{XIV}$-L$_{XVIII}$** were prepared following the same procedure: to a degassed solution of 3,8-dibromo-1,10-phenanthroline (13) (1 eq.) in dry DMF (30 mL) was added [PdCl$_2$(PPh$_3$)$_2$] (0.055 eq.). The reaction mixture was flushed with nitrogen and stirred for 20 minutes. Then the appropriate alkyne 18a-e (2.8 eq.), diisopropylamine (2.8 eq.) and copper iodide (0.115 eq.) were added. The reaction mixture was flushed with nitrogen and heated to 82 °C for 48 hours. The mixture was allowed to cool to room temperature and poured into an aqueous 2% solution of KCN (100 mL). Then the solution was extracted with CHCl$_3$. The organic layer was washed with H$_2$O and dried over MgSO$_4$. The solvent was removed under reduced pressure and the crude product was purified on a silica column with CH$_2$Cl$_2$/MeOH (99:1) as the eluent.

Ligand L$_{XIV}$
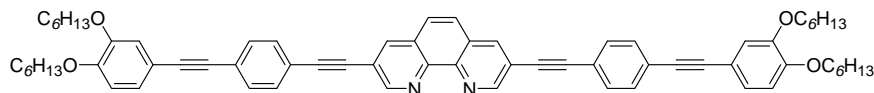
Yellow powder. Yield: 75%. δ$_H$ (400 MHz, CDCl$_3$): 0.91-0.93 (m, 12H, CH$_3$), 1.36-1.50 (m, 24H, CH$_2$), 1.79-1.87 (m, 8H, CH$_2$-CH$_2$-O), 4.02 (t, 8H, CH$_2$-O), 6.85 (d, 2H, H-aryl, J_o = 8.3 Hz), 7.05 (s, 2H, H-aryl), 7.10 (d, 2H, H-aryl, J_o = 8.3 Hz), 7.52-7.60 (m, 8H, H-aryl), 7.81 (s, 2H, H-aryl), 8.38 (d, 2H, H-aryl, J_m = 1.6 Hz), 9.29 (d, 2H, H-aryl, J_m = 1.6 Hz). δ$_C$ (100 MHz, CDCl$_3$): 13.97, 22.58, 25.67, 29.21, 31.56, 69.21, 69.36, 87.46, 88.00, 92.28, 113.38, 114.99, 116.84, 119.74, 121.72, 124.39, 125.15, 126.90, 128.13, 131.48, 131.72, 138.01, 144.55, 148.87, 150.10, 152.43. Calcd. for C$_{68}$H$_{72}$N$_2$O$_4$·H$_2$O: C 81.73, H 7.46, N 2.80. Found: C 82.18, H 7.81, N 2.75.

Ligand L$_{XV}$
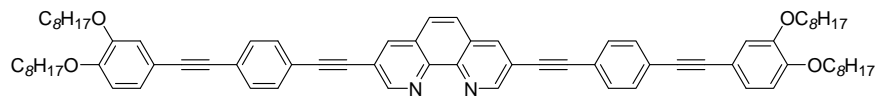
Yellow powder. Yield: 71%. δ_H (400 MHz, CDCl$_3$): 0.89 (t, 12H, CH$_3$), 1.30-1.48 (m, 40H, CH$_2$), 1.79-1.87 (m, 8H, CH$_2$-CH$_2$-O), 4.02 (t, 8H, CH$_2$-O), 6.84 (d, 2H, H-aryl, J_o = 8.3 Hz), 7.05 (d, 2H, H-aryl, J_m = 1.6 Hz), 7.09 (dd, 2H, H-aryl, J_o = 8.3 Hz, J_m = 1.6 Hz), 7.51-7.58 (m, 8H, H-aryl), 7.77 (s, 2H, H-aryl), 8.34 (d, 2H, H-aryl, J_m = 1.9 Hz), 9.26 (d, 2H, H-aryl, J_m = 1.9 Hz). δ_C (100 MHz, CDCl$_3$): 14.06, 22.65, 26.01, 29.25, 29.35, 31.81, 69.21, 69.37, 87.46, 88.00, 92.29, 93.89, 113.39, 114.99, 116.85, 119.72, 121.71, 124.38, 125.17, 126.89, 128.12, 131.47, 131.72, 138.00, 144.50, 148.86, 150.10, 152.40. Calcd. for C$_{76}$H$_{88}$N$_2$O$_4$·H$_2$O: C 82.12, H 8.16, N 2.52. Found: C 82.60, H 8.61, N 2.47.

Ligand L$_{XVI}$
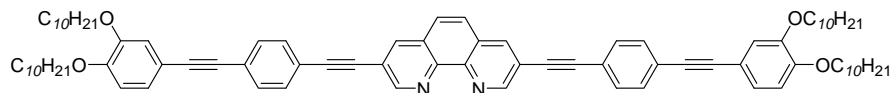
Yellow powder. Yield: 76%. δ_H (400 MHz, CDCl$_3$): 0.89 (t, 12H, CH$_3$), 1.28-1.48 (m, 56H, CH$_2$), 1.82-1.84 (m, 8H, CH$_2$-CH$_2$-O), 4.02 (t, 8H, CH$_2$-O), 6.85 (d, 2H, H-aryl, J_o = 8.4 Hz), 7.05 (s, 2H, H-aryl), 7.10 (d, 2H, H-aryl, J_o = 8.4 Hz), 7.52-7.60 (m, 8H, H-aryl), 7.81 (s, 2H, H-aryl), 8.38 (d, 2H, H-aryl, J_m = 1.5 Hz), 9.28 (d, 2H, H-aryl, J_m = 1.5 Hz). δ_C (100 MHz, CDCl$_3$): 14.06, 22.66, 26.01, 29.25, 29.32, 29.39, 29.56, 29.60, 31.90, 69.23, 69.38, 87.45, 88.00, 92.28, 93.89, 113.42, 114.99, 116.88, 121.72, 124.40, 125.15, 126.90, 128.14, 131.49, 131.72, 138.02, 144.56, 148.88, 150.11, 152.44. Calcd. for C$_{84}$H$_{104}$N$_2$O$_4$·H$_2$O: C 82.44, H 8.73, N 2.29. Found: C 82.62, H 8.58, N 2.30.

Ligand L$_{XVII}$
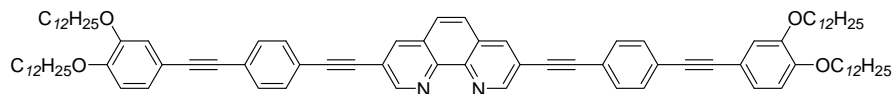
Yellow powder. Yield: 78%. δ_H (400 MHz, CDCl$_3$): 0.89 (t, 12H, CH$_3$), 1.27-1.48 (m, 72H, CH$_2$), 1.79-1.87 (m, 8H, CH$_2$-CH$_2$-O), 4.01 (t, 8H, CH$_2$-O), 6.85 (d, 2H, H-aryl, J_o = 8.3 Hz), 7.05 (d, 2H, H-aryl, J_m = 1.6 Hz), 7.10 (dd, 2H, H-aryl, J_o = 8.3 Hz, J_m = 1.6 Hz), 7.51-7.59 (m, 8H, H-aryl), 7.79 (s, 2H, H-aryl), 8.36 (d, 2H, H-aryl, J_m = 1.8 Hz), 9.27 (d, 2H, H-aryl, J_m = 1.8 Hz). δ_C (100 MHz, CDCl$_3$): 14.07, 22.66, 26.02, 29.25, 29.34, 29.40, 29.62, 29.68, 31.91, 69.22, 69.38, 113.41, 116.87, 125.16, 126.91, 131.48, 131.72, 138.03, 148.87, 150.11, 152.41. Calcd. for C$_{92}$H$_{120}$N$_2$O$_4$·H$_2$O: C 82.71, H 9.20, N 2.10. Found: C 82.41, H 9.44, N 2.04.

Ligand L$_{XVIII}$
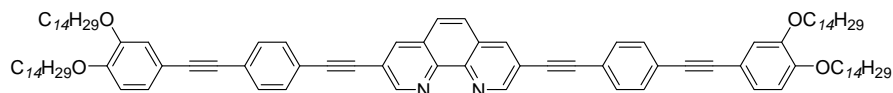
Yellow powder. Yield: 74%. δ_H (400 MHz, CDCl$_3$): 0.87-0.90 (m, 12H, CH$_3$), 1.27-1.48 (m, 88H, CH$_2$), 1.80-1.87 (m, 8H, CH$_2$-CH$_2$-O), 4.02 (t, 8H, CH$_2$-O), 6.85 (d, 2H, H-aryl, J_o = 8.4 Hz), 7.05 (s, 2H, H-aryl), 7.09 (d, 2H, H-aryl, J_o = 8.4 Hz), 7.53-7.60 (m, 8H, H-aryl), 7.81 (s, 2H, H-aryl), 8.38 (b, s, 2H, H-aryl), 9.29 (b, s, 2H, H-aryl). δ_C (100 MHz, CDCl$_3$): 14.06, 22.66, 26.01, 29.24, 29.34, 29.39, 29.61, 29.69, 31.91, 69.22, 69.37, 87.45, 88.00, 92.29, 93.90, 113.42, 114.99, 116.88, 119.77, 121.73, 124.41, 125.16, 126.91, 128.15, 131.49, 131.73, 138.04, 144.54, 148.88, 150.11, 152.46. Calcd. for C$_{100}$H$_{136}$N$_2$O$_4$·H$_2$O: C 82.94, H 9.60, N 1.93. Found: C 82.58, H 9.91, N 1.92.

5.5.2 Synthesis of the rhenium(I) complexes

(h) Rhenium(I) Complexes L_{XIV}-L_{XVIII}

All the rhenium(I) complexes L_{XIV}-L_{XVIII} were prepared by adding a solution of rhenium(I) pentacarbonyl bromide (1 eq.) in toluene (10 mL) to a solution of the appropriate ligand L_{XIV}-L_{XVIII} (1 eq.) in toluene (25 mL). The mixture was refluxed for 3 hours. Then the solvent was removed under reduced pressure and the crude product was purified on a silica column with $CHCl_3$/hexane (50:50) as the eluent. The complex was dissolved in a small amount of $CHCl_3$ and precipitated in methanol. The precipitate was filtered off and dried in a vacuum oven at 50 °C.

Rhenium(I) Complex L_{XIV}
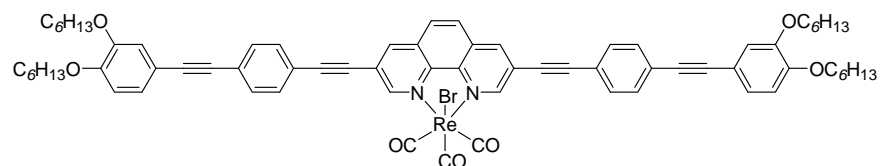
Orange powder. Yield: 60%. δ_H (400 MHz, $CDCl_3$): 0.92-0.94 (m, 12H, CH_3), 1.33-1.51 (m, 24H, CH_2), 1.76-1.85 (m, 8H, CH_2-CH_2-O), 3.96-4.03 (m, 8H, CH_2-O), 6.82 (d, 2H, H-aryl, J_o = 8.3 Hz), 7.00-7.03 (m, 4H, H-aryl), 7.44-7.52 (m, 8H, H-aryl), 7.86 (s, 2H, H-aryl), 8.30 (s, 2H, H-aryl), 9.36 (s, 2H, H-aryl). δ_C (100 MHz, $CDCl_3$): 13.98, 22.58, 25.66, 25.70, 29.18, 29.25, 31.59, 69.18, 69.40, 85.50, 87.31, 93.01, 97.05, 113.28, 114.71, 116.82, 120.32, 122.61, 125.29, 127.83, 130.17, 131.54, 131.96, 138.94, 144.86, 148.86, 150.25, 154.85, 188.49, 196.23. IR (KBr-pellet, cm^{-1}): 3441 (m, ν(N−H)), 2953, 2926, 2856 (s, aliphatic C−H stretch), 2018, 1920, 1896 (s, ν(CO)). Calcd. for $C_{71}H_{72}BrN_2O_7Re \cdot H_2O$: C 63.19, H 5.53, N 2.08. Found: C 62.86, H 5.62, N 2.08.

Rhenium(I) Complex L$_{XV}$
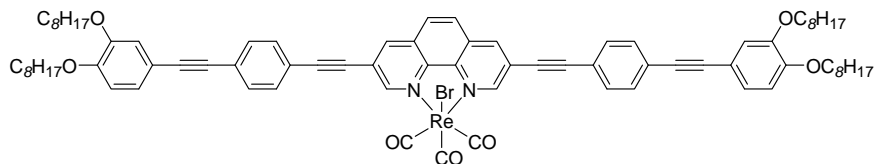
Orange powder. Yield: 54%. δ_H (300 MHz, CDCl$_3$): 0.89 (b, t, 12H, CH$_3$), 1.29-1.51 (m, 56H, CH$_2$), 1.78-1.89 (m, 8H, C**H**$_2$-CH$_2$-O), 3.98-4.05 (m, 8H, CH$_2$-O), 6.83 (d, 2H, H-aryl, J_o = 8.2 Hz), 7.04 (d, 2H, H-aryl, J_m = 1.8 Hz), 7.09 (d, 2H, H-aryl, J_o = 8.2 Hz), 7.51-7.59 (m, 8H, H-aryl), 7.95 (s, 2H, H-aryl), 8.47 (d, 2H, H-aryl, J_m = 1.8 Hz), 9.43 (d, 2H, H-aryl, J_m = 1.8 Hz). Calcd. for C$_{79}$H$_{88}$BrN$_2$O$_7$Re·H$_2$O: C 64.91, H 6.21, N 1.92. Found: C 64.90, H 6.37, N 1.93.

Rhenium(I) Complex L$_{XVI}$
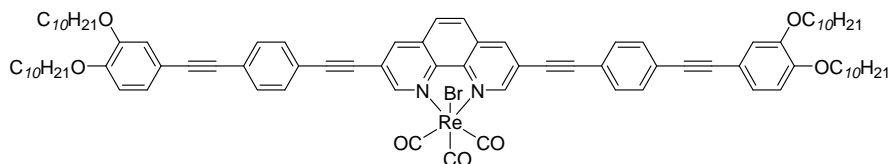
Orange powder. Yield: 55%. δ_H (300 MHz, CDCl$_3$): 0.89 (t, 12H, CH$_3$, J = 6.0 Hz), 1.28-1.49 (m, 56H, CH$_2$), 1.78-1.89 (m, 8H, C**H**$_2$-CH$_2$-O), 3.99-4.04 (m, 8H, CH$_2$-O), 6.84 (d, 2H, H-aryl, J_o = 8.2 Hz), 7.05 (s, 2H, H-aryl), 7.11 (d, 2H, H-aryl, J_o = 8.2 Hz), 7.54-7.62 (m, 8H, H-aryl), 7.98 (s, 2H, H-aryl), 8.53 (s, 2H, H-aryl), 9.46 (s, 2H, H-aryl). Calcd. for C$_{87}$H$_{104}$BrN$_2$O$_7$Re: C 67.16, H 6.74, N 1.80. Found: C 67.16, H 7.22, N 1.84.

174

Rhenium(I) Complex L$_{XVII}$
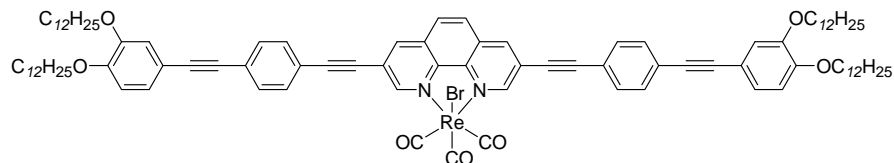
Orange powder. Yield: 52%. δ_H (300 MHz, CDCl$_3$): 0.89 (t, 12H, CH$_3$, J = 6.2 Hz), 1.28-1.49 (m, 72H, CH$_2$), 1.78-1.89 (m, 8H, C**H**$_2$-CH$_2$-O), 3.99-4.05 (m, 8H, CH$_2$-O), 6.84 (d, 2H, H-aryl, J_o = 8.2 Hz), 7.05 (s, 2H, H-aryl), 7.11 (d, 2H, H-aryl, J_o = 8.2 Hz), 7.53-7.61 (m, 8H, H-aryl), 7.97 (s, 2H, H-aryl), 8.51 (s, 2H, H-aryl), 9.45 (s, 2H, H-aryl). Calcd. for C$_{95}$H$_{120}$BrN$_2$O$_7$Re·H$_2$O: C 67.74, H 7.46, N 1.65. Found: C 67.82, H 7.37, N 1.70.

Rhenium(I) Complex L$_{XVIII}$
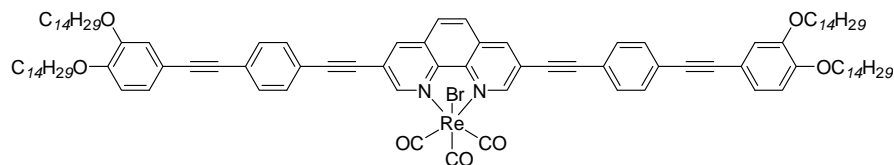
Orange powder. Yield: 53%. δ_H (300 MHz, CDCl$_3$): 0.88 (t, 12H, CH$_3$, J = 5.9 Hz), 1.27-1.51 (m, 72H, CH$_2$), 1.79-1.86 (m, 8H, C**H**$_2$-CH$_2$-O), 3.98-4.04 (m, 8H, CH$_2$-O), 6.83 (d, 2H, H-aryl, J_o = 8.3 Hz), 7.03 (s, 2H, H-aryl), 7.07 (d, 2H, H-aryl, J_o = 8.3 Hz), 7.50-7.58 (m, 8H, H-aryl), 7.93 (s, 2H, H-aryl), 8.44 (s, 2H, H-aryl), 9.42 (s, 2H, H-aryl). Calcd. for C$_{103}$H$_{136}$BrN$_2$O$_7$Re·H$_2$O: C 68.79, H 7.73, N 1.56. Found: C 68.83, H 8.08, N 1.60.

5.6 References

1. Sonogashira, K.; Tohda, Y.; Hagihara, N. *Tetrahedron Lett.* **1975,** 4467-4470.

2. Sonogashira, K. *J. Organomet. Chem.* **2002,** *653,* 46-49.

3. Corey, E. J.; Fuchs, P. L. *Tetrahedron Lett.* **1972,** 3769-3772.

4. Gehringer, L.; Bourgogne, C.; Guillon, D.; Donnio, B. *J. Am. Chem. Soc.* **2004,** *126,* 3856-3867.

5. Saitoh, Y.; Koizumi, T.; Osakada, K.; Yamamoto, T. *Can. J. Chem.* **1997,** *75,* 1336-1339.

6. Boldron, C.; Pitie, M.; Meunier, B. *Synlett* **2001,** 1629-1631.

7. Cardinaels, T. Liquid-crystalline complexes of transition metals and rare earths with substituted 1,10-phenanthroline ligands. K.U.Leuven, 2006.

8. Rowe, K. E.; Bruce, D. W. *J. Mater. Chem.* **1998,** *8,* 331-341.

9. Fazio, D.; Mongin, C.; Donnio, B.; Galerne, Y.; Guillon, D.; Bruce, D. W. *J. Mater. Chem.* **2001,** *11,* 2852-2863.

10. Allouchi, H.; Cotrait, M.; Guillon, D.; Heinrich, B.; Nguyen, H. T. *Chem. Mater.* **1995,** *7,* 2252-2258.

11. Hammond, C. *The Basics of Crystallography and Diffraction;* 2nd ed.; Oxford Science Publications: Oxford, United Kingdom, 2001.

12. Bury, I.; Heinrich, B.; Bourgogne, C.; Guillon, D.; Donnio, B. *Chem. Eur. J.* **2006,** *12,* 8396-8413.

13. Tschierske, C. *J. Mater. Chem.* **1998,** *8,* 1485-1508.

14. Duan, H.; Hudson, S. D.; Ungar, G.; Holerca, M. N.; Percec, V. *Chem. Eur. J.* **2001,** *7,* 4134-4141.

15. Yeardley, D. J. P.; Ungar, G.; Percec, V.; Holerca, M. N.; Johansson, G. *J. Am. Chem. Soc.* **2000,** *122,* 1684-1689.

16. Kutsumizu, S. *Curr. Opin. Solid State Mater. Sci.* **2002,** *6,* 537-543.

17. Diele, S. *Curr. Opin. Colloid Interface Sci.* **2002,** *7,* 333-342.

18. Imperor-Clerc, M. *Curr. Opin. Colloid Interface Sci.* **2005,** *9,* 370-376.

19. Levelut, A. M.; Clerc, M. *Liq. Cryst.* **1998,** *24,* 105-115.

20. Zeng, X. B.; Ungar, G.; Imperor-Clerc, M. *Nature Materials* **2005,** *4,* 562-567.

21. Percec, V.; Mitchell, C. M.; Cho, W. D.; Uchida, S.; Glodde, M.; Ungar, G.; Zeng, X. B.; Liu, Y. S.; Balagurusamy, V. S. K.; Heiney, P. A. *J. Am. Chem. Soc.* **2004,** *126,* 6078-6094.

22. Percec, V.; Holerca, M. N.; Nummelin, S.; Morrison, J. L.; Glodde, M.; Smidrkal, J.; Peterca, M.; Rosen, B. M.; Uchida, S.; Balagurusamy, V. S. K.; Sienkowska, M. J.; Heiney, P. A. *Chem. Eur. J.* **2006,** *12,* 6216-6241.

23. Percec, V.; Peterca, M.; Sienkowska, M. J.; Ilies, M. A.; Aqad, E.; Smidrkal, J.; Heiney, P. A. *J. Am. Chem. Soc.* **2006,** *128,* 3324-3334.

24. Donnio, B.; Heinrich, B.; Allouchi, H.; Kain, J.; Diele, S.; Guillon, D.; Bruce, D. W. *J. Am. Chem. Soc.* **2004,** *126,* 15258-15268.

25. Nguyen, H. T.; Destrade, C.; Malthête, J. *Adv. Mater.* **1997,** *9,* 375-388.

26. Stufkens, D. J.; Vlcek, A. *Coord. Chem. Rev.* **1998,** *177,* 127-179.

27. Donnio, B.; Guillon, D.; Deschenaux, R.; Bruce, D. W. Metallomesogens. In *Comprehensive Coordination Chemistry II;* McCleverty, J. A.; Meyer, T. J., Eds.; Elsevier: Oxford, United Kingdom, 2003; pp 357-627.

28. Donnio, B.; Rowe, K. E.; Roll, C. P.; Bruce, D. W. *Mol. Cryst. Liq. Cryst. Sci. Technol. , Sect. A* **1999,** *332,* 2893-2900.

29. Date, R. W.; Iglesias, E. F.; Rowe, K. E.; Elliott, J. M.; Bruce, D. W. *Dalton Trans.* **2003,** 1914-1931.

30. Malthête, J.; Nguyen, H. T.; Destrade, C. *Liq. Cryst.* **1993,** *13,* 171-187.

31. Nguyen, H. T.; Destrade, C.; Malthête, J. Phasmids and Polycatenar Mesogens. In *Handbook of Liquid Crystals;* Demus, D.; Goodby, J. W.; Gray, G. W.; Spiess, H.-W.; Vill, V., Eds.; Wiley-VCH: Weinheim, 1998; pp 865-886.

32. Kalsani, V.; Schmittel, M.; Listorti, A.; Accorsi, G.; Armaroli, N. *Inorg. Chem.* **2006,** *45,* 2061-2067.

Summary

The choice of 1,10-phenanthroline as primary building block for metallomesogens is justified by the ability of 1,10-phenanthroline to form complexes with *d*-block and *f*-block metals. In this way, it is possible to introduce the properties of transition metals into liquid crystals. The synthesis of new metallomesogens and their characterization was the aim of this PhD thesis.

In the first part, substituted imidazo*[4,5-f]*-1,10-phenanthrolines were used as building blocks for metal-containing liquid crystals. Imidazo*[4,5-f]*-1,10-phenanthrolines are versatile systems because they can form stable complexes with different *d*-block transition metals, including platinum(II) and rhenium(I), as well as with lanthanide(III) ions and uranyl, and they can be easily structurally modified by a judicious choice of the precursory benzaldehyde. None of the ligands designed for this study were liquid-crystalline. Mesomorphism could however be induced by their coordination to various metallic fragments. The thermal behavior of the metal complexes depended on the metal-to-ligand ratio. The lanthanide(III) complexes with a metal-to-ligand ratio of 1:2 (ML_2, with $M = Ln^{III}$) formed an enantiotropic cubic mesophase or were not liquid-crystalline, depending on the nature of the lanthanide(III) ion. Self-assembled monolayers of the europium(III) complex were investigated by scanning tunnelling microscopy (STM).

In the second part, imidazo*[4,5-f]*-1,10-phenanthroline and pyrazino*[2,3-f]*-1,10-phenanthroline are substituted with long alkyl chains and used as ligands for the design of metallomesogens, this because of the ease of ligand substitution. Whereas the ligands and the corresponding rhenium(I) complexes were not liquid-crystalline, mesomorphism was observed for ionic ruthenium(II) complexes with chloride, hexafluorophosphate and bistriflimide counter ions. The mesophases were identified as a smectic A

phase (SmA) by high-temperature small-angle X-ray scattering (SAXS) using synchrotron radiation. The transition temperatures strongly depend on the anion, the highest temperatures being observed for the chloride salts and the lowest for the bistriflimide salts. The ruthenium(II) complexes are examples of luminescent ionic liquid crystals. The imidazo*[4,5-f]*-1,10-phenanthroline ligand and the corresponding ruthenium(II) chloride complex exhibited lyotropic mesomorphic behavior.

A different approach was to modify 1,10-phenanthroline so that a tetracatenar was formed. The tetracatenar ligands were obtained by substituting the 1,10-phenanthroline central core unit at the 3- and 8-positions by extended, rigid acetylene moieties, equipped at the termini with two alkoxy chains of various length ($n = 6, 8, 10, 12, 14$). These mesogens exhibited a rich mesomorphism including smectic C, cubic, hexagonal and rectangular columnar phases, depending on the alkoxy chain length. The corresponding rhenium(I) complexes containing the bulky [ReBr(CO)$_3$] fragment were not liquid-crystalline. The ligands and rhenium(I) complexes were inverstigated by scanning tunnelling microscopy (STM) and both the ligands and the rhenium(I) complexes can be self-assembled into monolayers at the TCB-graphite and octanoic acid-graphite interfaces. The ligands and corresponding rhenium(I) complexes are luminescent.

Most of the objectives were obtained. In case of the 5,6-substituted 1,10-phenanthroline ligand, metallomesogens were obtained with lanthanide(III) and ruthenium(II) ions. The rhenium(I) complexes didn't exhibit mesomorphism. The ligand itself wasn't liquid-crystalline, but by combining the f-block or d-block element with the ligand, mesomorphism was obtained due to the geometry introduced by this metal ion. The 3,8-substituted 1,10-phenanthroline ligands were liquid-crystalline, but none of the complexes were liquid-crystalline. The objective of having luminescent properties was the least successful: the lanthanide(III) complexes showed

180

very weak luminescence and the ruthenium(II) complexes need further experiments for a unequivocal interpretation.

I hope that this PhD thesis is an invitation for people to perform further research on metallomesogens based on 1,10-phenanthroline. Not only the 5,6-substituted and 3,8-substituted phenanthrolines are interesting systems 2,9- and 4,7-substituted 1,10-phenanthrolines have a bended shape which can introduce totally different properties. Besides alkyl chains, mesogenic groups can be attached to the bent core.

Concerning the lyomesogens, described in chapter 4, investigation by XRD measurements is necessary to unequivocally determine the mesophases of the ligands and the ruthenium(II) complexes. Eventually a complete phase diagram can then be created in which the concentration is plotted in function of the temperature.

182

Samenvatting

De keuze voor 1,10-fenantroline als primaire bouwsteen voor metallomesogenen is gebaseerd op de mogelijkheid van 1,10-fenantroline om te complexeren met d-blok en f-blok metaalionen. Op deze manier is het mogelijk om de eigenschappen van de metaalionen te introduceren in vloeibare kristallen. De synthese en de karakterisatie van nieuwe metallomesogenen was de doelstelling van dit doctoraatsproefschrift.

In het eerste deel werden gesubstitueerde imidazo*[4,5-f]*-1,10-fenantrolines gebruikt als bouwsteen voor metaalhoudende vloeibare kristallen. De imidazo*[4,5-f]*-1,10-fenantrolines zijn veelzijdige systemen vanwege hun mogelijkheid om complexen te vormen met verschillende *d*-blok transitiemetalen, alsook met de driewaardige lanthanide-ionen en ze kunnen structureel makkelijk gevarieerd worden door de keuze van de benzaldehyde precursor. Geen enkel van de gemaakte liganden was vloeibaar kristallijn. Mesomorfisme kon echter wel geïnduceerd worden door de coördinatie met verschillende metaalionen. De lanthanide(III)-complexen met een metaal-ligandverhouding van 1:2 (ML$_2$, met M = Ln^{III}) vertonen een enantiotrope kubische mesofase of waren niet vloeibaar kristallijn, afhankelijk van het gekozen lanthanide(III)-ion. De spontaan gevormde monolagen van het europium(III)-complex werden onderzocht met scanning tunneling microscopie (STM).

In het tweede gedeelte, werden het imidazo*[4,5-f]*-1,10-fenantroline en het pyrazino*[2,3-f]*-1,10-fenantroline gesubstitueerd met lange alkylketens en gebruikt voor de synthese van metallomesogenen. De liganden en hun overeenkomstige rhenium(I)-complexen waren niet vloeibaar-kristallijn, de ionische ruthenium(II)-complexen van het chloride-, het hexafluorfosfaat- en het bistriflimide-tegenion waren daarentegen wel vloeibaar-kristallijn. Door middel van X-stralendiffractie op hoge temperatuur afkomstig van

183

synchrotronstraling werd de mesofase geïdentificeerd als een smectische A fase (SmA). De transitietemperaturen waren sterk afhankelijk van het anion, de hoogste temperaturen werden waargenomen voor de chloridezouten en de laagste voor de zouten van het bistriflimide. De ruthenium(II)-complexen zijn voorbeelden van luminescerende ionische vloeibare kristallen. Het imidazo*[4,5-f]*-1,10-fenantrolineligand en het overeenkomstige ruthenium(II)chloridecomplex vertoonden lyotroop mesofasegedrag.

Een andere benadering was het aanpassen van 1,10-fenantroline zodat een tetracatenar gevormd werd. De tetracatenarliganden werden bekomen door de substitutie van 1,10-fenantroline in de 3,8-positie door uitgebreide, rigide acetylenen voorzien van twee eindstandige alkylketens met verschillende lengtes (n = 6, 8, 10, 12, 14). Deze mesogenen bezitten een rijk mesofase-gedrag: smectische C, kubische, hexagonale en rechthoekige fasen afhankelijk van de ketenlengte. De overeenkomstige rhenium(I)-complexen met het grote [ReBr(CO)$_3$]-fragment waren niet vloeibaar-kristallijn. De liganden en de rhenium(I)-complexen werden onderzocht met scanning tunneling microscopie (STM) en zowel de liganden als de rhenium(I)-complexen vormden monolagen op TCB-grafiet en octaanzuur-grafiet-interfaces. De luminescerende eigenschappen van de liganden en de rhenium(I)-complexen werden onderzocht.

De vooropgestelde doelstellingen werden tijdens dit onderzoek voor het grootste gedeelte behaald. Voor de 5,6-gesubstitueerde liganden zijn we erin geslaagd metallomesogenen te maken met lanthanide(III) en ruthenium ionen. De rhenium(I)-verbindingen waren niet vloeibaar-kristallijn. Het ligand zelf was niet vloeibaar-kristallijn, maar door introductie van het d-blok of f-blok metaalion verkregen we metallomesogenen. De 3,8-gesubstitueerde liganden waren mesomorf, maar de metaalcomplexen vertoonden geen mesofasegedrag. De doelstelling om luminescente vloeibare kristallen te maken was het minst succesvol: de lanthanide(III)-complexen vertoonden enkel zwakke luminescentie en de ruthenium(II)-

complexen moeten nog verder onderzocht worden om een éénduidige interpretatie aan het resultaat te kunnen geven.

Hopelijk kan dit proefschrift een uitnodiging en een motivatie zijn om verder aan onderzoek te doen op metallomesogenen afgeleid van 1,10-fenantroline. Niet enkel de 5,6-gesubstitueerde en de 3,8-gesubstitueerde fenantrolines zijn interessant, ook de 2,9- en 4,7-gesubstitueerde 1,10-fenantrolines zijn interessante systemen en dit omdat ze door hun gebogen vorm totaal andere eigenschappen kunnen bezitten. Naast de alkylketens kunnen ook mesogene groepen aan de gebogen kern gekoppeld worden.

Wat betreft de lyomesogenen, beschreven in hoofdstuk 4, is verder onderzoek met X-stralen nodig om eenduidig de mesofasen van het ligand en de ruthenium(II) complexen te identificeren. Dit zal het mogelijk maken om een volledig fasediagramma op te stellen waarin de concentratie in functie van de temperatuur uitgezet kan worden.

List of publications

1. Van Deun, R.; Ramaekers, J.; Nockemann, P.; Van Hecke, K.; Van Meervelt, L.; Binnemans, K.; "Alkali-metal salts of aromatic carboxylic acids: Liquid crystals without flexible chains", *European Journal of Inorganic Chemistry* **2005**, 563-571.

2. Cardinaels, T.; Ramaekers, J.; Guillon, D.; Donnio, B.; Binnemans, K.; "A propeller-like uranyl metallomesogen", *Journal of the American Chemical Society* **2005**, *127*, 17602-17603.

3. Cardinaels, T.; Ramaekers, J.; Nockemann, P.; Driesen, K.; Van Hecke, K.; Van Meervelt, L.; Lei, S.; De Feyter, S.; Guillon, D.; Donnio, B.; Binnemans, K.; "Promotion of liquid-crystalline behavior of metallomesogens by electrostatic interactions" *Chemistry of Materials* **2008** (DOI: 10.1021/cm070637i).

4. Cardinaels, T.; Ramaekers, J.; Nockemann, P.; Driesen, K.; Van Hecke, K.; Van Meervelt, L.; Wang, G.; De Feyter, S.; Iglesias, E.F.; Guillon, D.; Donnio, B.; Binnemans, K.; Bruce, D.W.; "Tetracatenar Liquid Crystals Derived from 1,10-Phenanthroline" *Chemistry of Materials* in preparation.

5. Ramaekers, J.; Nockemann, P.; Driesen, K.; Van Hecke, K.; Van Meervelt, L.; Goderis, B.; Binnemans, K.; Cardinaels, T.; "Promotion of Liquid-Crystalline Behavior of Metallomesogens by Electrostatic Interactions" *Chemistry of Materials* in preparation.

188

Appendix A

Techniques

Nuclear magnetic resonance (NMR) spectra were recorded on a Bruker Avance 300 spectrometer (operating at 300 MHz for ^{1}H) or a Bruker AMX-400 spectrometer (operating at 400 MHz for ^{1}H).

FTIR spectra were recorded on a Bruker IFS-66 spectrometer, using the KBr pellet method.

Elemental analyses were obtained on a CE Instruments EA-1110 elemental analyzer.

Optical textures of the mesophases were observed with an Olympus BX60 polarizing microscope equipped with a LINKAM THMS600 hot stage and a LINKAM TMS93 programmable temperature controller.

DSC traces were recorded with a Mettler-Toledo DSC822e module. Electrospray ionization (ESI) spectra were recorded on a Thermo Finnigan LCQ Advantage mass spectrometer.

Photoluminescence spectra have been recorded on an Edinburgh Instruments FS900 spectrofluorimeter. This instrument is equipped with a 450 W xenon arc lamp, a microsecond flashlamp and a red-sensitive photomultiplier (250-850 nm). All the photoluminescence spectra have been corrected for the sensitivity of the detector at the different wavelengths.

The absoption spectra were measured with a Varian Cary 5000 spectrofotometer.

The STM experiments were carried out using a PicoSPM (Molecular Imaging, Arizona, USA) at room temperature, in the constant-current mode: the color coding in the STM graphs reflects differences in height. Pt/Ir STM tips were prepared by mechanical cutting from Pt/Ir wire (80/20%, diameter: 0.2 mm). For analysis purposes, the imaging of a molecular layer was immediately followed by recording the graphite lattice at a lower bias voltage, under otherwise identical experimental conditions. Drift effects were corrected for using the Scanning Probe Image Processor (SPIP)

software (Image Metrology ApS). To reduce noise, the images were filtered. The filtering procedure does not change the molecular features, yet enhances the visual presentation. The sample preparation was as follows: about 1 mg of ligand or rhenium(I) complex was dissolved in 1 mL of solvent (1-octanoic acid or 1,2,4-trichlorobenzene (TCB)). Samples in octanoic acid were heated for about 15 minutes at about 50 °C while sonicating. No heating was necessary for TCB solutions. STM Samples were prepared by placing a 3 μL droplet of the prepared solution onto a freshly cleaved highly oriented pyrolytic graphite surface (HOPG, GE Advanced Ceramics).

The XRD patterns were obtained with two different experimental setups, and in all cases, the powdered sample was filled in Lindemann capillaries of 1 mm diameter and 10 μm wall thickness. A linear monochromatic $CuK\alpha_1$ beam ($\lambda = 1.5405$ Å) obtained with a sealed-tube generator (900 W) and a bent quartz monochromator were used (both generator and monochromator were manufactured by Inel). One set of diffraction patterns was registered with a curved counter Inel CPS 120, for which the sample temperature is controlled within ±0.05 °C from 20 to 200 °C; periodicities up to 60 Å can be measured. The other set of diffraction patterns was registered on Image Plate. Periodicities up to 90 Å can be measured, and the sample temperature is controlled within ±0.3 °C from 20 to 350 °C.

Small-angle X-ray experiments were carried out at the Dutch-Belgian Beamline (DUBBLE, BM26-B) of the European Synchrotron Radiation Facility (ESRF, Grenoble).[1] Data were collected using a X-ray wavelength, λ, of 0.775 Å on a two-dimensional position sensitive gas-filled wire chamber detector at 1.5 m from the sample. The covered scattering vector range $0.045 < q < 0.8$ Å^{-1} was calibrated with a Silver Behenate specimen ($q = (4\pi/\lambda)\sin\theta$, where 2θ is the scattering angle).[2] The isotropic data were corrected for the detector response, azimuthally integrated and normalized to the intensity of the primary beam, measured by an ionization chamber placed downstream from the sample. The background scattering due to the experimental setup and the sample holder was subtracted according to

standard procedures, taking into account transmission differences. The samples, sealed in aluminum pans, were mounted into a Linkam HFS 191 hot-stage for temperature control.

1. Bras, W.; Dolbnya, I. P.; Detollenaere, D.; van Tol, R.; Malfois, M.; Greaves, G. N.; Ryan, A. J.; Heeley, E. *J. Appl. Cryst.* **2003**, *36*, 791.

2. Huang, T.C.; Toraya, H.; Blanton, T.N.; Wu, Y. *J. Appl. Cryst*. **1993**, *26*, 180.